EXCITON SIMULATIONS OF THE OPTICAL PROPERTIES OF SEVERAL PHOTOSYNTHETIC LIGHT-HARVESTING COMPLEXES

A THESIS SUBMITTED TO
THE GRADUATE SCHOOL OF NATURAL AND APPLIED SCIENCE
OF
MIDDLE EAST TECHNICAL UNIVERSITY

BY

ERKUT İNAN İŞERİ

IN PARTIAL FULFILMENT OF THE REQUIREMENTS FOR THE DEGREE OF
DOCTOR OF PHILOSOPHY
IN
PHYSICS

JUNE 2004

Approval of the Graduate School of Natural and Applied Sciences

_____
Prof. Dr. Canan Özgen
Director

I certify that this thesis satisfies all the requirements as a thesis for the degree of Doctor of Philosophy

_____
Prof. Dr. Sinan Bilikmen
Head of Department

This is to certify that we have read this thesis and that in our opinion it is fully adequate, in scope and quality, as a thesis for the degree of Doctor of Philosophy

_____
Prof. Dr. Demet Gülen
Supervisor

Examing Committee Members

Prof. Dr. Cüneyt Can	(METU,PHYS)	_____
Prof. Dr. Demet Gülen	(METU,PHYS)	_____
Prof. Dr. H. Yılmaz Kaptan	(HU,PHYS ENG)	_____
Prof. Dr. Şenay Katırcıoğlu	(METU,PHYS)	_____
Prof. Dr. Hamit Yurtseven	(METU,PHYS)	_____

"I hereby declare that all information in this document has been obtained and presented in accordance with academic rules and ethical conduct. I also declare that, as required by these rules and conduct, I have fully cited and referenced all material and results that are not original to this work."

Name- surname: Erkut İnan İşeri

Signature   :

ABSTRACT

EXCITON SIMULATIONS OF THE OPTICAL PROPERTIES OF SEVERAL PHOTOSYNTHETIC LIGHT-HARVESTING COMPLEXES

İşeri, Erkut İnan

Ph. D., Department of Physics

Supervisor: Prof. Dr. Demet Gülen

June 2004, 137 pages

The work presented in this thesis was aimed to investigate the structure-function relationship of several photosynthetic Light-Harvesting Complexes (LHCs) including Chlorophyll Protein 29 (CP29) and Light-Harvesting Complex II (LHCII) of green plants, and Fenna-Matthews-Olson (FMO) complex of green sulfur bacterium *Chlorobium tepidum*. This was accomplished by developing a set of procedures based on the exciton model and Förster transfer mechanism which have been employed to carry out numerical simulations to determine the optical characteristics and the energy transfer processes of the studied LHCs.

Based on the exciton calculations, a model was proposed to the electronic excited states (EES) of both CP29 and LHCII complexes by incorporating a considerable part of the current information offered by structure determination, mutagenesis analysis and spectroscopy in the modeling. The essential parameters for characterizing the excited states, Q_y dipole orientations and site energies were

assigned by suggesting a model that can explain both the key features of the linear (polarized) absorption spectra and the time scales of the energy transfer processes in CP29 and LHCII. Energy transfer rate between a pair of Chlorophylls has been modeled by the Förster mechanism. The idea of offering structural information through setting connection between the spectroscopy and the spectral simulations were supported by the presented results on CP29 and LHCII.

New spectroscopic measurements (absorption, linear dichroism (LD) and circular dichroism), carried out at 4 K on the FMO complex were presented, and also the LD spectrum was corrected for the degree of orientation of the sample, in order to provide comparison of not only the shape but also the size of the simulated and experimental spectra. The EES structure of the FMO complex was studied by simulating the measured optical spectra with more realistic model than the previously applied models. Simulations have been carried out with a computer program based on exciton model, which includes inhomogeneous, homogeneous and lifetime broadenings explicitly. The suggested EES model was compared with a previous model for the FMO complex from another green sulfur bacterium known as *Prosthecochloris aestuarii* and some of the observed spectral and structural differences between the two species were related in the frame of suggested models.

ÖZ

ÇEŞİTLİ FOTOSENTETİK IŞIK-DERLEYİCİ KOMPLEKSLERİN OPTİK ÖZELLİKLERİNİN EKSİTON SİMULASYONLARI

İşeri, Erkut İnan

Doktora, Fizik Bölümü

Tez Yöneticisi: Prof. Dr. Demet Gülen

Haziran 2004, 137 sayfa

Bu tezde sunulan çalışmanın amacı, yeşil bitkilerin Klorofil Protein 29'u (CP29) ile Işık Derleyici Sistem II'sini (LHCII) ve de yesil kükürt bakteri *Chlorobium tepidum*'un Fenna-Matthews-Olson (FMO) komplesini içeren çeşitli fotosentetik Işık-Derleyici Sistemlerin yapısı ile fonksiyonu arasindaki ilişkiyi incelemektir. Bu, çalışılan LHC'lerin optik özelliklerini ve enerji transfer süreçlerini belirlemek için eksiton model ve Förster transfer mekanizması temelinde nümerik simulasyonlar yapmakta kullanılan bir dizi prosedür geliştirilerek yapıldı.

Eksiton hesaplarına dayalı olarak, CP29 ve LHCII'nin elektronik uyarılmış durumları (EES) için, yapı tayininden, mutasyon analizinden ve spektroskopiden elde edilen güncel bilgilerin büyük bir kısmı dahil edilerek model önerildi. Uyarılmış durumları karakterize etmek için gerekli olan parametreler, Q_y dipol moment yönelimleri ve klorofil öz soğurma enerjileri, CP29 ve LHCII'nin doğrusal (polarize) soğurma spektrumlarının anahtar özellikleri ile enerji transfer

süreçlerinin zaman skalalarını açıklayan model önerilerek belirlendi. Klorofil çiftleri arasındaki enerji transfer süreçleri Förster mekanizması ile modellendi. Spektroskopi ve spektral simulayonu arasında bağlantı kurularak, sistemin yapısı hakkında bilgi sunulabileceği fikri CP29 ve LHCII için sunulan sonuçlar tarafından desteklendi.

FMO kompleksinin 4 K'de yapılmış yeni spektroskopik ölçümleri (soğurma, doğrusal dikroizm (LD) ve dairesel dikroizm) sunuldu ve de simulasyon ile deney spektrumlarının şeklinin yanısıra boyututunun da karşılaştırılmasına olanak sağlamak için LD spektrumu örneğin yönelimler derecesi için düzeltildi. FMO kompleksinin EES yapısı, ölçülen optik spektrumlarının önceki modelere göre daha gerçekçi bir model kullanılarak yapılan simulasyonu ile çalışıldı. Simulasyonlar eksiton modele dayalı, homojen, homojen olmayan ve ömre bağlı genişlemeleri ayrı ayrı içeren bilgisayar programıyla yapıldı. Önerilen EES modeli başka bir yesil bakteri olan *Prosthecochloris aestuarii*'nin FMO kompleksi için daha önce önerilen modelle karşılaştırıldı ve önerilen modeller çerçevesinde iki kompleks arasında gözlemlenen spektral ve yapısal farklılıkların bir kısmı ilişkilendirildi.

Anahtar kelimeler: Soğurma, bakteriklorofil, klorofil, CP29, elektronik uyarılmış durum, enerji transferi, eksiton model, FMO, Förster mekanizması, LHCII, ışık derleyici kompleks, fotosentez.

TABLE OF CONTENTS

LIST OF TABLES

LIST OF FIGURES

LIST OF ABBREVIATIONS

ABS Absorption

BChl Bacteriochlorophyll

CD Circular Dichroism

Chl Chlorophyll

CP29 Chlorophyll Protein

EES Electronic Excited States

FLN Fluorescence Line Narrowing

FMO Fenna-Matthews-Olson

fwhm full-width at half-maximum

IDF Inhomogeneous Distribution Function

LD Linear Dichroism

LHC Light-Harvesting Complex

PW Phonon Wing

RC Reaction Center

ZPL Zero Phonon Line

CHAPTER 1

INTRODUCTION

1.1 Photosynthesis and Light-Harvesting Complexes

Photosynthesis is the process by which plants, algae and certain types of bacteria capture and efficiently convert the solar energy into storable chemical energy. Since photosynthesis provides directly or indirectly free energy for driving the complex physical and chemical processes of the living organisms directly or indirectly, this energy conversion has vital importance for the life on the Earth. The importance of photosynthesis has been realized for many years and research into its mechanisms has attracted scientist from several different disciplines. It is believed that the knowledge acquired from the natural photosynthesis could point the way to the development of efficient, robust artificial systems for solar energy storage and also should help with the breeding of new plants with improved photosynthetic efficiencies.

Photosynthesis is initiated when the light is absorbed by a pigment molecule, which is in a special protein environment. A large number of pigment molecules involved in the process of absorbing light energy are collectively referred to as light harvesting complex (LHC) or antenna. The purpose of LHC is to increase the absorption cross-section and to maintain a high rate of electron transfer in the reaction center, even at low light intensities. In order to absorb solar energy, nature has evolved some pigments such as (bacterio)chlorophyll ((B)Chl), carotenoid or bilin depending on the type of organisms. Pigments are organic molecules and reflect only certain wavelength of visible light. This makes them appear "colorful". More important than their reflection of light is their ability to

absorb light energy, and to convert it into chemical energy. Within the main classes, there are several different pigments, each of which absorbs light of slightly different frequencies. This allows the photosynthetic organism to make use of a broad frequency spectrum. Light energy is absorbed by LHC but is not used immediately for energy conversion. Instead the light energy is transferred to pigment molecules that are in another special protein environment where the light energy is used to trigger a series of electron transfers. The molecules and the protein involved in electron transfer events together are called as the reaction center (RC). A series of electron transfers in the RC finally leads to a charge separation across the membrane where the reaction center is embedded in. This potential gradient due to the charge separation provides the energy necessary to drive further chemical reactions leading to oxygen evolution and carbon fixation. Together LHC and RC constitute the photosynthetic unit (PSU) (see Figure 1.1).
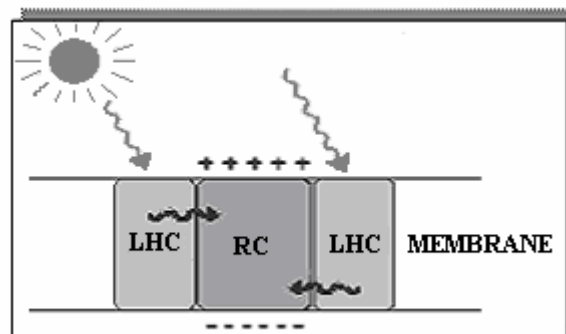
Figure 1.1. A schematic diagram of photosynthetic unit (PSU).

The transfer of excitation energy among the pigment molecules in the LHCs and the subsequent charge separation in the RC take place in picosecond time scale and are very efficient. The following are the current questions of interest:

- What are the structures of the LHC/RC complexes in different photosynthetic organisms?

- What are the physical mechanisms of the energy and electron transfer processes that make these particular structures to work in a very speedy and efficient way?

Owing to the recent advances in spectroscopic techniques, structure determination and molecular genetics these questions are now yielding answers [1-7]. Besides of these experimental techniques, considerable amount of information on these questions can also be obtained by setting connection between the structure and spectroscopy through modeling of the spectral properties. This has been the point of departure of this thesis. The connection between spectroscopy and structure together with the information gathered through genetic engineering has been used to investigate the molecular mechanisms of energy transfer in several photosynthetic LHCs.

1.2 (Bacteria)Chlorophylls (B(Chl)): Structure and Absorption

Chl a molecule is found in all plants, algae and cynaobacteria, which photosynthesize. Another kind of chlorophyll is Chl b, which occurs only in green algae and in the plants. BChl a molecule is found in photosynthetic bacteria.

The chemical structures of the BChl a and Chl a/b molecules are shown in Figure 1.2a and 1.3a. (Bacteria)Chlorophylls are molecules, which contain a porphyrin ring. Their central region is formed by four connected pyrrole-rings, coordinated by a magnesium atom. The peripheral region contains fifth ring, a long phytyl-chain and small side groups, which vary between different pigment species. The electronic and spectroscopic properties of (B)Chls, being porphyrin derivatives that is a stable ring-shaped molecule around which electrons are free to migrate, are determined to a large extend by the conjugate π system. Within this system, electrons are delocalized over larger distances than within a single covalent bond. This electronic charge distribution leads to a dipole which is quantum mechanically represented by a transition dipole moment. Pigment interacts with light through its electronic transition dipole moment, which must oscillate at the frequency of the light. The transition dipole moment of the first excited state, Q_y,

of (B)Chl a molecule is approximately along N_I and N_{III} as shown in Figure 1.2a. This is a vector and its length determines the amount of absorption and its direction gives the sensitivity to the polarization of the light. The second excited state, Q_x, has a transition dipole moment along N_{II} and N_{IV} (almost perpendicular to the Q_y transition dipole moment) [8]. The higher energy transitions, B_x and B_y (Soret transitions), also have transition dipole moments polarized along the X- and the Y-directions.
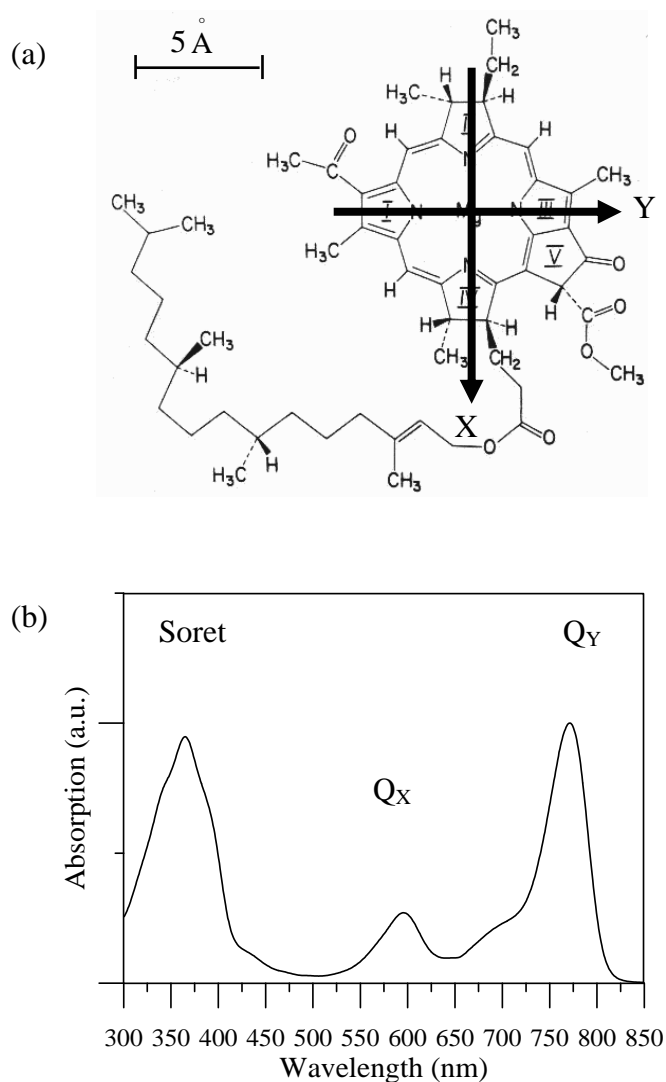
Figure 1.2. (a) Chemical structure of BChl a. (b) The absorption spectrum of BChl a in a polar organic solution (a mixture of methanol, acetonitrile, ethyl acetate and water) at room temperature [9].

4
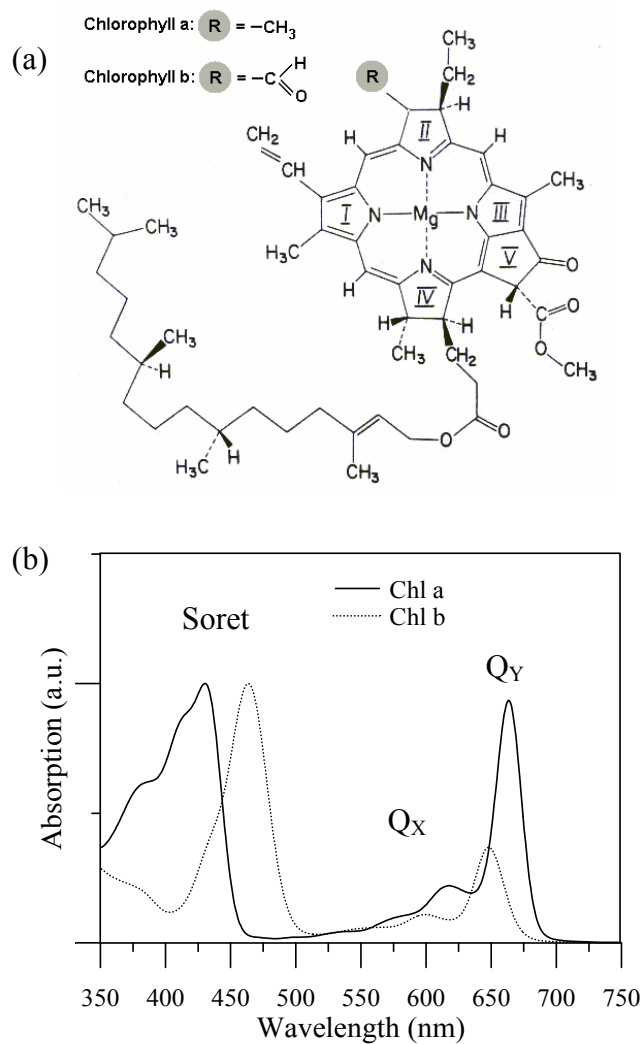
Figure 1.3. (a) Chemical structures of Chl a and Chl b. (b) The absorption spectrum of Chl a and b in a polar organic solution at room temperature [9].

The interaction of the molecule with the light in semiclassical approach can be described as follows [10]. The wave functions ψ^0 and $\Psi(t)$ of an unperturbed and a perturbed molecular systems must follow the Schrödinger equations

$$H^0\psi^0(t) = i\hbar \frac{\partial \psi^0(t)}{\partial t} \qquad (1.1)$$

$$(H^0 + H'(t))\Psi(t) = i\hbar\frac{\partial\Psi(t)}{\partial t} \tag{1.2}$$

where H^0 is a time-independent Hamitonian. Equation 1.2 also includes a time-dependent term $H'(t)$.

The solution to the equation (1.1) can be expressed as a normalized function of the form

$$\psi^0(t) = \sum_{n=0}^{\infty} a_n \psi_n^0(t) \tag{1.3}$$

where a_n are constants such that $\sum a_n^* a_n = 1$. The time-dependent functions $\psi^0(t)$ are wave functions of stationary states with energies E_n.

The equation (1.2) can be solved by using time-dependent perturbation theory in order to describe the states of the new perturbed system. One can thus substitute a sum as in equation (1.3) into (1.2) and obtain the coefficients from

$$i\hbar\sum_n \frac{da_n(t)}{dt}\psi_n^0 = \sum_n a_n(t)H'\psi_n^0 \; . \tag{1.4}$$

Recalling that the solution to a time-dependent Schrödinger equation can be written as

$$\psi^0(t) = \varphi^0 e^{-(i/\hbar)Et}$$

where φ^0 are now time-independent wave funcitons, one can determine the coefficents from the equation

$$\frac{da_m(t)}{dt} = -\frac{i}{\hbar}\sum_{n=0}^{\infty} a_n(t)e^{(i/\hbar)(E_m-E_n)t}\left\langle m^0\left|H'\right|n^0\right\rangle \tag{1.5}$$

where we have used Dirac notation (e.g. the wave functions φ_n^0 are represented as $\left|n^0\right\rangle$). Therefore, the probability to change the initial state n to another state m due

6

to the perturbation (absoption of light wave) is $\left| a_m \right|^2$. Now we need to know the form of the pertubation Hamiltonian in order to determine the transition probability. This is

$$H' = \sum \left\{ \frac{-q_j \hbar}{i m_j c}(\vec{A}.\vec{\nabla}) + \frac{q_j^2}{2 m_j c^2} \vec{A}^2 \right\} \tag{1.6}$$

where $\vec{A}$ is the vector potential of the light, and $\vec{\nabla}$ is the gradiant operator. The summation is made over all j charged particles, with charge q and mass m_j, $\hbar$ is Planck constant divided by 2π and c is the speed of light. In a wave model of light, the vector potential is

$$\vec{A} = A_0 \hat{\varepsilon}(\gamma e^{-i\omega t} + \gamma^* e^{i\omega y}) \tag{1.7}$$

where $\hat{\varepsilon}$ is the unit vector in the direction of polarization of the light wave, ω is the frequency of the light and $\gamma = e^{i\vec{k}\cdot\vec{r}}$ where $\vec{k} = 2\pi \hat{k}/\lambda$.

Using the electric dipole approximaion, which is based on the fact that the wavelength of the light is far longer than the molecular dimension, so that the series

$$\gamma = e^{i\vec{k}\cdot\vec{r}} = 1 + i\vec{k}\cdot\vec{r} - (\vec{k}\cdot\vec{r})^2 + ...$$

can be approximated by its leading term, 1 and also ignoring the $\vec{A}^2$ in equation (1.6), one can obtain the semiclassical result for the probability for light absoption per unit time as,

$$W = \frac{2\pi}{3\hbar} \left| \langle m | \hat{\mu} | n \rangle \right|^2 \rho(\nu) \tag{1.8}$$

where $\rho(\nu)$ is the radiation density and $\hat{\mu}$ is a dipole operator given by

$$\hat{\mu} = \sum_j q_j \vec{r}_j .$$

The intensity of the absorption band, which is also called as the dipole strength (absorption strength) is proportional to the squared transition dipole moment. To connect with the standard absorption measurements, it is more convenient to use the formula given below. The dipole strength (*D*) is related to the experimentally measurable molar extinction coefficient $\varepsilon(\omega)(M^{-1}cm^{-1})$ via the following equation:

$$D = \mu^2 = 9.180 \times 10^{-3} \left(\int \frac{\varepsilon(\omega)}{\omega} d\omega \right) \text{ debye}^2 \qquad (1.9)$$

where the integration is performed on a frequency scale across the absorption band. The molar extinction coefficient as a function of frequency can be obtained experimentally via the Beer-Lambert law;

$$OD(\omega) = \log_{10}(I_0 / I) = C\varepsilon(\omega)l \qquad (1.10)$$

where OD is called optical density or absorbance, I_0 is the intensity of the incident monochromatic light on the sample, *I* is the transmitted intensity by the sample, *C* is the molar concentration and *l* is the path length of the sample through which light actually travels (in cm). The normalized absorption spectra of BChl a, Chl a and b in a polar organic solution are shown in Figures 1.2b and 1.3b respectively [9]. The BChl a Q_y transition is around 775 nm and those of the Chl a and Chl b are around 665 nm and 645 nm respectively. The higher transitions, Q_x and Soret (B_x and B_y), for all pigments are around 550-600 nm and 400-480 nm respectively. These transitions remain present when the pigment is bound to a protein, but their properties are modified by interactions with neighboring pigments as well as the protein.

1.3 Structures

For an accurate/satisfactory interpretation of the spectroscopy of the LHCs and the RCs, the structure of pigment-protein complex involved in energy and electron transfer is critical. With exception of specific LHC and RC complexes

(such as the Fenna-Matthews-Olson complex of green sulfur bacteria), photosynthetic proteins are usually hydrophobic (repelled by water) membrane proteins. The hydrophobicity of membrane proteins, initially hampered attempts to elucidate the structure of these complexes, as they do not readily form the well-ordered crystals that are needed for high-resolution X-ray and electron diffraction studies which are the methods applicable in determining the 3-dimensional structure of complex biological molecules at atomic resolution. In the mid 1980's the investigators from the Max Planck Institute in Munich, Germany, found methods to crystallize the water insoluble membrane proteins [11]. By using certain small organic molecules with one end that is hydrophilic (attracted to water) and one end that is hydrophobic, which bind to the hydrophobic parts of the membrane, they have obtained aggregates of small molecules. Then the protein coated this way can be dissolved in aqueous solution and it can be crystallized which is known as the co-crystallization. Hartmut Michel, Robert Huber and Johann Deisenhofer, received the Nobel Prize in chemistry in 1988 for this research. Since then, the structures of various reaction centers and antenna complexes have been determined at atomic resolution. The structures of LHCs studied in this thesis have been summarized below.

1.3.1 Light-Harvesting Complex II (LHCII)

In photosystem II (PSII) of green plants light harvesting is performed by a collection of LHCs buried in the photosynthetic membrane (thylakoids). The LHC associated with PSII consists of two parts: an outer antenna binding Chl a, Chl b, and carotenoids and an inner antenna binding Chl a and carotenoids. The proteins forming the outer antenna are usually called as Lhcb proteins. The major Lhcb protein, LHCII, binds almost 65% of the PSII chlorophyll (accounting for 50% of the total Chls in the thylakoids) and the minor Lhcb proteins that have been identified so far (usually called as CP24, CP26 and CP29) bind altogether 15% of the PSII chlorophyll [12]. In Figure 1.4 an electron micrograph [13] of a PSII supercomplex of a PSII reaction center dimer and surrounding antenna is shown.
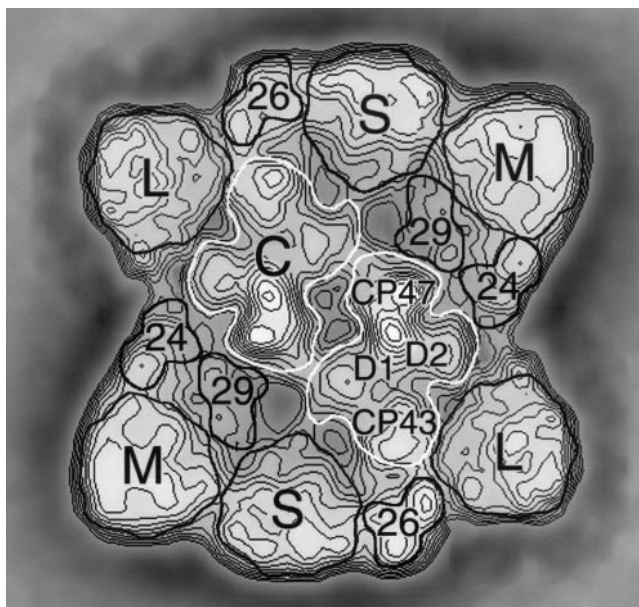
Figure 1.4. Electron micrograph of a PSII supercomplex of a PSII reaction center dimer (D1 and D2) and surrounding antennae [13]. Both the core antennae CP43 and CP47, and the peripheral antennae; CP29 (29), CP26 (26), CP24 (24) and LHCII (trimers L: loosely bound, M: moderately bound, S: strongly bound), are contained in this complex.

Currently, LHCII is the only Lhcb protein, which is structurally resolved. A large part of the structure of the LHCII is modeled by using electron diffraction to a resolution of 3.4 $\overset{\circ}{A}$ by Kühlbrant et al. [14]. The complex in the crystalline state forms a trimer with three symmetrically (C_3) arranged monomers (see Figure 1.5a). The arrangement of the polypeptide (helices) and the pigments in one of the monomeric subunits are shown in Figure 1.5b. The polypeptide consists of three transmembrane helices A, B, and C and another helix D that is roughly oriented parallel to the inner surface of the photosynthetic membrane. The helices A and B are related to each other by an approximate two-fold symmetry axis that runs perpendicular to the plane of the membrane and form an X-like cross-bridge in the center of the complex. The helix C located at the side of this symmetrical core is believed to be an evolutionary addition.

(a)

a2
b2
B3
A6
B1(a)
al
L1
b6
A3
L2
A7(b)
a4
b5
a5

20 Å

(b)

A
B
a1
a4
B1(a)
b2
b5
a2
a5
L1
L2
A3
B3
A6
b6
A7(b)
D
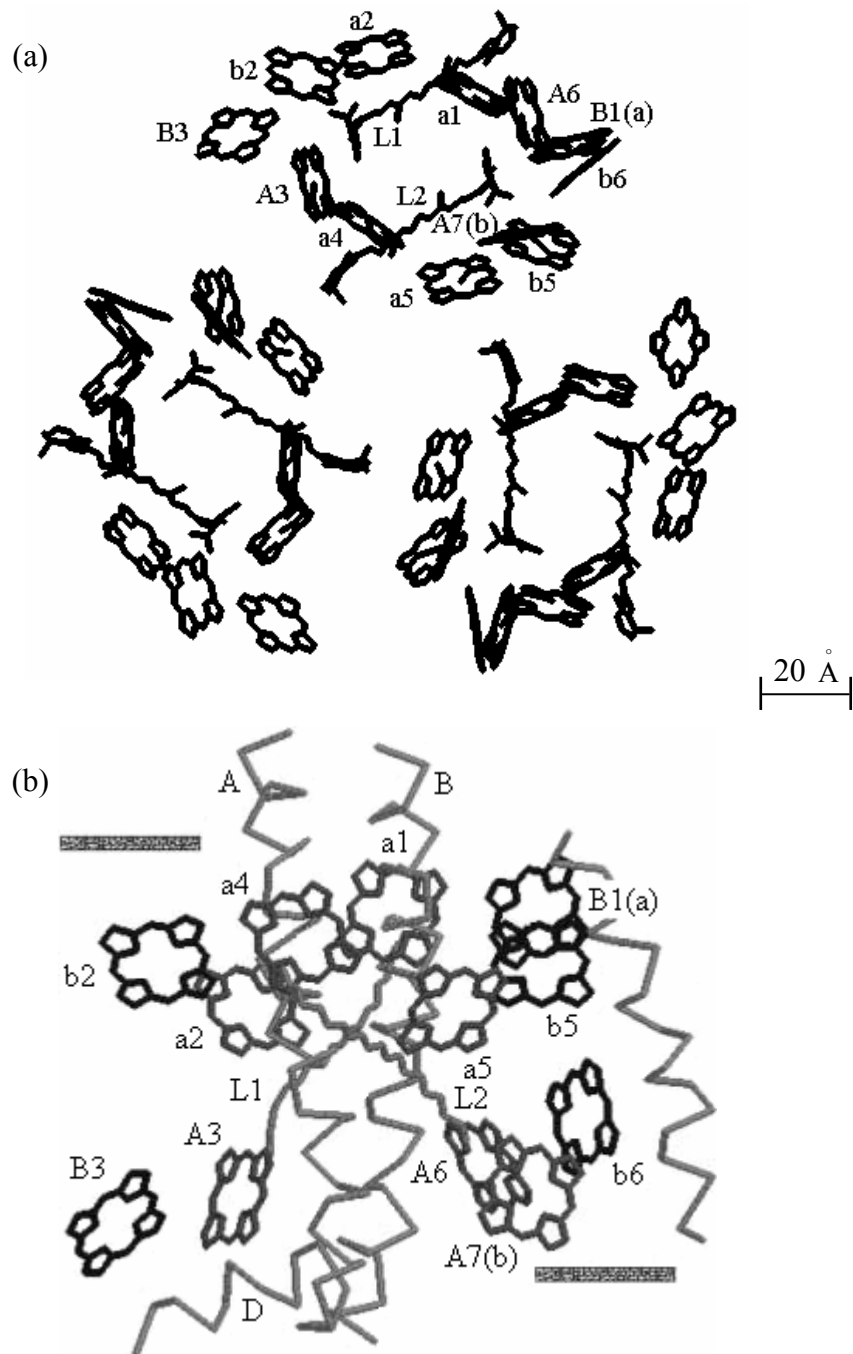
Figure 1.5. a) Top view of the pigment arrangement in the trimeric LHCII. b) A 2-dimensional side view of the monomeric LHCII structure and the presumed position of the thylakoid membrane. The protein folding of LHCII consists of three membrane-spanning helices (A, B, and C) and a fourth helix (D) running parallel to the presumed position of the photosynthetic membrane. The helices A and B are related to each other by a two-fold symmetry axis running perpendicular to the membrane (parallel to the C_3 symmetry axis). The 12 chlorophyll (Chl) molecules surround the two central carotenoids (L1 and L2). Horizontal solid thick lines indicate the approximate position of the photosynthetic membrane.

11

The LHCII pigments identified per monomeric subunit of the current model are 12 Chl a/b molecules surrounding two central carotenoid molecules. At the current resolution, the chlorophylls a and b cannot be distinguished. The Chls a and Chls b are labeled according to the recent site-directed mutagenesis study by Remelli et al. [15] where Chls a1, a2, a4, a5 and B1(a) are pure Chl a molecules and b2, b5, b6 and A7(b) are pure Chl b molecules. The binding sites for A3, B3 and A6 are idendified as the mixed sites, which may either bind a Chl a or a Chl b.

The chlorophylls are roughly arranged in two levels near the outer (upper) and the inner (lower) surfaces of the photosynthetic membrane. The upper level is a 'ring' of seven Chl molecules and the lower level contains five Chl molecules. Moreover, there is a pseudo 2-fold symmetry axis relating the three pairs in the upper level, a1-a4, a2-a5, b2-b5 and A3-A6 pair in the lower level. The Chl a1, a2, a4 and a5 core is conserved not only in Chl a/b binding proteins but also in Chl a/c binding proteins throughout the evolution [16].

Table 1.1. Center-to-center distances between the chlorophylls in a monomeric unit of the LHCII complex (in $\overset{\circ}{A}$).

	A1	A2	A3	A4	A5	A6	A7	B1	B2	B3	B5
A2	12.3										
A3	26.2	19.1									
A4	16.2	17.4	19.5								
A5	19.4	24.0	21.3	12.7							
A6	19.5	20.3	21.7	26.1	21.3						
A7	24.8	26.9	21.1	25.2	15.8	11.6					
B1	10.5	21.9	31.3	21.2	18.0	19.0	21.9				
B2	17.2	8.3	19.9	15.8	26.0	27.6	32.2	27.2			
B3	31.4	21.4	9.2	25.2	29.8	28.4	29.7	38.3	20.2		
B5	16.4	24.9	27.5	17.5	8.9	19.7	16.6	10.6	28.7	35.8	
B6	20.3	25.5	27.1	26.8	18.8	8.7	10.0	15.2	32.3	34.9	14.6

The center-to-center distances between the Chls in different levels are longer than 20 $\overset{\circ}{A}$. The closest distance is between chlorophylls A2 and B2 (8.3

$\overset{\circ}{A}$) and the largest distance is between chlorophylls B1 and B3 (38.3 $\overset{\circ}{A}$). Table 1.1 summarizes the center-to-center distances between the twelve chlorophylls of the monomeric unit of the LHCII.

At the current structural resolution there are two possible orientations (along Y or along X) for the Q_y transition dipole moment of each of the twelve Chls [17]. Two possible orientations (Y and X) for the Q_y transition dipole moments of the twelve Chls in the LHCII with respect to the C_3 symmetry axis are shown in Figure 1.6.
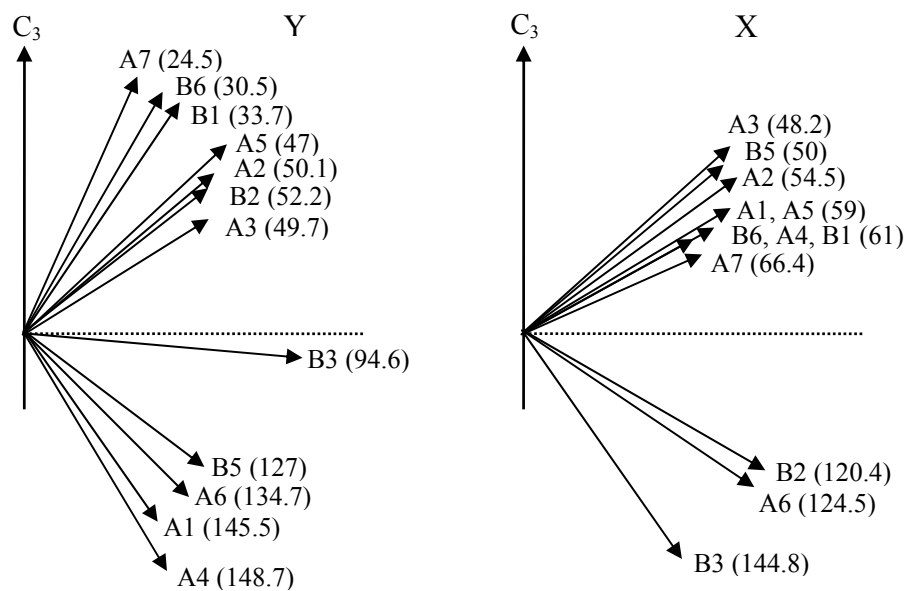
Figure 1.6. Two possible orientations (Y and X) for the Q_y transition dipole moment of each Chls with respect to the C_3 symmetry axis. The dotted line shows the plane parallel to the plane of membrane. The numbers in parentheses are the values of the angles that the dipole moments make with the C_3 symmetry axis.

1.3.2 Chlorophyll Protein 29 (CP29)

All the Lhcb proteins are highly homologous and are therefore believed to share a protein folding similar to that of the LHCII. Furthermore, the Chl binding sites are conserved. Therefore, the LHCII structure is not only important for the study of LHCII itself, but also serve as model for the structure of the minor Chl a/b binding Lhcb proteins CP29, CP26 and CP24 of PSII. All the minor Lhcb proteins have been predicted to play a role in the photoprotective dissipation of excess excitation energy, known as high-energy-state non-photochemical fluorescence quenching [18].
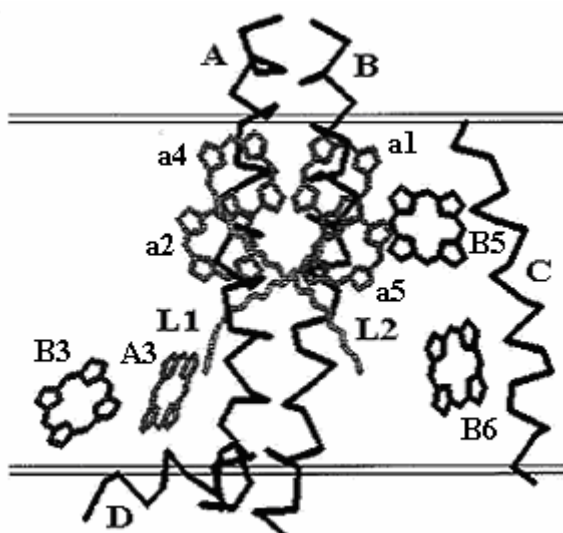
Figure 1.7. The model structure of CP29. The relevant part of the LHCII structural data resolved by Kühlbrandt et al. [14] is shown together with the Chl identities of Bassi et al. [16]. Horizontal lines indicate the approximate position of the photosynthetic membrane.

The LHCII pigments identified per monomeric subunit of the current model are twelve Chl molecules surrounding two central carotenoid (Car) molecules (see Figure 1.5). The minor Lhcb proteins bind a fewer number of Chls with varying

pigment-binding stochiometries. The Lhcb protein of interest in this work, CP29, is the largest of these minor Lhcb proteins which binds 2 Chl b, 6 Chl a and 2 Car molecules [16] (see Figure 1.7). In Figure 1.7 the Chls a and Chls b are labeled according to the recent site-directed mutagenesis study by Bassi et al. [16] where the evolutionarily conserved core consisting of the Chls a1, a2, a4, and a5 are identified as pure Chl a sites, and A3, B3, B5 and B6 are identified as mixed sites. We refer to table 1.1 for the distances between the relevant Chl molecules and to Figure 1.6 for the possible Q_y transition dipole moment directions of the Chl molecules associated with CP29.

1.3.3 Fenna-Matthews-Olson (FMO) complex

In photosynthetic green sulfur bacteria the FMO complexes are believed to mediate electronic energy transfers from the peripheral antenna to the reaction centers [19].

The 3-dimensional structure of the FMO complex of the green bacterium *Chlorobium* (*Cb.*) *tepidum,* currently at 2.2 $\overset{\circ}{\text{A}}$ resolution [20], reveals three identical subunits related by a crystallographic 3-fold axis of symmetry (C_3). Figure 1.8a shows a ribbon drawing of the polypeptide of the three symmetry related subunits. Each one of these protein envelopes, which consists of a large β-sheet of 23 strands and 9 helices, encloses seven BChl a molecules arranged in a rather non-symmetric fashion (see Figure 1.8b).

BChl 1 and BChl 2 (labeled according to the Fenna-Mathews numbering scheme [21]) are close the surface of the monomer protein while BChls 3, 4, 5, 6 and 7 are buried in the core of protein. BChl 7 is in the center of seven molecules and has the closest average distance towards the other six BChl molecules. The average center-to-center distance between nearest-neighbor BChls is $13.2 \overset{\circ}{\text{A}}$ in the same subunit and the closest distance between different subunits is $23.9 \overset{\circ}{\text{A}}$ (see Table 1.2). The Q_y transition dipole moment orientations of the BChl molecules with respect to the C_3 symmetry axis are shown in Figure 1.9. The dipole moments

for the BChls 1, 4 and 7 are approximately parallel to the C_3 symmetry axis while the dipole moment orientations for the BChls 2, 3, 5 and 6 are very close to the plane of trimer.

(a)

(b)

BChl 1
BChl 6
BChl 5
BChl 4
BChl 2
BChl 7
BChl 3

10 Å
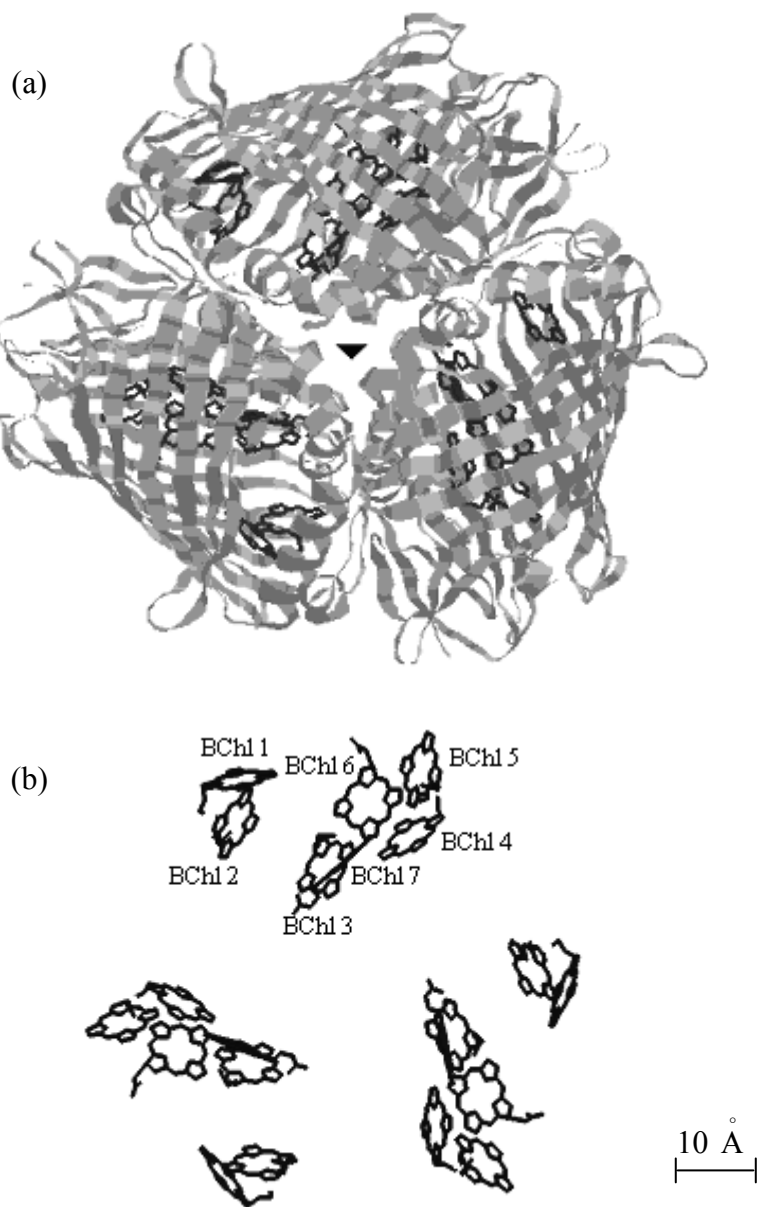
Figure 1.8. The structural model for the FMO complex of *Cb. tepidum* [20]. a.) Ribbon diagram of the polypeptide chain of the FMO trimer. C_3 symmetry axis is indicated with triangle. b.) Arrangement of the BChls of the trimeric FMO complex. The protein has been removed and the BChls are labeled in the Fenna-Matthews numbering scheme [21].

Table 1.2 . Center-to-center distances between the BChls in a subunit and between the BChls of the adjacent subunits of the trimeric FMO complex (in $\overset{\circ}{A}$).

Subunit	BChl no	1	2	3	4	5	6	7
	2	12.9						
	3	28.3	17.4					
1	4	30.9	23.6	11.1				
	5	24.4	23.3	21.0	13.6			
	6	16.0	19.1	24.2	21.1	11.5		
	7	19.9	13.8	12.4	13.2	14.4	12.7	
	1	46.4	43.3	46.0	51.3	54.4	47.1	41.6
	2	46.0	39.8	38.0	43.8	49.8	44.9	36.5
	3	40.7	30.5	24.8	33.1	42.1	40.1	28.5
2	4	34.3	23.9	23.8	33.9	41.1	37.9	27.1
	5	33.1	27.0	33.7	42.8	46.5	40.0	32.5
	6	32.4	29.4	36.2	43.0	44.9	36.8	31.5
	7	33.2	26.1	26.8	33.9	39.0	33.9	24.9
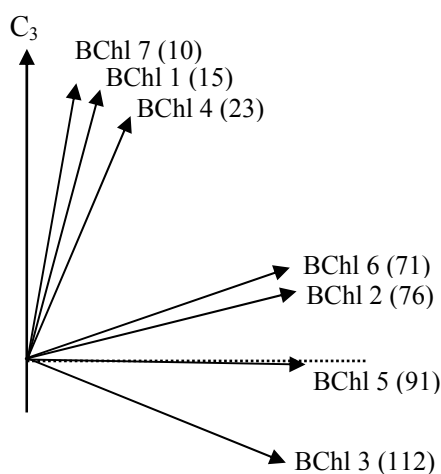
Figure 1.9. The Q_y transition dipole moment directions of the monomeric BChls a with respect to the C_3 symmetry axis. The dotted line shows the plane parallel to the plane of membrane. The numbers in parentheses are the values of the angles (in degrees) that the dipole moments make with the C_3 symmetry axis.

Being water soluble, the FMO complex from *Prosthecochloris (Pc.) aestuarii* has been the first photosynthetic pigment-protein complex to have its

17

three-dimensional structure determined to an atomic resolution by X-ray crystallography [21]. Currently, the structural model of the FMO complex from *Pc. aestuarii* is at 1.9 Å resolution [22]. The overall structures of the two complexes are very similar. The FMO complex from *Pc. aestuarii* also consists of three identical subunits related by a crystallographic C_3 symmetry axis. Each monomeric subunit encloses seven BChl molecules in a geometry that is very similar to that of the FMO complex of *Cb. tepidum*. Figure 1.10 shows a superposition of the structures of the FMO complexes of the two species. There are only minor differences in the positions and orientations of the various BChls. The amino acid sequences of the FMO from *Pc. aestuarii* and *Cb. tepidum* are also 78% homologous. Despite their very similar structures, the FMO proteins from *Pc. aestuarii* and *Cb. tepidum* have rather distinctive spectral features [20, 23].
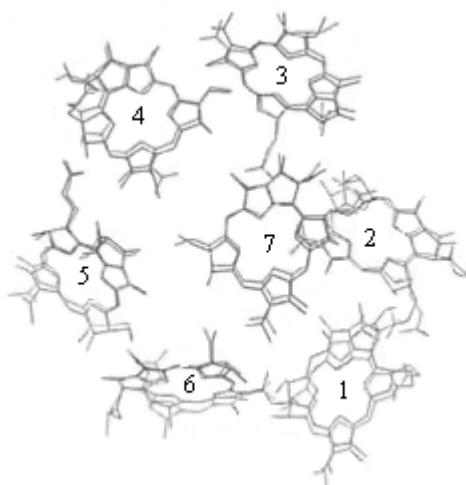
Figure 1.10. Superposition of the structures of the FMO complexes from *Cb. tepidum* (darker) and *Pc. aestuarii* (lighter) [23].

1.4 Theoretical Considerations

1.4.1 Intermolecular Interactions

The spectroscopic properties of LHCs are determined to a large extend by the interactions between the pigments due to the relatively small distances between the pigment molecules.

The Coulomb interaction between two molecules through their charge distributions ($\rho_1(r)$ and $\rho_2(r)$) in the medium characterized by the dielectric constant, ε, is given by

$$V_{Coulomb} = \frac{1}{4\pi\varepsilon}\iint \frac{\rho_1(\vec{r})\rho_2(\vec{r}')}{|\vec{r}-\vec{r}'|}d\vec{r}d\vec{r}' \qquad (1.11)$$

The equation (1.11) can be rewritten by using the method of multipole expansion. Taking as a reference point the center $\vec{r}_i$ of the ith molecule, for instance its center of mass, one defines as multipole moments of its charge distribution $\rho_i(\vec{r})$ relative to this center as;

$$q_i = \int \rho_i(\vec{r})d\vec{r} , \qquad (1.12)$$

$$\vec{\mu}_i = \int \rho_i(\vec{r})(\vec{r}-\vec{r}_i)d\vec{r} , \qquad (1.13)$$

$$\theta_{i,\alpha\beta} = \int \rho_i(\vec{r})\{3(\vec{r}-\vec{r}_i)_\alpha(\vec{r}-\vec{r}_i)_\beta - \delta_{\alpha\beta}(\vec{r}-\vec{r}_i)^2\}d\vec{r} \qquad (1.14)$$

monopole, dipole moment and quadrupole tensor respectively and higher multipole moments which are not shown. The interaction energy between two molecules with relative position vector $\vec{R}=\vec{r}_j -\vec{r}_i$ and corresponding unit vector $\hat{R}$ is then written as

$$V(\vec{R}) = \frac{1}{4\pi\varepsilon}\left\{\frac{q_i q_j}{R} + \frac{q_i(\vec{\mu}_j \cdot \hat{R}) - q_j(\vec{\mu}_i \cdot \hat{R})}{R^2} + \frac{\vec{\mu}_i \cdot \vec{\mu}_j - 3(\vec{\mu}_i \cdot \hat{R})(\vec{\mu}_j \cdot \hat{R})}{R^3} + \right.$$

$$\left. \sum_{\alpha,\beta=1}^{3} \hat{R}_\alpha \hat{R}_\beta \left\{ q_i \theta_{i,\alpha\beta} + q_i \theta_{i,\alpha\beta} \right\} \frac{1}{2R^3} + \ldots \right\}. \tag{1.15}$$

Unfortunately, the multipolar description of the electrostatic effects, such as equation (1.15), encounters serious problems because of the divergent nature of the multipole expansion. The equation (1.15) is valid only if the distance R between the molecules is considerably larger than the size of the molecules (~1 nm x 1 nm) which must be well separated in order to guarantee proper convergence of the series expansion of $V(\vec{R})$. The first two terms in equation 1.15 correspond to the ion-ion and ion-dipole interactions, respectively. These are important in charged pigments and in the case of coupling between charge-transfer states. However, in many cases one is dealing with uncharged molecules and the third term of equation (1.15) thus becomes dominant which corresponds to the dipole-dipole coupling between two molecules.

Another reasonable criteria in the dipole-dipole approximation is to inquire that R to be larger than the dipole radius a, where a= μ/e (μ is the transition dipole moment and e is the elementary unit of charge). The successive higher order terms in the expansion can be negligible since they get smaller and smaller with distance as in most cases. As a consequence, the changes in spectroscopic properties of the interacting pigments are determined to a large extend by the dipole-dipole coupling term compared to those of the individual pigments and the excitation energy transfer. For the small intermolecular distances that are comparable to the intramolecular distances, the multipole series expansion will diverge and the exact distribution of charges should be fully considered for the Coulomb energy between the monomers. However, even if this is the case, the dipole-dipole approximation may give at least a qualitative description. In Table 1.3, recent *ab initio* calculations of Coulombic interactions between the transition densities (V_{td}) are compared with the point dipole approximation (V_{d-d}) for the various distances

20

between the BChl molecules of the LH2 complex of *Rhodopseudomonas acidophila* [24]. The Q_y-Q_y interactions of BChl molecules are well described in the point-dipole approximation (V_{d-d}) for pairwise separations greater than 15 $\overset{\circ}{A}$ and deviations are significant (25-30%) only at separations around 9-9.5 $\overset{\circ}{A}$.

Table 1.3. Intermolecular separation and calculated couplings, V_{td} and V_{d-d} between various BChls of the LH2 complex of *Rhodopseudomonas acidophila*.

Distance ($\overset{\circ}{A}$)	V_{td} (cm^{-1})	V_{d-d} (cm^{-1})
9.1	213	284
9.5	238	367
17.6	27	27
17.8	-46	-48
18.6	-37	-37
21.2	-27	-26
23.9	-13	-12
31	7	7
36.3	5	5

1.4.2 Photosynthetic Exciton Concept

Excitons exist by virtue of intermolecular interactions. When the pigment molecules are located sufficiently close to each other; they interact each other through their transition dipole moments giving rise to the formation of new delocalized excited states. The corresponding delocalized electronic states are called as the exciton states [25].

The exciton concept is generally applied to describe the spectroscopic properties, the electronic excitation dynamics and the flow of excitation energy in biological structures, amorphous media and molecular aggregates, from liquid helium temperature to room temperature [26].

A system of N molecules whose positions and orientations are 'fixed' in space (e.g. Chl molecules embedded in a protein environment) is considered. The ground state wave function can be expressed as

$$\Psi_G = \phi_1\phi_2\phi_3..........\phi_N = \prod_{j=1}^{N}\phi_j \ , \qquad (1.16)$$

and the lowest-energy singlet excited state of the aggregate can be represented by the wave function

$$\varphi_i = \phi_1\phi_2\phi_3....\phi_i^*.....\phi_N = \phi_i^*\prod_{\substack{j=1\\j\neq i}}^{N}\phi_j \ . \qquad (1.17)$$

In equation (1.17), ϕ_i^* indicates that the molecule i is in its lowest singlet excited state, and the remaining molecules are in their ground states, ϕ_j. So the kth one-exciton state wave function is then described by

$$\psi_k = \sum_{i=1}^{N} c_{ik}\varphi_i \ , \qquad (1.18)$$

i.e., each one-exciton state is linear combination of the N singly excited states. The corresponding energies ε_k can be found by using Schrödinger equation as;

$$\varepsilon_k c_{ik} = E_i c_{ik} + \sum_{j}^{N} c_{jk} V_{ij} \qquad (1.19)$$

where, $|c_{ik}|^2$ determines the probability that the ith molecule is excited, E_i's are the individual transition energies (site energies) of each molecule and V_{ij} is the interaction between the molecules . These eigenfunctions and the corresponding eigenenergies are obtained by diagonalizing the Hamiltonian matrix, H, given by equation (1.22) as described below.

Suppose each molecule has a dipole allowed transition (a singly excited state) in the spectral region of interest. The dipolar interaction between a pair of molecules in the point dipole approximation is given by

$$V_{ij} = 5.04 \frac{\mu_i \cdot \mu_j \cdot \kappa_{ij}}{r_{ij}^3 \cdot n} (cm^{-1})$$ (1.20)

where μ_i is the effective magnitude of the dipole moment vector of the ith molecule (in debye); r_{ij} is the center-to-center distance from the ith molecule to the jth molecule (in nm); n is the refractive index medium and equal to $\sqrt{\varepsilon}$ and κ_{ij} depends on the orientations of the transition dipole moments and is given by

$$\kappa_{ij} = \hat{\mu}_i \cdot \hat{\mu}_j - 3(\hat{\mu}_i \cdot \hat{r}_{ij})(\hat{\mu}_j \cdot \hat{r}_{ij}).$$ (1.21)

Here, $\hat{\mu}_i$ is the unit vector in the direction of the transition dipole moment of the ith molecule. $\hat{r}_{ij}$ is the unit vector along the line connecting the 'centers' of these molecules.

In the basis of N singly excited states ($i=1,…,N$), the electronic structure of a system can be described by its Hamiltonian, H, which for interacting pigments can be formulated by using Dirac notation (e.g., $|i\rangle \equiv \varphi_i$) as follows ;

$$H = \sum_{j=1}^{N} E_j |j\rangle\langle j| + \sum_{\substack{i,j=1 \\ i \neq j}}^{N} V_{ij} (|j\rangle\langle i| + |i\rangle\langle j|)$$ (1.22)

where the matrix elements of the H of the system are;

$$\langle i|H|j\rangle = V_{ij} , i \neq j$$

$$\langle i|H|j\rangle = E_i , i = j$$

where E_i's are the site energies of each molecule and V_{ij} is defined in equation (1.20).

If one lets Z and Λ be respectively, the eigenvector and the eigenvalue matrices of H satisfying the eigenvalue problem H·Z= Λ·Z. Each column of Z (an N×N matrix) corresponds to the eigenstate vector of a one-exciton state and the off-diagonal elements of Λ (an N×N matrix) are zero and the diagonal elements are the energies of the one-exciton states.

1.4.3 Excitonic Stick Spectra in the Point-Dipole Approximation

In this section, we describe how to calculate excitonic stick-spectra of absorption (ABS), linear dichroism (LD) and circular (CD), by using the formalism of one-exciton states. One can refer to references [25] and [27] for an extensive account of this formalism.

The ABS, the LD (difference between absorption parallel and perpendicular to a macroscopically defined axis) and the excitonic CD strengths (the difference in the absorption of the system exposed alternately to left and right circularly polarized light) corresponding to the kth one-exciton transition (k=1,…,N) are defined as;

$$ABS_k = \left|\vec{\mu}_k\right|^2 = \sum_{i,j=1}^{N} \mu_i \mu_j (\hat{\mu}_i \cdot \hat{\mu}_j) Z_{ik} Z_{jk} \qquad (1.23)$$

$$LD_k = ABS_{k,\parallel} - ABS_{k,\perp} \qquad (1.24)$$

where,

$$ABS_{k,\parallel} = \left|\vec{\mu}_{k,\parallel}\right|^2 = \sum_{i,j=1}^{N} \mu_i \mu_j (\hat{\mu}_i \cdot \hat{d})(\hat{\mu}_j \cdot \hat{d}) Z_{ik} Z_{jk} \qquad (1.25)$$

$$ABS_{k,\perp} = \left|\vec{\mu}_{k,\perp}\right|^2 = \sum_{i,j=1}^{N} \mu_i \mu_j \left[\hat{\mu}_i \cdot \hat{\mu}_j - (\hat{\mu}_i \cdot \hat{d})(\hat{\mu}_j \cdot \hat{d})\right] Z_{ik} Z_{jk} \qquad (1.26)$$

which satisfy

$$3ABS_k = ABS_{k,\parallel} + 2ABS_{k,\perp}$$

and

$$CD_k = R_k = 1.7 \times 10^{-9} \sum_{i,j=1}^{N} v_i \mu_i \mu_j r_{ij} [\hat{r}_{ij} \cdot (\hat{\mu}_i \times \hat{\mu}_j)] Z_{ik} Z_{jk} \qquad (1.27)$$

In (1.25) - (1.27), $\vec{\mu}_k$ is the dipole moment (in debye) of the kth one-exciton transition, Z_{ik} is the ith element of the eigenstate vector corresponding to the kth one-exciton transition; v_i is the site energy (in cm^{-1}) of the ith molecule; $\hat{d}$ is the unit vector in the direction of a macroscopically defined alignment axis; conserved excitonic CD is expressed in rotational strength R_k (in Debye-Bohr magnetons) of the kth excitonic transition, and $\vec{\mu}_{k,\parallel}$ and $\vec{\mu}_{k,\perp}$ are the components of $\vec{\mu}_k$ respectively parallel and perpendicular to $\hat{d}$.

The spectrum obtained by plotting the one-exciton energies (the diagonal elements of Λ) versus the intensities found using the equation (1.25),(or (1.26) and (1.27)) is termed as the 'excitonic stick spectrum'.

1.5 Broadening Mechanisms

The stick spectra described above has infinitely sharp transitions. However, in reality, transitions are not infinitely sharp, for example, due to the vibrations of the pigments and the coupling between the environment and the excitonic transitions (exciton-phonon coupling). Different broadening mechanisms, inhomogeneous, homogeneous and lifetime broadenings that are used to convolute the excitonic transitions in this thesis will be introduced below.

1.5.1 Inhomogeneous Broadening

It is very likely that there always exists some static disorder in the system that an additional averaging over the different possible quantities such as the site

energies, vibrational frequencies, dipole moments etc. is necessary. Every molecule feels a somewhat different protein environment and as a result molecular properties may differ from molecule to molecule. This particular situation may lead to absorption band broadening in the linear optical spectroscopy of the respective transition. Since this broadening is caused by different values of the transition frequency found for different molecules located at different points in the probed sample, it is called inhomogeneous broadening, and the distribution of the site energies per molecule is referred to as the inhomogeneous distribution function (IDF). At low temperatures proteins can be frozen in a particular conformation and macroscopic measurements are performed for an ensemble of many different substates, generally leading to a Gaussian distribution of the site energies. Therefore IDF is generally taken to be a Gaussian with a certain width at half maximum (fwhm). In the simulations, Monte Carlo approach [25, 28] is usually used to account the inhomogeneous broadening. For every Monte Carlo iteration, the site energy of each of the pigment molecule of LHC's is randomly taken from its own Gaussian distribution function independently from the site energies of the other molecules.

An alternative method for accounting the inhomogeneous broadening is the Gaussian synthesis method. The basic idea is to assign a single symmetric Gaussian line shape to each excitonic transition by keeping the integrated area under each Gaussian equal to the intensity of the transition. The intensity of the dressed one-exciton transition as a fuction of wavelength (λ) is given by;

$$\varepsilon_k(\lambda) = \varepsilon_{pk} \exp\left[-4\ln 2(\lambda - \lambda_k)^2 / W_{\lambda k}^2\right] \qquad (1.28)$$

where,

$$\varepsilon_{pk} = \left[(\ln 2)/\pi\right]^{1/2} (2I_k \lambda_k) / W_{\lambda k}$$

in which I_k corresponds to one of the ABS_k, LD_k or CD_k depending on which spectrum is to be constructed, λ_k is the peak position (in nm) of the kth one-exciton transition and $W_{\lambda k}$ is the full-width at half-maximum (band width, nm) of the kth

one-exciton transition. The simulated spectrum is the sum of the Gaussian dressed intensities.

1.5.2 Homogeneous Broadening

If the modulation of molecular properties by the environment is fast with respect to the time of the measurement, there exists dynamical disorder. It may result in the so-called homogeneous broadening, which can be rationalized in terms of dephasing rates, which have to be added to the transitions. Homogeneous broadening is accounted for in the simulations by convoluting each excitonic line with a homogenous lineshape. A homogeneous line generally consists of a zero-phonon line (ZPL) due to the pure transition and a phonon wing (PW) due to a simultaneous electronic and (protein) phonon or other low frequency transition (see Figure 1.11). The ZPL has generally a Lorentzian shape which has a width determined by the lifetime of the exciton state and the shape of the PW is a function of the phonon density of states and the coupling strength of the phonons to the electronic transition.

The homogeneous absorption spectrum $I(\omega)$ at 0 K can be written as

$$I(\omega) = \sum_{i=0}^{\infty} \frac{S^i \cdot e^{-S}}{i!} \cdot l_i(\omega) \tag{1.29}$$

where i runs over the Franck-Condon progression of phonons and vibrations, l_0 is the ZPL and l_i is the convolution of l_{i-1} with the one-phonon-vibration profile $\phi(\nu)$. Here, S is the Huang- Rhys factor. The area of $\phi(\nu)$ is normalized to unity. The ZPL l_0 is assumed to be a Lorentzian with a width determined by the lifetime of the exciton state (see below).
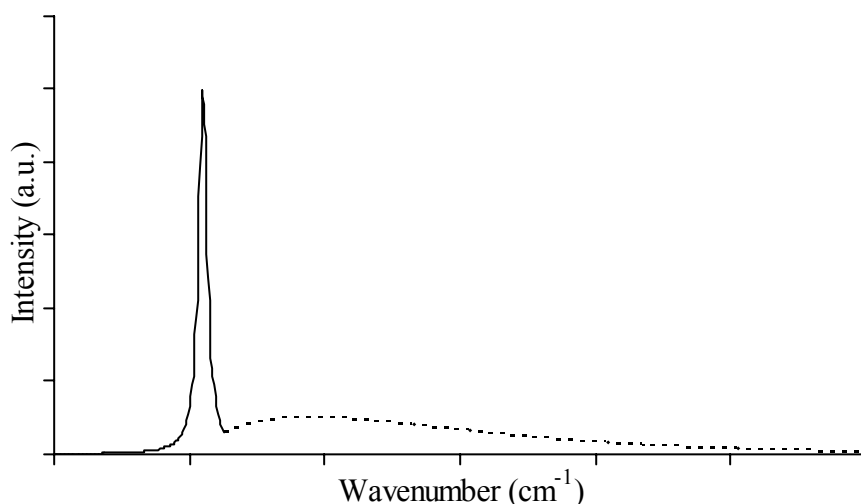
Figure 1.11. Homogeneous absorption spectrum. It consists of zero phonon line (ZPL) (solid line) and a phonon wing (PW) (dotted line).

1.5.3 Lifetime Broadening

The homogeneous lineshape broadened depending on the lifetime of each exciton state. At low temperatures the homogenous absorption band has a Lorentzian shape with linewidth of (fwhm, in cm^{-1}) $1/\pi Tc$. Here c is the speed of light (in cm s^{-1}) and T is the lifetime of the excited state.

When the broadening of absorption band is larger than the intermolecular coupling strength, the Förster mechanism is adequate to describe the rate of energy transfer between a pair of molecules (donor and acceptor). On the other hand, when the coupling strength is of similar magnitude or stronger than the amount of broadening the excitations are not localized on the individual molecules. One then describes the dynamics by the rates of transitions between the excitonic states.

In the later, the transitions between the excitonic states are visualized as the phonon-assisted (environmental) relaxations. For the case of weak and linear exciton-phonon coupling there exist several studies in which the relaxation rates are formulated [25, 29]. In the formalism by Leegwater et al. [29], $\Gamma_{JJ,KK}$: the

28

population transfer rate from the Jth exciton state to the Kth exciton state is given by;

$$\Gamma_{JJ,KK} = 2\delta_{J,K}\sum_{m,L}\gamma(\omega_K - \omega_L)\left|c_{Jm}\right|^2\left|c_{Km}\right|^2 - 2\sum_{m}\gamma(\omega_K - \omega_J)\left|c_{Jm}\right|^2\left|c_{Km}\right|^2 \qquad (1.30)$$

where δ is the Kronecker delta and c_{Jm} is the mth component of the eigenvector for the Jth exciton state, i.e., $\left|c_{Jm}\right|^2$ stands for the probability density of excitations on molecule m in the Jth exciton state. $\gamma(\omega)$ is the spectral density describing the frequency dependent coupling of the electronic states of the complex to their environment. The lifetime of the exciton state J is then equal to $T_J = 1/\Gamma_{JJ}$ where $\Gamma_{JJ} = \sum_K \Gamma_{JJ,KK}$, and the Lorentzian ZPL of that exciton state will have a fwhm given by $1/\pi T_J c$. The PW will also become broader as a result of using a lifetime-broadened ZPL in equation (1.29).

1.6 Förster Energy Transfer

If the intermolecular interactions are weak enough to consider the excitations essentially localized on the individual molecules, the energy transfer process between a pair of molecules can be described by the Förster expression [30, 31].

Upon absorption of a photon the donor molecule is promoted to the excited state, and the dipole-dipole interaction between the donor molecule and a neighboring acceptor molecule that is in the ground state leads to a transition where the donor is de-excited and the acceptor is excited (see Figure 1.12). This type of energy transfer is referred to as the hopping or the incoherent energy transfer and has been quantified by Förster [30, 31]. On close proximity of polarizable molecule (e.g. unexcited accepter molecule) with a molecule having a dipole (e.g. excited donor molecule), the electric field from the dipole of the excited molecule induce a dipole in the unexcited molecule, which results in the dipole-dipole interaction between the two molecules.
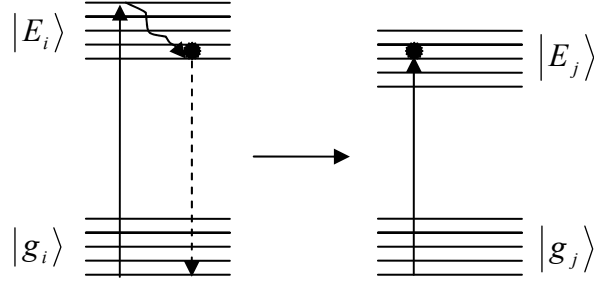
Figure 1.12. A schematic representation of the Förster excitation energy transfer between a pair of donor-acceptor molecules. $|g_i\rangle(|E_i\rangle)$ is the ground(excited) state of ith molecule.

The physics underlying the Förster energy transfer expression can be quantum mechanically expressed by the Fermi's Golden Rule. For a donor-acceptor pair in which each molecule has a dipole-allowed transition, the probability for energy transfer is given by

$$F_{ij} = \frac{2\pi}{\hbar} \left| \langle i^* j | V_{ij} | ij^* \rangle \right|^2 \rho(E) \tag{1.31}$$

where V_{ij} is the dipole-dipole interaction between the two molecules given by equation (1.20), $|i^* j\rangle (|ij^*\rangle)$ is the initial (final) state with i (j) excited and j (i) in the ground state , $\rho(E)$ is the density of states at $E_i \approx E_j$.

Förster has shown that the rate of energy transfer is proportional to overlap integral between the emission spectrum of the donor molecule and absorption spectrum of the acceptor molecule, given that the intramolecular vibrational relaxation time is shorter than the intermolecular transfer time.

The Förster rate of energy transfer [30, 31] is given by

$$F_{ij} = C_{ij} \kappa_{ij}^2 r_{ij}^{-6} n^{-4} . \tag{1.32}$$

Here, C_{ij} is the overlap integral between the donor's emission (J_i) and the acceptor's absorption (ε_j) spectra and is proportional to

$$\int_0^\infty J_i(v)\varepsilon_j(v)v^{-4}dv \qquad (1.33)$$

where v is the frequency. All the other quantities in equation (1.32) are defined in section 1.4.2 (see equation (1.20)).

The C_{ij} coefficients for the pairwise transfers are estimated by using the method suggested originally by Shipman et al. [32] and later modified by Jean et al. [33]. This is an analytic method, which approximates the absorption and emission spectra as symmetric Gaussians.

Each symmetric Gaussian spectrum is defined by a width (σ), a peak wavelength (λ), and a transition dipole strength (μ). If the spectra are narrow enough, so that v can be taken out of the integration, an analytical expression for the C_{ij} coefficients can be offered [32]. For a donor-acceptor pair whose emission and absorption maxima are separated by Δ_{ij};

$$C_{ij} = \mu_i^2 . \mu_j^2 . I_{ij}$$

where,

$$I_{ij} = \text{constant} \ \frac{1}{\sqrt{2\pi(\sigma_j^2 + \sigma_i^2)}} . \exp[\frac{-\Delta_{ij}^2}{2(\sigma_j^2 + \sigma_i^2)}] \qquad (1.34)$$

in which the constant in front is 29.99 Debye^{-4}ps^{-1}nm^{-6}cm^{-1}.

1.7 The Overall Purpose and Outline

Photosynthetic organisms contain light-harvesting pigment-protein complexes that absorb light and transfer energy efficiently to the reaction centers to initiate the photochemistry of photosynthesis. The key to the efficiency of light-

harvesting processes is the ultrafast energy transfers in the LHCs of green plants, bacteria and algae which are mainly governed by pigment-pigment and pigment-protein interactions. For a comprehensive understanding of the ultrafast energy transfer processes, it is essential to relate the structure of these complexes to both the steady-state and time-resolved spectra [34].

The purpose of thesis has been to investigate the structure-function relationship of several photosynthetic light-harvesting complexes in the frame of the exciton theory and the Förster transfer mechanism. Our approach was based on the fact that the connection between any two of the structure, the spectroscopy and the electronic excited state (EES) model of a particular LHC which could give considerable information about the missing one of the relevant LHC. By combining the spectral information with the EES model, we have obtained the structural information of the two complexes CP29 and LHCII of green plants as we discuss in Chapters 2 and 3, respectively. In Chapter 4, the refinement of the suggested EES model by using the detailed structural and spectroscopic information on the FMO complex of *Cb. tepidum* is discussed. A summary of our results and observations on the investigated complexes is finally given in Chapter 5.

CHAPTER 2

ELECTRONIC EXCITED STATES AND ENERGY TRANSFER KINETICS OF THE CP29 ANTENNA COMPLEX OF GREEN PLANTS

2.1 Introduction

In photosystem II of green plants, the reaction center is surrounded by several chlorophyll-binding proteins, that efficiently absorb and transport the solar energy. The chlorophyll-binding proteins associated with PSII consist of two parts: an outer antenna binding Chl a, Chl b, (called as Lhcb proteins) and carotenoids and an inner antenna binding Chl a and carotenoids. Considerable information about the Lhcb proteins of PSII can been obtained from elucidation of the major

antenna complex, LHCII, structure to a resolution of 3.4 $\overset{\circ}{A}$ by Kühlbrandt and co-workers [14]. Since, all the Lhcb proteins are highly homologous and are therefore believed to share a protein folding similar to that of the LHCII. The LHCII pigments identified per monomeric subunit of the current model are 12 Chl molecules surrounding 2 central carotenoid (Car) molecules (see Figure 1.5). The minor Lhcb proteins bind a fewer number of Chls with varying pigment-binding stochiometries. The Lhcb protein of interest in this chapter is CP29. CP29 binds 2 Chl b, 6 Chl a and 2 Car molecules [16] (see Figures 1.7). We refer to Chapter 1 for further structural information about LHCII and CP29.

The Lhcb proteins are spectroscopically complex objects, exhibiting considerably heterogeneous spectra in the spectral range of 630-685 nm (Q_y band) and many spectral forms are commonly observed in all the Lhcb proteins in this absorption region. The number of spectral bands decomposed in the Q_y band

almost matches the number of bound Chls in all these complexes [35]. Owing to a fewer number of Chls, the minor antennae show a lower degree of complexity and their spectral data may prove more easily interpretable than that of LHCII. In particular, the spectral bands resolved in the Chl a absorption region of the LHCII and CP29 proteins are essentially identical, suggesting an identical organization for the Chls a common to both complexes [15, 35, 36]. In addition, the energy equilibration in CP29 is observed to be very similar to part of the energy equilibration in LHCII both in terms of temporal and spectral characteristics [17]. It is therefore expected that a better interpretation of the light-harvesting process in the major plant antenna, LHCII, which is studied in the next chapter, can be obtained by understanding a less complicated Lhcb protein like CP29.

The LHCII model available does not allow a direct access to several parameters that are essential for understanding of the light-harvesting function. At the current resolution, the Chls could only be modeled as naked tetrapyrrole rings. Therefore the model does not provide any distinction between the Chls a and the Chls b (the identity problem) and no distinction could be made between the molecular x and y axes of the Chl molecules (the orientation problem). However, most of the chlorophyll-binding sites in LHCII are disclosed by the structural model, which led to the identification of the probable binding sites in highly homologous CP29 [16, 37]. Site-directed mutagenesis of chlorophyll binding residues has allowed construction of several mutant proteins lacking individual Chl molecules. Biochemical and spectral characterization of these mutants have recently been used for determination of the Chl identities in CP29 [16].

Determination of the Chl identities is a major step in correlating the spectra with the structure. But the orientation problem is still an open question to be answered. In this work we have looked for an answer to this question through modeling of the steady-state spectra using exciton calculations [27].

Recently, an electronic excited state structure for CP29 (orientation of the transition dipole moments and transition energies) has been suggested [38] by assuming a structure common with the relevant part of the LHCII. This model of

Simonetto and co-workers has been based on the interpretation that the pigment-protein interactions determine the spectral heterogeneity in the absorption region from 630 nm to 685 nm and, the effects of pigment-pigment interactions have been totally neglected. In this interpretation differential spectroscopy of mutant proteins missing single Chls have been used for the reconstruction of the absorption (ABS) and the linear dichroism (LD) spectra of CP29 under the observation that difference spectra can be fitted to one major and one or two minor Gaussians. However, a good fit to the LD spectra could only be obtained under a rather unconventional choice of the monomeric Chl transition dipole moment directions.

In this work we have re-addressed the orientation problem. We have provided simultaneous simulations that can explain the key features of the low temperature ABS and LD spectra in the same spectral range. We have discussed that a spectral decomposition including both pigment-pigment and pigment-protein interactions, yet yielding a spectral decomposition very similar to that reported by Simonetto et al. [38] is feasible with a more conventional definition of the individual transition dipole moment directions. We have also discussed that the model we have proposed can explain the observed features of the equilibration of energy in CP29 [17] on the basis of our preliminary energy transfer rate estimates.

2.2 Materials and Methods

Coulomb interaction between pairs of Chls is assumed to be the relevant physical mechanism and the interactions between the Chls are treated in the point dipole approximation. As we have discussed in Chapter 1, the point-dipole approximation is reasonable for pairwise separations greater than 15 $\overset{\circ}{\text{A}}$ and deviations are significant (25-30%) at separations around 9-9.5 $\overset{\circ}{\text{A}}$ of the BChl molecules in the LH2 complex of *Rhodopseudomonas acidophila* [24]. Calculations with the same degree of accuracy are not available for determining the extent of deviations from the point-dipole approximation in CP29 as well as in several other photosynthetic antenna in which the major interactions originate from

several Chl/Bchl pairs with pairwise separations of 12-15 $\overset{\circ}{\mathrm{A}}$. The recent models using the point-dipole approximation have yielded very satisfactory results in simultaneous simulations of several steady-state spectra of one such complex, the FMO complex [39-41]. The success in FMO has usually been taken as a good support for using point-dipoles as a good approximation down to distances 11-12 $\overset{\circ}{\mathrm{A}}$. In CP29 a word of caution is necessary for two of the pairs b3-a3 and b5-a5 (both around 9 $\overset{\circ}{\mathrm{A}}$) for which the interaction strengths are most likely to be subjected deviations, all the other Chl pairs are separated by distances greater than 12 $\overset{\circ}{\mathrm{A}}$.

Pigment-protein interactions, as in [38], are only described through a wavelength shift of the Chl site energies (the transition energies in the protein environment in the absence of pigment-pigment interactions).

The ABS and LD spectra are simulated using the exciton formalism [27] as we have described in Chapter 1 and elsewhere in detail [42].

The information needed to simulate the experimental spectra at the level of approximation we have used involves:

- Identities of the Chl molecules as a and b

- Distances between the Chl molecules

- Effective absorption strengths of the Chls in the protein environment corresponding to the Q band (0-0) transitions

- Orientations of the individual Q_y (Q_x) transition dipole moments for the Chl a and Chl b molecules

- Site energies of the Chl molecules

The relevant part of the LHCII structural model as suggested earlier [38] via homology between the two complexes is used for the organization of the Chls in

CP29 (see Figure 1.5). The atomic coordinates of the tetrapyrrole rings of the LHCII complex are used to determine the distances between the Chls and the orientation of the planes in which the transition dipole moments are assumed to lie.

The Chl identities determined recently by Bassi et al. [16] are used: a1, a2, a4, and a5 are pure Chl a sites and the Chl a binding affinities of the four mixed sites are respectively, 70% (A3), 60% (B5), 30% (B3) and 40% (B6). Note that we use A/B for the binding sites and indicate the identities with a/b.

The effective absorption strength corresponding to the Q_y (0-0) transitions of each Chl a is taken as μ_a^2=21 debye^2, following the recent determination by Kleima et al. [43] for monomeric Chl a in the protein environment of *Amphidinium carterae* and that of each Chl b is taken as μ_b^2=14 debye^2 by keeping μ_b^2/μ_a^2=0.7 [44]. This effective value is estimated to correspond to a refractive index of 1.6± 0.1 [43].

The Q_x transitions and assumed to carry 10% of the Q_y absorption strength and have been assigned around 620 nm (for Chl a) and around 595 nm (for Chl b). We have determined the remaining parameters (the site energies in the Q_y and the orientations) through a simultaneous simulation the key features of the ABS and LD spectra.

The nomenclature of Gülen et al. [45] for the two possible directions of the molecular y axis, i.e., 0 (along the N_A-N_C axis) and 1 (along the N_B-N_D axis) is maintained. Here the subscripts refer to the convention of the LHCII structure file provided by Prof. Dr. Werner Kühlbrandt.

The Q_y transition dipole moment direction of each Chl is shown in Figure 2.1 and the direction for each Chl is selected as described below (see section 2.3). The selection is basically guided by the previous results of Gülen et al. [45, 46] and Gradinaru et al. [47]. The Q_x transitions are taken perpendicular to the Q_y transitions. The sense of the rotations, "+ /-", defined as the c.w./c.c.w. rotations of the vectors from N_D to N_B and from N_A to N_C.

Each excitonic transition in the Q_y region is dressed by a symmetric Gaussian of bandwidth 9 nm and the bandwidths for the Q_x transitions are taken to be 28 nm.

Table 2.1. Probability of occurrence of the 16 configurations in CP29.

Configuration	A3	B5	B3	B6	Probability
1	a	a	a	a	0.0504
2	a	a	a	b	0.0756
3	a	a	b	a	0.1176
4	a	b	a	a	0.0336
5	b	a	a	a	0.0216
6	a	a	b	b	0.1764
7	a	b	b	a	0.0784
8	a	b	a	b	0.0504
9	b	a	a	b	0.0324
10	b	a	b	a	0.0504
11	b	b	a	a	0.0144
12	b	b	b	a	0.0336
13	b	b	a	b	0.0216
14	b	a	b	b	0.0756
15	a	b	b	b	0.1176
16	b	b	b	b	0.0504

The LD analysis is performed in the same convention as Simonetto et al. [38]. The pseudo 2-fold internal symmetry axis of the LHCII monomers is defined as a normal to "the molecular plane" which is the plane in which the membrane presumably lies (see Figure 1.5). It has been assumed that the macroscopic alignment axis of the LD measurements is parallel to the molecular plane and

$LD = A_{||} - A_{\perp}$ where $A_{||(\perp)}$ is the absorption parallel (perpendicular) to the macroscopic alignment axis.

Due to presence of 4 mixed sites there are 16 different configurations for the 8 Chls of the CP29 complex. These configurations are listed in Table 2.1 with their respective probabilities of occurrence determined by the Chl a/b binding affinities of the mixed sites. The spectra of CP29 are simulated as weighted sums of the Gaussian dressed spectrum of each of the 16 configurations given in Table 2.1. The experimental spectra are taken from [37].

2.3 Results and Discussion

The need for including the Chl-Chl interactions is already apparent in view of the emerging picture of the energy transfer pattern in the CP29 complex. Gradinaru and co-workers [47] have followed the suggestion of Prof. Robert S. Knox [48], and voiced that the energy transfer in CP29 has a compartmental nature: energy equilibrates very fast (on subpico- to pico-second scale) in the compartments consisting of a few Chl molecules, and a less rapid equilibration ($\geq$ 10 ps) takes place between the compartments. Recent results of Simonetto et al. [38] also support this description. The details of the energy transfer pathways are somewhat different in these two models: in part due to different assumptions on the extent of Chl-Chl interactions and in part owing to the differences in the assignments of the molecular y-axis for some of the Chls, and also in the orientations of the Q_y transition dipole moment directions in the tetrapyrrole plane. What is clear however is that there are several pairs/groups of Chls (e.g., a1-a2, a4-a5-(B5) and A3-B3) which always equilibrate on subpico- to a few pico-seconds scale. In fact, the LHCII model forces the rapid energy transfers between three of the pairs (i.e., a1-a2, a4-a5 and A3-B3) irrespective of their identities and orientations.

The strong pairwise interactions causing ultrafast transfers from Chls b to Chls a are not expected to cause delocalization of excitation due to large energetic

separation. However, delocalization effects especially for the pairs/groups of Chls a (or Chls b) belonging to the same compartment are to be expected, and this has set the point of departure of this work.

We have assigned the direction of the Q_y transition dipole moment of each Chl a molecule along the molecular y axis (i.e., 0 or 1). We have based this assignment on a number of studies in which either monomeric or a pair of very weakly interacting Chl a molecules in a very well-defined geometry are analyzed. In all these analyses the Q_y transition dipole moment of Chl a is found to be almost (within about 5^0) along the molecular y axis. In the recent model of Simonetto et al. [38], it has been concluded that unless there is a $20^0 (30^0)$ deviation from the molecular y axis for the Chl a (b) transition dipole moments, the LD of CP29 could not be explained in the absence of Chl-Chl interactions.

In angle-resolved fluorescence depolarization experiments on monomeric Chl a oriented in anhydrous nitrocellulose films the Q_y transition dipole moment for absorption is found to be along the molecular y-axis [49].

In the monomeric unit of PCP (Peridinin-Chlorophyll a-Protein) from *Amphidinium carterae* [50]-a very weakly interacting pair of Chl a molecules (interaction strength less than 10 cm^{-1}) in a very well-defined geometry ($2 \overset{\circ}{A}$ resolution)-the Chl a dipole moment corresponding to the Q_y absorption is concluded to lie very close to the molecular y-axis [43].

A similar result has also been reported in a dimer of zinc chlorophyllide, embedded in the heme pockets of hemoglobin [51].

In addition, it has recently been possible to explain the key features of several steady-state spectra of the FMO protein by assigning the Q_y transition dipole direction of each of the seven Bchl a molecules along the molecular y-axis [39-41].

We are not aware of any study of the kind in which a very well defined geometry is used for the determination of the transition dipole moment direction of

the Chl b molecule. In the literature there are reports suggesting a 10^0 difference between the Q_y dipole moment directions of the Chl a and the Chl b molecules [e.g., 52 and the references therein].

We have based the selection of the Q_y transition dipole moment orientations (0 or 1) of each of the Chls on the assignments reported in a series of work by Gülen et al. [45, 46] and by Gradinaru et al. [47]. In [45-47] the most probable orientations have been suggested upon performing a quite extensive search in a large space of possible combinations of individual dipole moment orientations. The combinations that can comply with the global features of both the steady-state and the temporal and spectral behavior of kinetic observations have been selected using a set of relatively mild restrictions. The LD features in both Chl a and Chl b regions and the CD characteristics in Chl a region were evaluated in the presence of Chl-Chl interactions and the excited state kinetics were evaluated on the basis of Förster transfer.

Although the search procedure mentioned above has been applied to CP29 prior to the full Chl identification, the model used has been very similar to the one suggested in the recent work of Bassi and co-workers [16]. The same eight Chl molecules identified by Bassi and co-workers have been included and the organization of these eight molecules was assumed to be identical to those binding to the same sites in LHCII. The identities of the molecules in the Chl a-binding core (a1, a2, a4, and a5) have been assigned correctly. The mixed identities of the sites A3, B3, B5, and B6 have not been taken into account. However, those binding mostly Chl b (B3 and B6) have been assigned as Chls b and similarly, those binding mostly Chl a (A3 and B5) have been assigned to be Chls a.

The selection process that is described above has used very mild selection criteria and therefore, did not yield an unambiguous solution for the orientations. It did however provide a very restricted set of possible orientational configurations. The most probable orientational assignments (judged mostly by the polarized absorption characteristics) have been: a1(0), a2(0 or 1), A3 (a, 0 or 1), a4(0), a5(0), B5(a, 0 or 1), B3(b, 1) and B6(b, 0) (see Figure 2.1). We note that none of these

orientational assignments contradicts the "individual" LD signs of the Chls suggested in [38] by using the difference spectra of CP29 versus mutants.
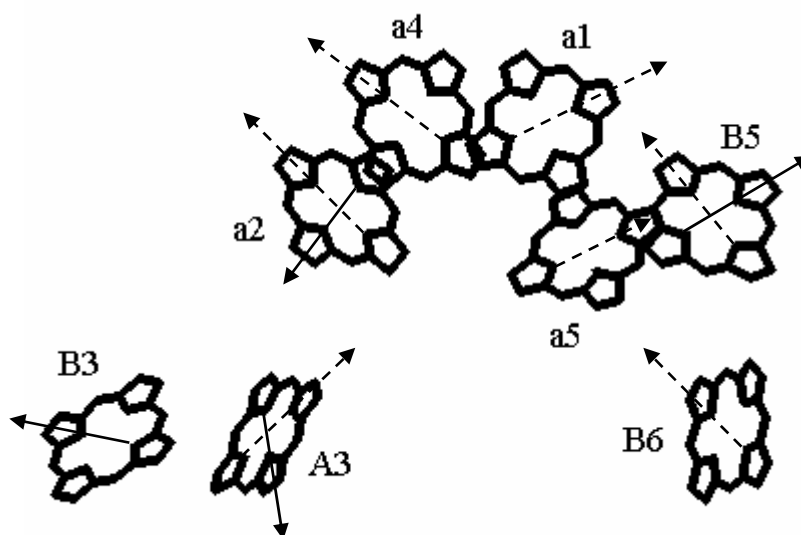
Figure 2.1. Model structure of CP29. The protein and the carotenoids are stripped off for clarity. a1, a2, a4, and a5 are pure Chl a sites and the Chl a binding affinities of the mixed sites are, 70%(A3), 60%(B5), 40%(B6), and 30%(B3). The diagonal arrows on the tetrapyrrole rings of the Chls indicate approximately the most probable Q_y transition orientation assignments directions (Y(1), solid arrow and X(0), dotted arrow) of each Chl molecule [45-47].

We have tested the orientations discussed above to determine the best solution, which can give a simultaneous explanation of all the prominent features of ABS and LD spectra. Although we have not provided any simultaneous fits, we shall discuss that this solution can also explain the key features of the CD spectrum and the excitation transfer kinetics.

Under the assumption that the mixed sites bind Chls a and b in the same geometry, the best solution we have found has the following parameters. The orientational assignments: a1(0), a2(1), A3(0), a4(0), a5(0), B5(1), B3(1), (see Figure 2.2) and B6(0), and the site energies (in nm): a1(670), a2(672), A3(a, 672),

a4(670), a5(670), B5(a, 670), B3(a, 669), B6(a, 670), A3(b, 637), B3(b, 635), B5(b, 644), and B6(b, 648).
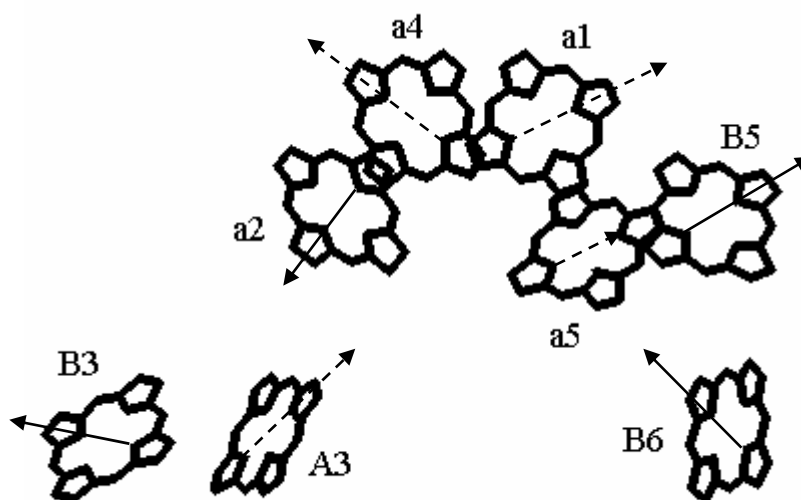
Figure 2.2. The Chl arrangement in CP29. The protein and the carotenoids are stripped off for clarity. The diagonal arrows on the tetrapyrrole rings of the Chls indicate approximately the directions (Y(1), solid arrow and X(0), dotted arrow) of the Q_y transition dipoles determined in this study.

To have a satisfactory fit of the Chl b region LD properties, it has been necessary to allow some deviation from the molecular y-axis for the dipole moments of the Chl b molecules. For A3(b), B5(b), and B6(b) rotations of around 5-10° was sufficient for fine-tuning the LD signal in the 645-660 nm range. The blue-most LD signal (peaking around 635 nm) is mainly associated with the B3(b) molecule, which has a very large positive monomeric LD. In the absence of Chl a Q_x band, which should also contribute to the blue tail of the Chl b absorption [44], the intensity of this signal could still match the experimental one if we allow a rotation of around 15-20° for the dipole moment of B3(b) in the molecular plane. The overall effect of the Chl a Q_x transitions is a predominantly negative LD signal, which helps to reduce the intensity of the 635 nm LD. When Q_x transitions are included, it was sufficient to rotate the dipole moment of B3 by 5-10° in the

molecular plane. (Further details of the rotations are explained in the caption of Figure 2.3).
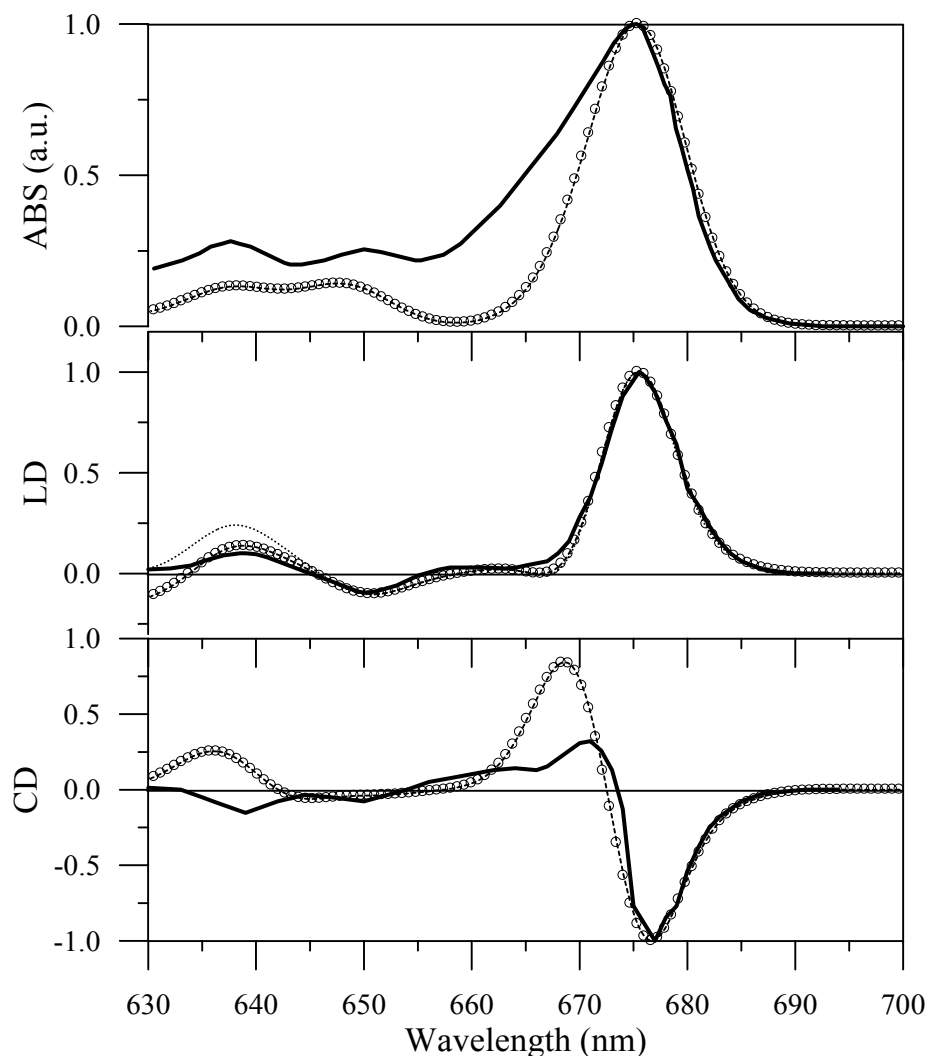
Figure 2.3. Experimental ABS, LD, and CD spectra versus simulations. Experimental data (ABS at 130 K, LD and CD at 77 K) are reproduced from [37] (solid lines). Open dots are the simulation results including Q_x bands. Dashed line in LD is the simulation with only the Q_y transitions. In all simulations the dipole moment directions of all the Chl a molecules are taken along the molecular y-axis, while those of the Chl b molecules deviate by: -10° (A3 and B5), by +10° (B3), by -5° (B6) from the y-axis in the tetrapyrrole plane of each molecule.

In Figure 2.3 the ABS and LD spectra of CP29 are presented for the solution given above and compared with the experimental data [37]. Each spectrum

given in Figure 2.3 is constructed as a weighted sum of the Gaussian dressed spectrum corresponding to the 16 configurations as listed in Table 2.2 with the weights given in Table 2.1. In Table 2.2 we detail the resolution given in Figure 2.3 by giving the transition wavelengths, the absorption intensities, and the delocalization characteristics for each of the 16 configurations making up the spectra. Each of the 16 configurations have a different excited state structure, the average over all configurations yield a composition which can be approximated by eight independent Gaussian subbands with midpoints and widths very similar to those presented in the model by Simonetto et al.[38].

The electronic excited state structure in the Chl a region ($\approx$665-685 nm) is mainly governed by the interactions within four pairs: a1-a2 ($\approx$-65 cm^{-1}), a4-a5 ($\approx$ 45 cm^{-1}), B5(a)-B6(a) ($\approx$45 cm^{-1}), B3(a)-A3(a) ($\approx$-155 cm^{-1}) and by the weaker cross-couplings between the first three of these dimers. Much stronger pairwise coupling of B3(a)-A3(a) prevents any mixing with the others, when unpaired these molecules also mix with the others.

Each Chl a in these dimers contributes both to the blue and the red spectral bands. The blue-most ($\approx$663 nm) and the red-most ($\approx$678 nm) bands originate from the A3(a)-B3(a) interaction. A3(a)-B3(a) pair is a dimer with about equal contributions of both molecules to the delocalized states. a1 and a2 molecules predominantly contribute to the spectra around 668 nm and around 675 nm. a4, a5, B5(a), and B6(a) are associated with the bands in the middle of the absorption ($\approx$670-674 nm). a1- a2 character is also observed in the middle bands due to cross-coupling with the a4-a5 pair. Similary, a4-a5 character is also observed in the blue bands. When unpaired the mixed sites A3 and B3 mainly merge into the bands in the middle as well.

Table 2.2. Transition energies, absorption strengths and delocalization characteristics of the 16 configurations. For each configuration, the first row gives the transition energy (nm), absorption strength (debye^2). The molecules contribution to each transition and their percentage contribution, in parenthesis, are given in the second row. The molecules are labeled as 1 (a1), 2 (a2), 3 (A3), 4 (a4), 5 (a5), 6 (B5), 7 (B3) and 8 (B6). The data for the Q_y band transitions are shown, but in the calculations the Chl a and b Q_x bands are also include.

Config. No.								
1	681.1, 34.4	677.5, 11.3	676.0, 48.0	674.4, 30.6	671.0, 10.5	670.9, 11.6	670.4, 3.2	666.2, 18.6
	3 (.59), 7 (.39)	2 (.47), 1 (.28)	6 (.31), 5 (.19)	8 (.51), 4 (.22)	4 (.54), 5 (.35)	1 (.64), 2 (.31)	6 (.45), 8 (.32)	7 (.59), 3 (.40)
2	681.1, 34.4	677.5, 11.3	675.8, 54.7	672.2, 11.2	671.0, 11.0	670.8, 7.4	666.2, 17.7	648.9, 14.2
	3 (.59), 7(.39)	2 (.48), 1 (.28)	4 (.27), 5 (.27)	6 (.66), 4 (.30)	1 (.32), 2 (.23)	5 (.35), 1 (.33)	7 (.59), 3 (.40)	8 (.99)
3	677.5, 11.4	676.4, 77.3	675.6, 3.3	674.4, 32.2	670.9, 11.9	670.8, 7.8	670.4, 2.8	637.9, 14.9
	2 (.47), 1(.28)	3 (.46), 5 (.17)	3 (.45), 6 (.19)	8 (.47), 4 (.26)	1 (.45), 2 (.26)	4 (.35), 5 (.22)	5 (.44), 8 (.30)	7 (.98)
4	681.1, 32.1	677.3, 16.6	674.9, 41.8	672.8, 17.4	671.0, 11.0	670.9, 11.2	666.2, 18.7	647.0, 12.9
	3 (.59), 7 (.39)	2 (.57), 1 (.32)	4 (.47), 5 (.39)	8 (.94)	4 (.44), 5 (.38)	1 (.62), 2 (.23)	7 (.59), 3 (.40)	6 (.99)
5	677.6, 15.3	676.1, 61.3	674.4, 33.3	672.8, 13.6	671.0, 10.3	670.1, 12.2	670.4, 2.2	639.8, 14.0
	2 (.50), 1 (.28)	6 (.32), 5 (.23)	8 (.53), 4(.20)	7 (.89)	4 (.52), 5 (.34)	1 (.62), 2 (.33)	6 (.45), 8 (.31)	3 (.97)
6	677.5, 11.3	676.4, 74.9	675.4, 14.1	672.2, 9.2	670.9, 12.0	670.7, 4.7	648.9, 14.2	637.9, 14.9
	2 (.48), 1 (.28)	3 (.53), 5 (.17)	3 (.41), 4 (.26)	6 (.68), 4(.27)	1 (.53), 2(.29)	5 (.48), 4 (.26)	8 (.99)	7 (.98)
7	677.4, 21.2	676.1, 37.7	674.8, 30.4	673.1, 19.1	670.9, 11.9	670.8, 6.9	647.0, 12.8	637.9, 14.9
	1 (.32), 2 (.59)	3 (.84)	4 (.49), 5 (.30)	8 (.94)	1 (.44), 2 (.25)	5 (.38), 4 (.28)	6 (.99)	7 (.98)
8	681.1, 31.7	677.3, 17.1	674.9, 37.6	671.0, 11.8	670.9, 10.9	666.2, 17.7	649.9, 19.6	646.3, 10.0
	3 (.59), 7 (.39)	2 (.58), 1 (.32)	4 (.48), 5 (.42)	4 (.41), 5 (.36)	1 (.56), 2 (.24)	7 (.59), 3 (.40)	8 (.76), 6 (.24)	6 (.76), 8 (.24)

Table 2.2. Continued.

9	677.6, 15.4	675.9, 70.3	672.8, 9.4	672.2, 14.4	670.9, 10.7	670.8, 7.9	648.9, 13.7	639.8, 14.1
	2 (.51), 1 (.29)	5 (.31), 4 (.26)	7 (.82)	6 (.63), 4 (.23)	5 (.32), 1 (.26)	1 (.45), 5 (.24)	8 (.99)	3 (.97)
10	677.5, 12.3	676.0, 57.4	674.4, 31.7	671.1, 11.6	670.9, 11.4	670.4, 2.8	643.3, 12.8	635.8, 15.4
	2 (.48), 1 (.28)	6 (.31), 5 (.21)	8 (.52), 4 (.21)	4 (.55), 5 (.33)	1 (.62), 2 (.30)	6 (.44), 8 (.31)	3 (.63), 7 (.37)	7 (.63), 3 (.37)
11	677.4, 25.0	675.0, 51.1	673.1, 19.2	672.8, 10.7	671.0, 11.1	670.9, 11.1	647.0, 13.7	639.8, 13.5
	2 (.59), 1 (.32)	4 (.44), 5 (.42)	8 (.93)	7 (.89)	4 (.46), 5 (.42)	1 (.61), 2 (.29)	6 (.99)	3 (.97)
12	677.4, 20.8	675.0, 46.6	673.1, 17.6	671.1, 11.4	670.9, 10.8	647.0, 14.4	643.2, 11.8	635.8, 15.3
	2 (.59), 1 (.32)	4 (.45), 5 (.41)	8 (.94)	4 (.46), 5 (.39)	1 (.58), 2 (.26)	6 (.99)	3 (.63), 7 (.37)	7 (.63), 3 (.37)
13	677.4, 24.1	674.9, 43.8	672.7, 14.5	671.0, 12.8	670.9, 10.6	649.9, 19.2	646.3, 9.8	639.9, 14.4
	2 (.59), 1 (.32)	4 (.47), 5 (.45)	7 (.92)	4 (.44), 5 (.40)	1 (.59), 2 (.28)	8 (.77), 6 (.23)	6 (.77), 8 (.23)	3 (.98)
14	677.5, 12.5	675.8, 65.1	672.2, 11.6	671.0, 10.0	670.8, 7.9	648.9, 14.2	643.3, 12.6	635.8, 15.5
	2 (.50), 1 (.29)	5 (.29), 4 (.26)	6 (.65), 4 (.32)	5 (.32), 4 (.26)	1 (.43), 5 (.25)	8 (.99)	3 (.63), 7 (.37)	7 (.63), 3 (.37)
15	677.4, 22.0	676.1, 36.8	674.8, 27.7	671.0, 11.7	670.8, 7.2	649.9, 19.4	646.3, 9.0	637.9, 14.9
	2 (.59), 1 (.32)	3 (.86), 5 (.11)	4 (.50), 5 (.33)	1 (.42), 2 (.24)	5 (.37), 4 (.27)	8 (.76), 6 (.24)	6 (.76), 8 (.24)	7 (.98)
16	677.4, 21.3	674.9, 41.7	671.1, 12.0	670.9, 10.5	649.9, 19.2	646.3, 11.1	643.2, 11.3	635.8, 15.4
	2 (.59), 1 (.32)	4 (.47), 5 (.44)	4 (.45), 5 (.39)	1 (.57), 5 (.26)	8 (.77), 6 (.23)	6 (.77), 8 (.23)	3 (.63), 7 (.37)	7 (.63), 3 (.37)

The blue side of the Chl b absorption (630-640 nm) is mainly attributed to the B3 and A3 molecules. B3(b)-A3(b) interaction ($\approx$-110 cm^{-1}) delocalizes the two transitions around (633.5 and 635.5 nm) into two transitions around 631.5 nm and 638 nm. The red side of the Chl b absorption is contributed by the B5 (644 nm) and B6 (648 nm) molecules. B5-B6 interaction is rather weak ($\approx$30 cm^{-1}) and the composition of the two red Chl b bands are about $\geq$ 90% monomeric.

Large energetic separation between Chls b and Chls a precludes any significant delocalization between these two spectral regions. Less than 2% mixing is observed in the most strongly coupled a-b pair, A3-B3.

We would like to note that we have only considered the 0-0 transitions and have not made any attempt to introduce vibrational transitions. The absorption offset observed in the Q_y region between 630 and 660 nm, which is also present in the ABS construction of Simonetto et al. [38], is mostly related to the neglect of vibrational tails in the Chl a absorption forms.

We have not attempted to fit the CD spectrum, but our model also produces the overall character of the CD spectra in the Chl a absorption region: the strongly biphasic signal, negative on the red and positive on the blue (see Figure 2.3). The non-conservative negative CD signal in the Chl b absorption region remains to be understood. It is a fact that in CP29, LHCII, CP26, and also in reconstituted complexes with varying Chl a/b ratios (see e.g., [53]) there exists a non-conservative negative CD signal in the Chl b band. Existence of a negative, non-excitonic CD signal in the Chl b region may offer a resolution.

Experimental measurements of transient absorption on CP29 upon selective excitation of the two Chl b subbands around 640 nm and 650 nm [17], have indicated that the blue Chls b (absorbing around 640 nm) transfer excitation to the red Chls a with a time constant of 350$\pm$100 fs, while the red Chls b (absorbing around 650 nm) transfer on a picosecond time scale (2.2$\pm$0.5 ps) towards a Chl a pool more on the blue. Furthermore, both fast (280$\pm$50 fs) and slow (10-15 ps) equilibration among the Chl a molecules have been observed. Moreover, it has

been concluded that these rates as well as their associated spectra are very similar to those observed in LHCII [47, 54, 55].

In view of the results we have presented above, it is necessary to evaluate the energy equilibration by taking the delocalized nature of the excited states into account and therefore it is not entirely proper to talk in terms of the Förster rates between the pairs of molecules. However to guide the rest of the discussion on energy equilibration and to connect with the previous models [47, 38] we have provided a block diagram in Figure 2.4. We have estimated the rate constants of this diagram using the Förster mechanism as we have described in Chapter 1 and elsewhere in detail [56, 47].

It was already evidenced by the previous studies that excitation delocalization will be important within the compartments. Our calculations show that the delocalization of excitation is not only limited to the compartments: there is considerable delocalization over the entire core region Chls a (a1, a2, a4, a5) and cross-couplings with the core also induce delocalization over the entire Chl a pool. Excitation equilibration among all these delocalized levels in the Chl a spectral region needs to be detailed. It is however clear that all the Chls a will be fully equilibrated since there are several bi-directional pathways between "the compartments" (see Figure 2.4). We avoid any strong comments on the time scales and on the spectral properties of the equilibration among the Chl a states on the basis of Förster rates given in Figure 2.4. Nevertheless, the time scales of the intra- ($\approx$500 fs-1 ps) and inter-compartmental ($\approx$5-10 ps) transfers correlate well with the experimentally observed equilibration rates.

B3(b)-A3(b) pair is highly delocalized and equilibrates very rapidly, but transfer of excitation from this Chl b pair to the Chl a pool is rather slow ($\approx$15 ps). The monomeric B3(b) and A3(b) molecules are responsible for the ultrafast de-excitation of the 640 nm band. Both molecules transfer to a pool of weakly coupled Chls a in which the leading contribution will be due to B3(b) to A3(a) and A3(b) to B3(a) transfers at a rate ($\approx$250-300 fs) consistent with the experiments. In the model of Simonetto et al. these two molecules are also responsible for the 640

nm band. But the orientational assignments of these two molecules are such that they become not only weakly coupled to the Chl a pool but also to each other. Therefore this assignment is unlikely to explain the ultrafast energy transfer out of the 640 nm band.

Our model attributes the slow de-excitation (2.2±0.5 ps) of the 650 nm band to B5(b) and B6(b) molecules. These molecules equilibrate with each other in several picoseconds and as a pair transfer to the Chl a pool via B5(b)-a5 coupling (≈5 ps), which is also the route of de-excitation for the monomeric B5(b). B6(b) transfers to the Chl a pool through its interaction with B5(a) (≈3.5 ps). B5 (b) transfers to a pool of strongly coupled Chls a, while B6 (b) transfers to a weakly coupled Chl a pool. In the model proposed by Simonetto et. al. B5(b) also de-excites through its coupling to the a4-a5 pair. However their orientational assignment (a4=1 and a5=1, B5=1) yields an extremely fast (<100 fs) de-excitation. Such a combination of orientations would also be inconsistent with the steady-state spectra, as it would yield an interaction strength greater than the spectral splitting observed experimentally. In [38] slow de-excitation of the 650 nm band is attributed only to the B6(b) molecule, which de-excitates through its interactions with the group of Chls a4-a5-B5.

Very recently the site-directed mutagenesis approach has also been applied to LHCII [15] and it has been reported that most of the sites present in both CP29 and LHCII induce similar absorption characteristics. Combination of this information with extensive spectroscopic data on LHCII and with the orientational assignments that we have proposed in this study can provide a better understanding of the structure-function relationship in both the LHCII (see Chapter 3) and the other minor LHCs of the PSII.

636 nm 0.25 b,
638 nm 0.53 b (B3)
640 nm 0.12 b (A3)
643 nm 0.18 b

670 – 671 nm 0.40 a
673 – 676 nm 1.30 a
677 nm 0.30 a

670 – 71 nm 0.05 a
673 – 75 nm 0.50 a
676 – 77 nm 0.45 a

0.2

A3 ↔ B3

0.5

A2 ↔ A1

B6

0.3

10

B3

666 nm 0.15 a
670 – 75 nm 0.10 a (B3)
670 – 75 nm 0.35 a (A3)
681 nm 0.30 a

0.1

10

1

B5

5

A3

5

A4 ↔ A5

1

3.5

3.5

670 – 71 nm 0.35 a
673 – 74 nm 0.30 a
675 – 76 nm 1.25 a
677 nm 0.10 a

5

B5

B6

2

646 nm 0.17b
647 nm 0.15 b (B5)
649 nm 0.35 b (B6)
650 nm 0.33 b

51
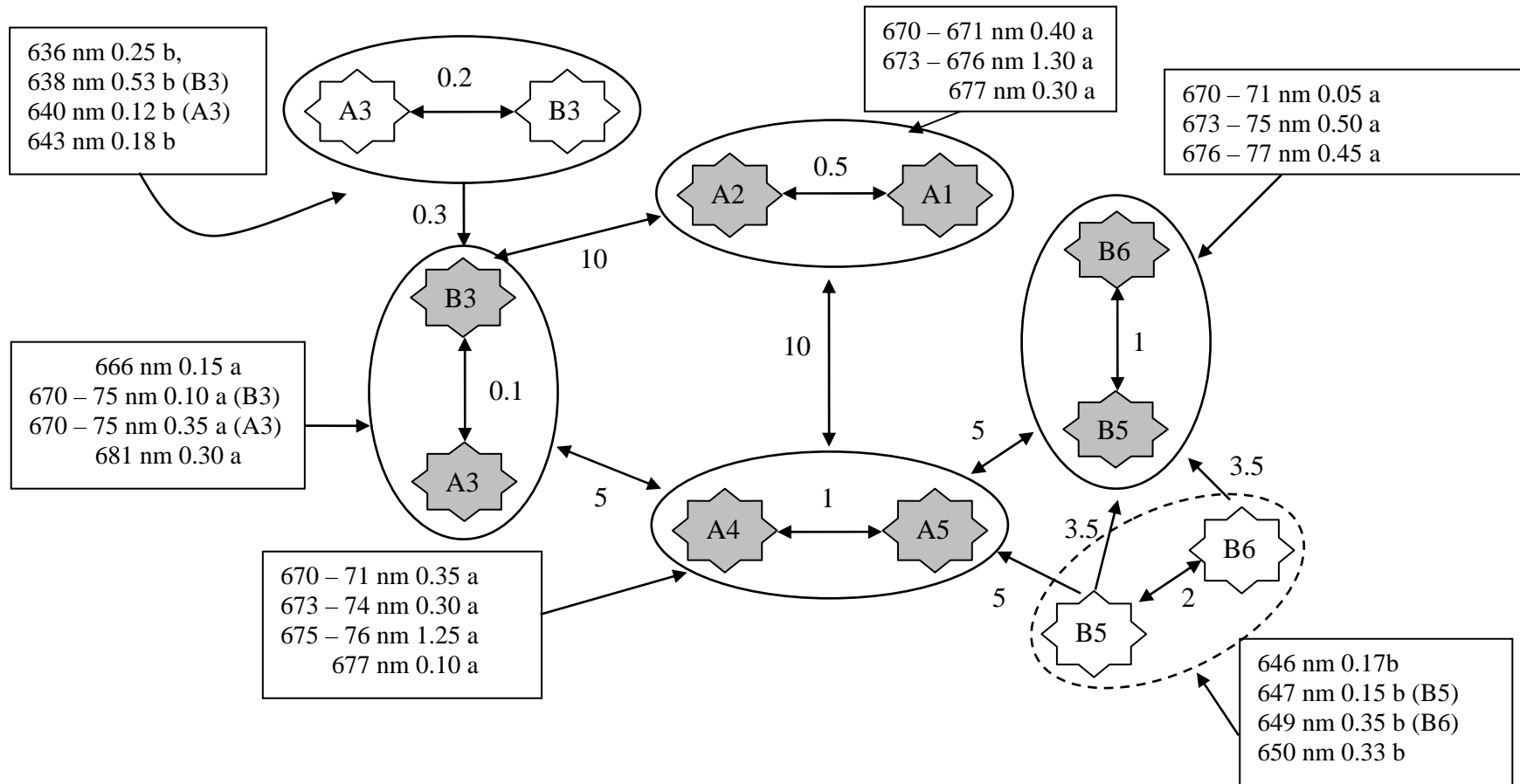
Figure 2.4. Block diagram representation of the excitation pathways in CP29 (in ps). Relative contributions of the Chls to the excitation energy transfers of particular states are also shown. Shaded symbols corresponds to the Chl a molecules.

CHAPTER 3

CHLOROPHYLL TRANSITION DIPOLE MOMENT ORIENTATIONS, EXCITED STATES AND PATHWAYS FOR FLOW OF EXCITATION ENERGY AMONG THE CHLOROPHYLLS OF THE MAJOR PLANT ANTENNA, LHCII

3.1 Introduction

In Chapter 2, we have suggested an electronic excited state structure for the CP29 complex [57] by assuming a structure common with the relevant part of the LHCII and using the Chl identities reported by the mutational analysis of Bassi et al. [16]. We have suggested the orientations of the Q_y transition dipole moments of all Chls of CP29 by a simultaneous simulation of the key features of the low-temperature absorption (ABS) and linear dichroism (LD) spectra [37]. We have also discussed that the model we proposed can explain the general character of the energy equilibration in CP29 [17] on the basis of our preliminary energy transfer rate estimates.

In this Chapter we have attempted to assign the orientations of all the LHCII chlorophylls using our recent orientational assignments for the CP29 Chls and most of the identities of the LHCII Chls recently reported [15]. We have evaluated a considerable part of the extensive spectroscopic data on the Chl excited states and Chl interactions in LHCII [47, 54, 55, 58-71] in the presence of both the Coulombic interactions between the Chls and the pigment-protein interactions. We have suggested an assignment, which satisfactorily reproduces the polarized linear absorption characteristics as well as the prominent spectral and temporal features of the energy transfer processes among the chlorophylls.

3.2 Materials and Methods

We used the same basic principles and assumptions as described in section 2.2. The LHCII structural model is used for the organization of the Chls in the LHCII (see Figure 1.5). The calculations are restricted to a monomeric unit of the C_3 symmetric LHCII trimer shown in Figure 1.5. The atomic coordinates of the tetrapyrrole rings of the LHCII complex are used to determine the distances between the Chls and the two possible directions of the molecular y-axis for each of the 12 Chls (see Figure 1.6).

Except for the identity of the molecule binding to site A7, the Chl identities recently determined by Remelli et al. [15] are used: a1, a2, a4, a5 and B1(a) are Chl a molecules; b2, b5, and b6 are Chl b molecules; and A3, B3, and A6 are mixed sites In this mutagenesis study, A7 is suggested to be a pure Chl b site. However, for reasons discussed below we have assigned this site also as a mixed one. We have assumed equal a and b binding probabilities for A7 for the sake of simplicity. Owing to presence of four mixed sites there are 16 different configurations for the 12 Chls of the LHCII complex. Since all the mixed sites have/are assumed to have equal (50%) Chl a and Chl b occupancies, all 16 configurations given in Table 3.1 have equal probability of occurrence (6.25%).

Again as in Chapter 2, the effective absorption strength corresponding to the Q_y (0-0) transitions of each Chl a is taken as $\mu_a^2 = 21$ debye^2, following the recent determination by Kleima et al. [43] for the monomeric Chl a in the protein environment of *Amphidinium carterae* [50]. The effective absorption strength for each Chl b is taken as $\mu_b^2 = 14$ debye^2 by keeping $\mu_b^2/\mu_a^2 = 0.7$ [44]. This effective value is estimated to correspond to a refractive index of 1.6±0.1 [43]. The remaining parameters (the site energies in the Q_y band and the direction of the molecular y-axis for each Chl) have been determined through a satisfactory simultaneous simulation of the key features of the ABS and LD spectra.

Table 3.1. The 16 LHCII configurations.

Configuration	A3	A6	A7	B3
1	a	a	A	a
2	a	a	B	a
3	a	b	a	a
4	a	b	b	a
5	b	a	a	a
6	b	a	b	a
7	b	b	a	a
8	b	b	b	a
9	a	a	a	b
10	a	a	b	b
11	a	b	a	b
12	a	b	b	b
13	b	a	a	b
14	b	a	b	b
15	b	b	a	b
16	b	b	b	b

The orientations of the Chl a1 (0), a2 (1), A3 (0), a4 (0), a5 (0), B3 (1), b5 (1), and b6 (0) in the nomenclature of Gülen et al. [44, 45], are fixed using our results on the CP29 chlorophylls (see Figure 2.2). The Q_y transition dipole moment direction of each Chl a molecule is assigned along the molecular y-axis (i.e. 1 or 0), while those of the Chl b molecules are rotated by ±5-10° from the molecular y-axis, which is the case in CP29 simulations.

The LD analysis is performed in the convention of Simonetto et al. [38], as in Chapter 2. The C_3 symmetry axis of the trimeric LHCII (or the pseudo-two-fold internal symmetry axis of the LHCII monomers) is defined as a normal to "the molecular plane", which is the plane in which the membrane presumably lies (see

Figure 1.5). It is assumed that the macroscopic alignment axis of the LD measurements is parallel to the molecular plane.

The spectra are simulated as weighted sums of the Gaussian dressed spectrum of each of the 16 configurations. Each excitonic transition in the Q_y region is dressed by a symmetric Gaussian of bandwidth 8 nm.

We have compared the simulations with the low-temperature ABS and LD data for the trimeric LHCII [62], in the absence of low-temperature spectra of the reconstituted monomeric LHCII. The ABS spectrum of the reconstituted monomeric LHCII at room temperature is almost identical to that of the native trimeric LHCII [15]. Although there exist low-temperature data for several monomeric LHCII prepared by other techniques [65], we have avoided comparing with these as the samples are likely too have Chl a/b binding properties not identical to that of the reconstituted monomeric LHCII.

3.3 Results

The aim has been to propose the orientations and the site energies of all 12 chlorophylls of an LHCII monomer by a simultaneous simulation of the ABS and LD spectra. Having fixed the Q_y dipole moment directions of eight of the Chls common to both CP29 and LHCII, there remain four Chl dipole moment directions to be determined. We start with the 2 possible orientations for the molecular y-axis suggested by Gradinaru et. al. [17] and there are 2^4=16 possible dipole moment conformations to be judged.

We have tested each of these 16 dipole moment conformations to determine the best solution. Although we have not provided any simultaneous fits, we have also inspected whether a selected conformation can account for the general character of the b-b, b-a, and a-a excitation transfer kinetics. We have not attempted to fit the circular dichroism (CD) spectrum since it is very sensitive to minor changes in the orientations of the Chls. Furthermore, the experimental CD spectrum at room temperature (and also at low temperature) is not conservative;

especially, the origin of the large, non-conservative, negative CD signal in the Chl b absorption region is unknown. Such a signal is also present in CP29, LHCII, CP26, and reconstituted complexes with varying Chl a/b ratios (see e.g. reference [53]). In our calculations, one would obtain a conservative CD spectrum by definition.
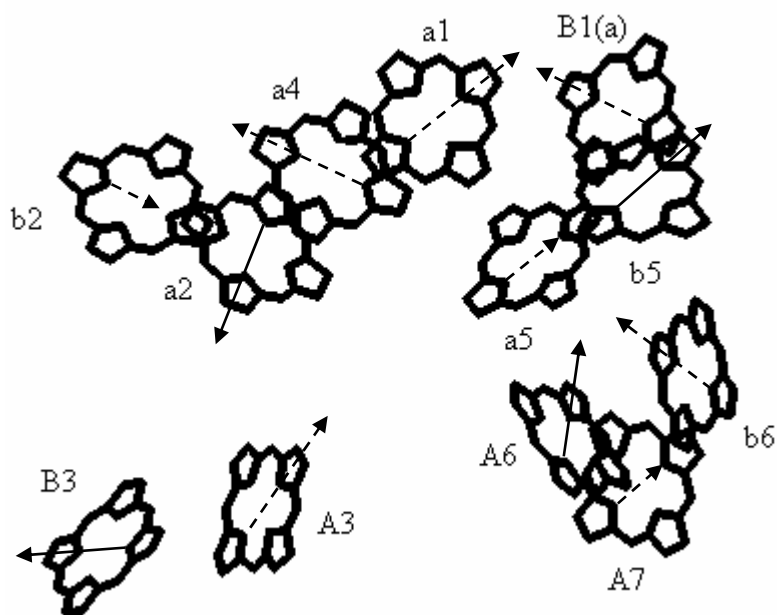
Figure 3.1. The Chl arrangement in monemeric LHCII. The protein and the carotenoids are stripped off for clarity. The diagonal arrows on the tetrapyrrole rings of the Chls indicate approximately the directions (Y(1), solid arrow and X(0), dotted arrow) of the Q_y transition dipoles determined in this study.

Under the assumption that the mixed sites bind Chls a and b in the same geometry, the best solution we have found has the following parameters: orientational assignments: a1(0), a2 (1), a4 (0), a5 (0) B1(a) (0), b2 (0), b5 (1), b6 (0), A3 (0), B3 (1), A6 (1), and A7 (0) (see Figure 3.1); site energies (in nm): a1 (668), a2 (672), a4 (a, 673), a5 (674), B1(a, 667), A3 (a, 672), B3 (a, 665), A6 (a, 673), A7 (a, 667), b2 (645), b5 (647.5), b6 (649.5), A3 (b, 653), B3 (b, 651), A6 (b, 653), and A7 (b, 649). Note that we have not fixed the site energies of the Chls common to the LHCII and CP29 complexes. Although most of the sites present in

both complexes induce similar absorption characteristics, some sizable differences have been observed in several binding sites (e.g. A3, B3 and a2), such changes may be attributed to different pigment-protein interactions [15].

To have a satisfactory fit of the Chl b region LD properties, it has been necessary to allow around $\pm 5\text{-}10^0$ deviations from the molecular y-axis for the Chl b dipole moments and this has also been the case in the CP29 simulations. The rotations have been b2 (-10^0), b6 (10^0), A3 (-10^0), B3(10^0), A6(5^0), and A7 (10^0), the effect of rotations on the interaction matrix elements is negligible.

In Figure 3.2 the ABS and LD spectra have been presented for the solution given above and have been compared with the LHCII experimental data [62]. Each of the simulated spectra is the weighted average of the Gaussian dressed spectrum for each of the 16 LHCII configurations.
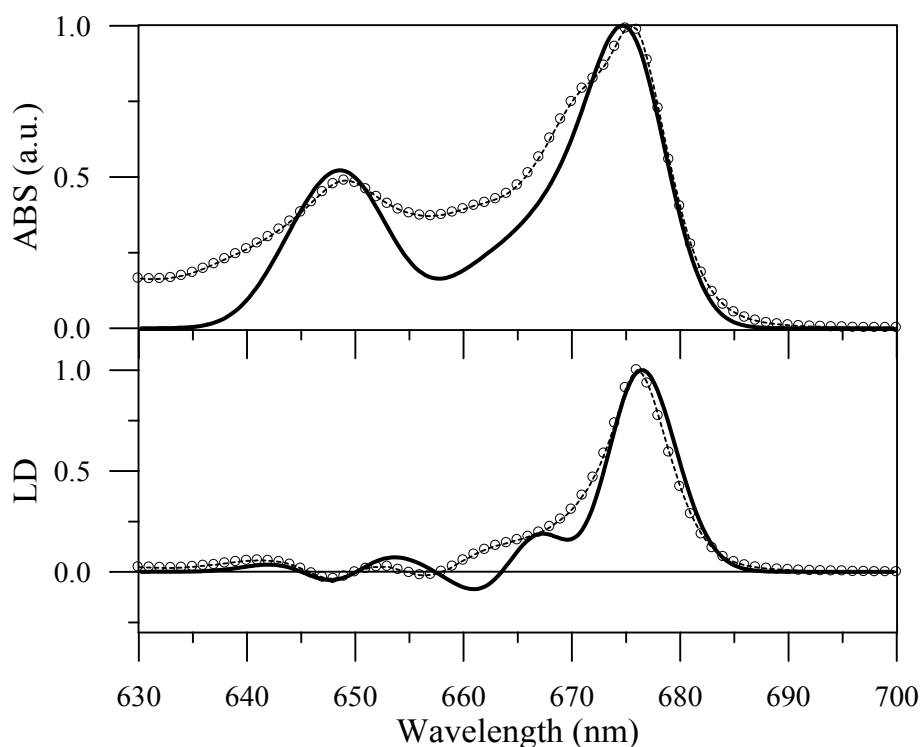
Figure 3.2. Experimental spectra (open circles) versus simulations (solid lines): a) ABS; b) LD. Experimental data at 77 K are reproduced from [62].

Table 3.2. Properties of the "Chl a" region (660-677 nm) transitions in LHCII.

	Wavelength (nm)	ABS strength (debye^2)	Composition[a]	Configurations
I	660.7	19	A3(a), B3(a) (28, 72)	1, 2, 3, 4
II	662.6	12	a1, B1, (47, 49)	All
IIIa	666.7	6	A3(b), B3(a) (10, 80)	5, 6
IIIb	666.8	18	A3(b), B3(a) (11, 87)	7, 8
IVa	667.7	35	A7(a), b6 (88, 5)	1, 3, 9, 11, 13, 15
IVb	667.9	50	A7(a), B3(a), b6 (81, 7, 5)	5, 7
V	670	8	a1, a2, B1 (23, 35, 40)	All
VIa	671.5	6	A3(a), a4, a5 (22, 34, 37)	9, 10, 11, 12
VIb	671.9	7	a4, a5(45, 45)	1, 2, 3, 4
Vic	672	9	a4, a5 (49, 45)	5, 6, 7, 8
VId	672.1	11	a4, a5 (50, 47)	13, 14, 15, 16
VIIa	673.7	31	A3(a), a4, A6(a) (54, 20, 13)	9, 10
VIIb	673.8	18	A3(a), a4 (71, 20)	11, 12
VIIc	674	21	A6(a) (92)	1, 2, 5, 6, 13, 14
VIId	674.1	6	A3(a), A6(a) (17, 75)	9, 10
VIIIa	675	35	a1, a2, a4, b1 (23, 46, 12, 10)	1, 2, 3, 4
VIIIb	675.1	54	a1, a2, a4, b1 (26, 50, 7, 11)	Others
IXa	676.2	8.5	a1+a2, a4, a5 (15, 40, 37)	1, 2, 3, 4
IXb	676.3	15	a1+a2, a4, a5 (10, 42, 47)	5, 6, 7, 8, 13, 14, 15, 16
IXc	676.3	18	a1+a2, a4, a5 (10, 40, 49)	9, 10, 11, 12
X	676.8	45	A3(a), a5, B3(a) (62, 12, 23	1, 2, 3, 4

[a]The molecules contributing and the respective percentage contribution (in parentheses). The numbers in the first three columns are the values averaged over the configurations given in the last column.

Table 3.3. Properties of the "Chl b" region (644-656 nm) transitions in LHCII.

	Wavelength (nm)	ABS strength (debye^2)	Composition[a]	Configurations
Ia	664	6	A7(b), b2, b5, b6 (16, 40, 10, 25)	4, 8, 12, 16
Ib	644.1	12	b2 (9395)	Others
IIa	644.3	11	A7(b), b2, b6 (16, 56, 17)	4, 8, 12, 16
IIb	644.8	2	A7(b), b5, b6 (38, 16, 38)	2, 6, 10, 14
IIc	645	11	A6(b), b5, b6 (15, 30, 45)	3, 7, 11, 15
IId	645.9	7.5	b5, b6 (50, 44)	1, 5, 9, 16
IIIa	647.7	17-20	A7(b), b5 (23, 75)	2, 4, 6, 8, 10, 12, 16
IIIb	647.8	14	A7(b), b5 (22, 65)	14
IV	648.1	20	A3(b), B3(b) (35, 65)	13, 14, 15, 16
Va	648.7	27	b5, b6 (67, 23)	3, 7, 11, 15
Vb	649.2	23	b5, b6 (47, 49)	1, 5, 9, 13
VI	649.8	12-20	A3(a), B3(b) (5, 93)	9, 10, 11, 12
VIIa	650.4	38	A3(b), A6(b), A7(b) b5, b6 (13, 21, 35, 10, 20)	8
VIIb	650.5	28	A6(b), A7(b) b5, b6 (24, 42, 10, 24)	4, 12, 16
VIIIa	651	13	A3(b), B3(a) (88, 12)	5, 7
VIIIb	651.1	26	A3(b), B3(a) (77, 10)	6
VIIIc	651.1	7	A3(b), B3(a) (75, 11)	8
IXa	651.3	29	A3(b), A7(b), b6 (15, 40, 37)	2, 10
IXb	651.8	18	A3(b), A7(b), b6 (15, 31, 46)	6
IXc	652	26	A7(b), b6 (45, 47)	14
Xa	655.5	4	A6(b), b6 (73, 24)	3, 7, 11, 15
Xb	655.6	7	A6(b), b6 (64, 33)	4, 8, 12, 16
XIa	655.9	13	A3(b), B3(b) (62, 37)	13, 14, 15, 16

[a]The molecules contributing and the respective percentage contribution (in parentheses). The numbers in the first three columns are the values averaged over the configurations given in the last column.

We would like to note that we have only considered the 0-0 transitions and have made no attempt to introduce the phonon wing/vibrational transitions. The Chl a wing contributes significantly around 660 nm for a Chl a 0-0 transition around 675 nm. We attribute the difference between the simulated and measured ABS spectra and the inconsistencies in the LD spectra around 662 nm to the neglect of phonon wing/vibrational transitions. An absorption offset between 630 and 660 nm is also present in the ABS simulations of CP29 [38, 57] and is attributed similarly to the neglect of the vibrational tails in the Chl a absorption forms.

The transitions, which occur in the 16 different LHCII configurations, can be classified in terms of their delocalization characteristics. The classifications for the "Chl a" (660-677 nm) and the "Chl b" (645-656 nm) spectral regions are given, respectively, in Table 3.2 and 3.3. The electronic excited state structure in the "Chl a" spectral region is decided to a large extend by the interactions within the following groups of Chls a: a1-a2-B1(a) (a1-a2≈-65 cm^{-1} and a1-B1(a)≈100 cm^{-1}), a4-a5 (≈45cm^{-1}), B3(a)-A3(a) (≈-155 cm^{-1}). There are also several weaker cross-couplings between these three groups, which cause further delocalization of excitation. The pairs, a4-a5 and A3-B3 are cross-coupled through the interactions of A3 with both a4 and a5 (≈-10 and ≈-20 cm^{-1}, respectively). The a1-a2-B1(a) triplet is cross-coupled with the a4-a5 pair via the interactions of a1 and B1 with both a4 and a5, with strengths ranging from -6 to 15 cm^{-1}. The a4-a5 pair predominantly contributes to the bands in the middle (671.5-674 nm) and in the red (675-676 nm), while the a1-a2-B1 triplet and B3-B3 pair are associated with both the red and the blue (660-667 nm) sides of the spectrum. In addition, the strong coupling between the B3(a) and A3(b) molecules delocalizes the excitation between the two spectral regions and yields a band around 667 nm. One of the remaining two Chls a, A6, has the strongest interaction with A7 (≈-35 cm^{-1}) and is also weakly coupled with A3 and a4 (both ≈-10 cm^{-1}). In addition to the A6-A7 coupling, A7 is also coupled with a5 (≈25 cm^{-1}). Moreover, both A6 and A7 are also coupled strongly with Chl b6 (A6-b6≈-105 cm^{-1} and A7-b6≈100 cm^{-1}). However, owing to their widely differently site energies, A6 and A7 do not mix

with each other. A6 mixes with A3 and a4 and contributes to a band around 674 nm. A7 contributes to a blue state ($\approx$667 nm), which is delocalized over the Chl A7 and the Chl b6 molecules. A similar b-a excitation delocalization via the equally strong b6-A6 coupling is more limited (2-3%, not shown in Table 3.2) owing to a larger separation in the site energies.

The Chl b region transitions (644-656 nm) are more congested than that of the Chl a region transitions. There are several important pairwise b-b interactions shaping up the spectra: A3(b)-B3(b) ($\approx$-110 cm^{-1}), A6(b)-b6 ($\approx$-90 cm^{-1}), A7(b)-b6 ($\approx$85 cm^{-1}), b5-b6 ($\approx$35 cm^{-1}), and A6(b)-A7(b) ($\approx$-25cm^{-1}). In particular, the coupling of b6 with A6, A7 and b5, and a further A6-A7 interaction offer a multitude of possibilities for the transitions ranging between 645 and 652 nm as shown in Table 3.3. In addition, the b-a couplings between B3 and A3 ($\approx$-130 cm^{-1}) contribute to the spectra around 650-651 nm. The most uncoupled Chl b, b2, contributes to the blue-most transitions ($\approx$644-645 nm) and the red-most transitions ($\approx$656 nm) are attributed to the A3(b)-B3(b) and A6(b) b6 interactions.

3.4 Discussion

The assignment of the Q$_y$ transition dipole moment of each Chl molecule along the molecular y-axis is based on a number of studies in which either monomeric or a pair of very weakly interacting Chl molecules in a very well-defined geometry are analyzed [43, 49-51].

The point of departure for assigning the orientations of the CP29 has been the results reported in a series by Gülen et al. [45, 46] and by Gradinaru et al. [47]. In these series of papers the most probable orientations have been suggested upon performing a quite extensive search in a large space of possible combinations of the individual dipole moment orientations. Although this search procedure has been applied to CP29 prior to the "full" Chl identification, the model used has been very similar (in terms of structural and identity assumptions) to the one suggested in the recent work of Bassi and co-workers [16]. The combinations that can comply with the global features of both the polarized steady-state spectra and the temporal and

spectral behavior of the kinetic observations have been selected. An unambiguous solution for the orientations could not be found since the selection is based on a set of relatively mild criteria, but a very restricted set of possible orientational configurations has been offered. The most probable orientational assignments for the CP29 chlorophylls (judged mostly by the polarized absorption characteristics) have been: a1 (0), a2 (0 or 1), A3 (a, 0 or 1), a4 (0), a5 (0), B5 (a, 0 or 1), B3 (b,1), and B6 (b, 0). We have recently suggested a unique, most probable orientation set by fixing the orientations of a2 (1), A3 (0), and B5 (1) through an analysis similar to the one presented in this work [57]. In Gradinaru et al. [17], for the remaining LHCII Chls, only the orientation of A7 has been found to prefer one of the orientations (0) but it was assigned as a pure Chl a site. Moreover, B1, b2, and A6 are assigned as pure Chl b sites. We have therefore carried out our calculations with two possible orientations for each of these four Chls.

The existence/absence of several Chls a cause some notable differences between the delocalization characteristics of the transitions associated with the Chl a core common to CP29 and LHCII. These differences can be attributed mainly to the existence of B1(a) and the absence of B5(a) in the LHCII. The coupling between the a1-a2 and a4-a5 pools (mainly via a1-a5≈15cm^{-1}) causes considerable delocalization of excitation over these four Chls a in the CP29. However, a much stronger B1(a)-a1≈100cm^{-1} coupling in the LHCII limits the mixing between these two pairs of Chls a. Similarly, A3(a)-a5 coupling (≈-20 cm^{-1}), which leads to non-negligible delocalization of A3(a) with the a4-a5 pool in the LHCII, does not yield any significant delocalization in the CP29, since in this case the coupling of the a4-a5 pair with B5(a) overtakes. Furthermore, the delocalization between the Chl b and the Chl a pools originating from the B3-A3 interactions is more pronounced in the LHCII in these molecules as Chls b absorb 10 nm to the red compared to their absorption in the CP29.

The spectral complexity in the Chl b absorption region is almost entirely a result of the recent Chl b identify assignments [15]. If A3, A6, and A7 had no Chl b character, as in the original Kühlbrandt et al. [14] assignment, the only important

b-b interaction would be the b5-b6 interaction and the excitation delocalization in the Chl b region would be mush more restricted.

Remelli et al. [15] have also assigned the transition energies of all the Chls in LHCII by comparing the spectral properties and pigment composition of LHCII with and without binding a specific Chl. It has been noted that the excitonic effects are present in the difference spectra, but the conclusions about the spectral decomposition of the Q_y band have been mainly drawn without taking the interactions between the pigments into account. Nonetheless, there is considerable agreement between the spectral decomposition proposed by Remelli and co-workers and out results on the composition of the energy bands. For instance, the Chls B1(a), a1, and a2 contribute to a large extent to the main absorption band on the red side and there are minor contributions to 663 nm band by a1. The absorption of the Chls a4 and a5 peaks is near 675 nm. The Chl A3(a) is partly responsible for an absorption band peaking near 662-663 nm. Owing to several stronger excitonic couplings, it is more difficult to compare the Chl b region assignments. However, the blue-most Chl b is b2 and the other Chls b are more on the red side in both studies.

Energy transfer processes in the LHCII, both in monomeric and trimeric forms, have been studied extensively by various time-resolved techniques (e.g. see references [47, 54, 55, 58, 61, 63; 64, 65; 67, 70, 71]). The "intra-monomeric" b-a, a-a, and b-b transfers with time scales ranging between 150 fs and 10 ps have been identified. In two-color transient absorption experiments exciting the Chl b region around 650 nm, three different time scales for the Chl b to Chl a transfers have been distinguished (=200 fs, ≈600 fs, and 2-6 ps) [54, 55, 71]. Their contribution to the Chl b to Chl a transfers have been found to be around 40%, 40%, and 20%, respectively.

648 nm 0.34 b
650 nm 0.28 b (B3)
651 nm 0.23 b
655 nm 0.16 b

671-673 nm 0.40 a
674-675 nm 0.26 a
676 nm 0.65 a

644 nm 0.11 b
645 nm 0.09 b (A6, B6)
647 nm 0.16 b (A7)
649 nm 0.35 b (B6)
650-651 nm 0.87 b
655 nm 0.19 b (A6, B6)

677 nm 0.47 a
674-671 nm 0.19 a
660 nm 0.17 a
666 nm 0.12 a

662 nm 0.57 a (A1, B1)
670 nm 0.37 a (A1, A2, B1)
675 676 nm 2.10 a (A1, A2, B1)
644 nm 0.78 b (B2)

644-645 nm 0.14 b (B5)
648 nm 0.50 b (B5)
649 - 651 nm 0.55 b (B5)
673-674 nm 0.41 a (A6)
667-668 nm 0,81 a (A7)

64

Figure 3.3. Block diagram representation of the excitation pathways in LHCII (in ps). Relative contributions of the Chls to the excitation energy transfers of particular states are also shown. Shaded symbols corresponds to the Chl a molecules.

Transient absorption measurements have indicated that the Chl(s) a absorbing around 663 nm transfers to the low-energy ones (absorbing 679 nm), either directly or via the 670 nm pool with a time constant of 5±1 ps. The 670 nm excitation is transferred to the low-energy Chls a in two phases (300±50 fs and 12±2 ps) and a fast equilibration (450±50 fs) takes place within the main absorption band (675-680 nm) [30]. In a recent 3 PEPS (three-pulse photon echo peak shift) experiment [71], two decay channels of lifetimes around 320 fs and 5 ps upon 670 nm excitation have also been found. Chl b to Chl b transfers in the 650 nm band have been observed for the first time in the same 3PEPS study and a biexponential transfer (with lifetimes 300 and 800 fs) between a "pair" of Chls b has been reported. These observations have also suggested that the slows b to a transfer is linked with a strongly coupled Chls b involved in the biexponential b-b transfer and, in addition, these groups of molecules are associated with a Chl b to Chl a decay pathway of lifetime 600 fs.

According to the results we have presented above, again as in the case of CP29, it is necessary to evaluate the energy equilibration by taking the delocalized nature of the excited states into account. Therefore it is not entirely proper to talk in terms of the Förster rates [31] between the pairs of molecules. However, in order to discuss that one can in principle understand quite well the pathways and the time scales for flow of excitation energy within the proposed assignment, we have provided a block diagram in Figure 3.3. The rate constants for this diagram are estimated using the Föster mechanism as described elsewhere in detail [47, 56]. The lowest excited states of the isolated chlorophylls are used in estimating the rate constants.

It was already evidenced by several previous studies that the excitation transfer in the LHCII and CP29 complexes are compartmental to a large extent [38, 47, 56, 57]. Compartment refers to a group of molecules that transfer to/equilibrate with each other very fast (<1 ps) but has significantly slower transfers (5 ps) with the rest of the molecules in the system. The compartments, defined by the assignments of this study are shown in Figure 3.3.

Excitation is extensively delocalized among the Chls a belonging to the same compartment. The electronic excited state structures presented in this work furthermore indicate that the delocalization of excitation is not only limited to the compartments. Inter-compartmental interactions cause further delocalization of excitation. It is clear that excitation will be fully equilibrated over the compartmental Chls a since there are several bi-directional pathways between them. One of the two non-compartmental Chls a, A6, also equilibrates with this core through A6-a3 interaction ($\approx$20 ps; not shown in Figure 3.3). The other one, A7, is the only unidirectional Chl a and it feeds the a4-a5 pair. Excitation equilibration among all these delocalized levels in the Chl a spectral region needs to be detailed with further simulations of energy transfer processes. Nevertheless, the time scales of the intra- ($\leq$1 ps) and inter-compartmental ($\approx$5-10 ps) transfers correlate well with the experimentally observed equilibration rates.

The fastest transfers from the 650 nm band flow out of the Chls b, B3, A3, and b2. The B3(b)-A3(b) pair is highly delocalized and equilibrates very rapidly ($\leq$200 fs), but transfer of excitation from this Chl b pair to the Chl a pool is rather slow (=10 ps, via B3-a2 interaction). Therefore the Chl b molecules B3 and A3 in the monomeric form are responsible for part of the ultrafast b to a transfer from the 650 nm band. Each, as a Chl a molecule, is weakly coupled with the rest of the Chl a molecules. The B3(b) to A3(a) and A3(b) to B3(a) transfers take about 250 fs. The other ultrafast Chl b, b2, on the other hand, transfers to a pool of strongly coupled Chls a via b2-a2 coupling ($\approx$250 fs). In our model, the b5 molecule transfers to several Chl a molecules (a4, a5, A6, and B1) with transfer times ranging from 5 ps to 15 ps, yielding an overall de-excitation rate of around 2 ps. It is therefore likely to contribute both to the intermediate and slow b to a transfers. The remaining Chls b, A6, A7, and b6, constitute a strongly coupled group of molecules. In the compartment of these Chls b there are two subpicosecond transfers, b6-A6 (350 fs) and b6-A7 (500 fs). There is also b6-b5 equilibration, but this is several times slower ($\geq$2 ps) and is not shown in the block diagram. Moreover, the b to a transfers which exit from this pool have two different time scales (subpico- and several picoseconds). The slow one proceeds mainly via

A6(a) to A7(a) and A7(b) to A6(a) and a5 connections with the respective lifetimes of around 5 ps and 2.5 ps. The third Chl b of this pool, b6, de-excites by transferring both to A7(a) and A6(a). Each of these transfers is on the sub-picosecond scale, b6-A7 (800 fs) and b6-A6 (500 fs), yielding an overall de-excitation rate of around ≥ 300 fs. All these b-b and b-a transfer properties associated with the A7, A6, and b6 molecules are perfectly in agreement with the conclusions of the recent 3PEPS study of Agarwal et al. [71]. With these estimates of the rate constants, the contributions of the Chls b in the monomeric LHCII to the Chl b- Chl a transfers around 40% (fast), 30% (intermediate), and 30 % (slow).

LHCII in vivo is probably an aggregated form of the trimeric LHCII. Therefore, in addition to the intramonomeric transfers described above, one also expects intermonomeric and intertrimeric transfers. With the suggested orientations and the spectral assignments, the a4-a5 interaction between the adjacent monomers is the most favorite intermonomeric channel (estimated to have a Förster rate of around 15-20 ps).

Our choice on the identity of the molecule binding to site A7 has not been fully justified by site-directed mutagenesis. A7 has been suggested to be a pure Chl b binding site by Remelli et al. [15]. With the identity assignments of this mutagenesis work, however, the Chl a/b stochiometry (6.5a/5.5b) of the LHCII (7a/5b) is not satisfied. It has already been discussed that one of the sites A6 and A7 might be binding Chl a with a higher affinity [15] and our choice has been to assign A7 as a mixed site with equal binding probability. Several remarks on this choice are necessary. Note that unless both A6 and A7 sites bind Chl b molecules it would not be possible to have a biexponential b-b transfer process with the transfer times observed [71] in the Chl b spectral region with the current identity assignments. Consequently, it would also not be possible to associated part of the slow b to a transfer with a group of strongly coupled Chls b. The dipole moment direction of the molecule binding to site A7 is very extreme: either almost in the molecular plane (0) or almost parallel to the C_3 symmetry axis (1). The orientation 0 gives a large positive LD and the orientation 1 yields a large negative LD signal. For this reason, it has been assigned to be in orientation 0 as a Chl a in the previous

models [47, 72]. In this respect, it becomes rather difficult to explain the relative strengths of the LD signals and the values of the reduced LD in the Chl b and the Chl a bands if no Chl a character is associated with this molecule. One is referred to, for example, Gülen et al. [46] for more a comprehensive discussion on this point.

3.5 Conclusions

We have assigned in this work the Q_y dipole moment orientations for all the chlorophylls in the major plant antenna, LHCII. We have assumed that the electronic excited states of the complex have been decided by the Chl-Chl and Chl-protein interactions and have modeled the Coulombic interaction between a pair of Chls in the point dipole approximation and the Chl-protein interactions are treated as empirical fit parameters. A considerable part of the current information offered by structure determination, site-directed mutagenesis, and spectroscopy has been included in the modeling. The assignment proposed has been discussed to yield a satisfactory reproduction of all the prominent features of the polarized linear absorption spectra as well as the prominent spectral and temporal features of the energy transfer processes among the chlorophylls.

It is believed that, given the complexity of the system, the orientations and the spectral assignments obtained by relatively simple exciton calculations have been necessary, in order to provide a good point of departure for more detailed treatments of both steady-state spectra [33, 73] and the excitation kinetics [29, 74, 75].

CHAPTER 4

OPTICAL PROPERTIES AND THEIR SIMULATIONS FOR THE FMO COMPLEX OF *CHLOROBIUM TEPIDUM*

4.1 Introduction

With the availability of more and better resolved structural data for the photosynthetic systems, there has been progress towards understanding of structure-function relationship in these systems. On the other hand, a complete understanding of even the best-structurally and spectroscopically characterized systems, such as the FMO complex of green sulfur bacteria, is still elusive.

This water soluble complex from *Pc. aestuarii* has been the first photosynthetic pigment-protein complex to have its three-dimensional X-ray structure determined to an atomic resolution by X-ray crystallography [21]. Currently, there exist structural models of the FMO complex from *Pc. aestuarii* and *Cb. tepidum* at $1.9 \overset{\circ}{A}$ and $2.2 \overset{\circ}{A}$ resolutions respectively [20, 22, 23]. The overall structures of the two complexes are very similar. Both FMO complexes consist of three identical subunits related by a crystallographic 3-fold rotational symmetry axis (C_3) (see Figure 1.7). Each monomeric subunit encloses seven BChl molecules arranged in a rather non-symmetric fashion as shown in Figure 1.7b. We refer to Chapter 1 for further structural information.

Because of the detailed structural information, the FMO complex has been attractive for the study of excitonic effects, both theoretically and experimentally [27, 34, 39-41, 76-87]. However, because the seven BChl a molecule in a subunit can experience different site energy due to the different protein environments and the different conformational properties and there is no reliable method for

calculating the site energies, the problem is not simple and the complete understanding of functioning of this system couldn't be attained. Nevertheless, recently several reasons for the failure of the earlier models have been identified [75, 78-82] and there has been significant progress [39-41, 84-86] towards understanding of the structure-function relationship in the FMO complex. Currently there exists good qualitative explanation of a number of spectra such as absorption (ABS), linear dichroism (LD), triplet-singlet absorption difference (T-S) and circular dichroism (CD) of *Pc. aestuarii* and ABS, LD, and CD of *Cb. tepidum* and their excited-state dynamics [39-41, 84-87].

There is a general agreement in these studies, that the lowest energy band (around 825 nm) is due to the states that stem from the lowest Q_y-state of each subunit. For this state excitation localized to a large extend on a single molecule. Moreover, the assignment of the red-most band is of particular interest because this lowest energy state is thought to participate in a trapping of energy to the reaction center. Lately, there has been a convergence into the models in which the BChl 3 is the lowest energy absorbing pigment [40, 41, 84-87].

Particularly important to note is the level of treatment of the key factors in the above mentioned studies. Most of the current models used the point-dipole approximation to account for the pigment-pigment (excitonic) interactions. The site energies are treated as empirical fit parameters and Gaussian synthesis is used to dress the calculated excitonic stick spectra with symmetric Gaussians to account for the spectral broadening. Homogeneous and inhomogeneous broadenings were not explicitly considered until recently. In the very recent study, Wendling et al. [86] have included three different broadening mechanisms, inhomogeneous, homogeneous and lifetime broadening, explicitly into the simulations. Monte Carlo approach was used to treat inhomogeneous broadening and fluorescence line narrowing (FLN) measurements were used to construct the homogeneous (line shape) broadening [88].

In all the current simulations except that of Wendling et al. [86], only the shape of the spectra was simulated whereas the size (relative to the absorption

spectrum) was not considered. Since the degree of ordering of the complexes in the LD measurements was unknown, the size of the LD could not be simulated. Recently, Wendling et al. [86] have combined LD and polarized fluorescence results to deduce the absolute LD spectra of the FMO from *Pc. aestuarii*, i.e., the spectra that would be measured if the complexes had been perfectly oriented [86].

In that study [86] the simulations for the trimeric FMO from *Pc. aestuarii* have been carried out and BChl 3 was assumed to be the red-most pigment. The effective dipole strength, in the protein environment, was determined to be 30.6 debye^2. This is in qualitative accord with the study of İşeri and Gülen [40] which argued that the key features of several steady-state spectra and the temporal and spectral evolution of absorption difference spectra of FMO complex from *Pc. aestuarii* can be explained using dipole strength between 30 and 40 debye^2 provided that BChl 3 is the lowest energy pigment. In particular, this study has shown that inclusion of the different broadening mechanisms into the simulations of absorption (difference) spectra leads to considerable improvement.

In this Chapter we have present the new experimental absorption, LD and CD spectra for *Cb. tepidum* and have carried out simulations of these spectra with the same basic assumptions used earlier for the FMO complex from *Pc. aestuarii* [86].

4.2 Material and Methods

4.2.1 Sample Preparation

The FMO complex from *Cb. tepidum* was kindly provided by Dr. Thijs J. Aartsma, which was isolated as described by Francke and Amesz [89]. For the low temperature ABS and CD measurements samples were dissolved in a buffer 50 mM Tris/HCl and 200 mM sodium chloride (pH = 8.3), and also 66% (v/v) glycerol was added to obtain clear glass upon cooling. For the LD measurement, the same buffer was used with 8% acrylamide (w/v), 0.3% (v/v) TEMED, 0.03% (w/v) ammonium persulphate and 55 % (v/v) glycerol to obtain gel. Orientation of the FMO

complexes for LD measurement was achieved by a gel compression technique. The gel was compressed in two perpendicular directions allowing expansion along the third axis by a factor of 1.6. Samples were cooled in a helium flow cryostat, which allowed measurements at different cryogenic temperatures.
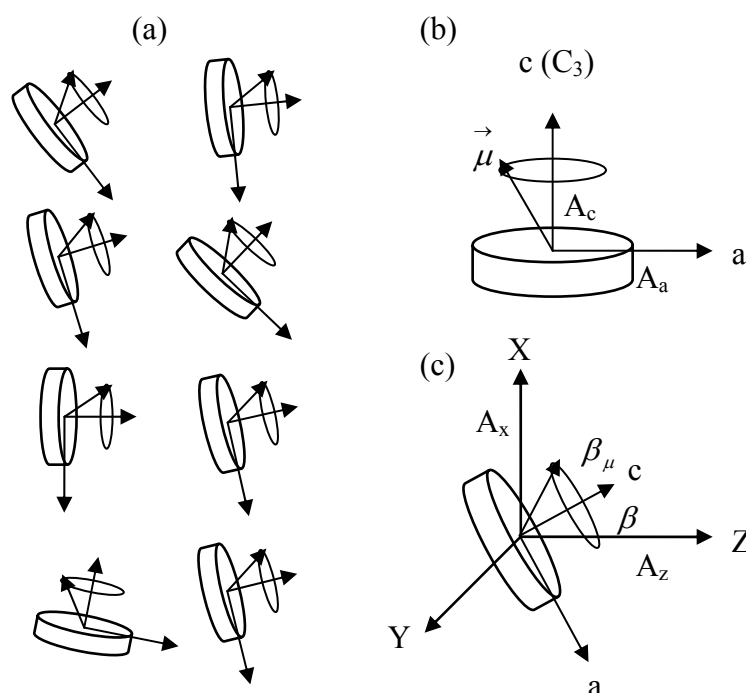
4.2.2 Absolute LD and Scaling of the Spectra

Figure 4.1. The FMO trimer is presented as a disc-shaped particle. a) Randomly oriented FMO trimers in the compressed gel. b) c and a are molecular axes of coordinates and A_c and A_a are polarized absorption of oriented FMO proteins with respect to the molecular frame of the complex. $\vec{\mu}$ is the dipole moment vector of BChl a Q_y transition.c) X, Y and Z are the laboratory axes of coordinates. A_Z and A_X are polarized absorption of oriented FMO proteins with respect to the laboratory frame. β_μ is the angle between the transition dipole moment and the C_3-symmetry axis of the trimeric complex. β is the angle between the C_3-symmetry axis and the Z-axis of the gel.

In the LD experiment, one measures the difference in absorption, $\Delta A(\lambda) = A_Z - A_X$, where A_Z and A_X are respectively the absorption of light polarized along and perpendicular to the Z-axis. The Z-axis is the axis along which the gel expands after squeezing in both the X- and Y-direction with respect to the laboratory frame (see Figure 4.1). The LD spectrum that one calculates using the exciton theory is the absolute LD ($\Delta A^{mol}(\lambda)$) by assuming that all complexes are oriented with their c-axis parallel to each other. The degree of orientations of the complexes in the squeezed gel is not known in the conventional LD measurements. Therefore, in order to compare theoretical and experimental spectra quantitatively an additional correction should be done on the measured spectra. We next describe how to obtain absolute LD.

The absolute LD and the reduced-LD ($\Delta A_{red}^{mol}(\lambda)$) spectra with respect to the molecular frame of the complex are defined by;

$$\Delta A^{mol}(\lambda) = A_c - A_a \tag{4.1}$$

$$\Delta A_{red}^{mol}(\lambda) = \frac{\Delta A^{mol}(\lambda)}{3A_{iso}(\lambda)} = <\mathrm{P}_2(\cos\beta_\mu)>_\lambda \tag{4.2}$$

$$3A_{iso}(\lambda) = A_c(\lambda) + 2A_a(\lambda) \tag{4.3}$$

Here, A_c and A_a are respectively the absorption of light polarized along and perpendicular to the C_3-symmetry axis of the complex. β_μ is the angle between the transition dipole moment and the C_3-symmetry axis of the disc-like trimeric complex (see Figure 4.1). $\mathrm{P}_2(x) = (3x^2-1)/2$ is the second order Legendre polynomial and the brackets indicate a weighted average over different pigments (or excitonic states) contributing to the absorption at wavelength λ. $\Delta A_{iso}(\lambda)$ is the isotropic absorption spectrum. The term $<\mathrm{P}_2(\cos\beta_\mu)>_\lambda$ is an intrinsic property of the complex and depends entirely on the excitonic transition dipole moment orientations within the trimer.

In reference [90] it was shown in detail how $< P_2(\cos\beta_\mu) >_\lambda$ can be obtained from the reduced-LD spectrum $\Delta A_{red}(\lambda)$ and the fluorescence excitation anisotropy $r(\lambda)$. The reduced-LD spectrum is defined as;

$$\Delta A_{red} \equiv \frac{\Delta A}{3A_{iso}} = \frac{A_Z - A_X}{A_Z + A_X + A_Y} = \frac{A_Z - A_X}{A_Z + 2A_X} = \langle P_2(\cos\beta) \rangle P_2(\cos\beta_\mu) \qquad (4.4)$$

Here the term $\langle P_2(\cos\beta) \rangle$ describes the average orientation of the complexes in the squeezed gel, β being the angle between the C_3-symmetry axis and the Z-axis of the gel. The brackets indicate averaging over all possible orientations of the complexes in the gel. $\langle P_2(\cos\beta) \rangle$ is also called the degree of orientation or orientation factor. It equals 0 in the absence of compression, whereas it is -0.5 in the case of maximal ordering upon squeezing, i.e. the C_3-axis of all complexes is oriented perpendicularly to the Z-axis and randomly within the X-Y plane of the gel. For the complex, which contains several pigments with different absorption bands and different orientations of the transition dipole moments with respect to the symmetry axis, ΔA_{red} becomes wavelength (λ) dependent and it is given by

$$\Delta A_{red}(\lambda) = \langle P_2(\cos\beta) \rangle \langle P_2(\cos\beta_\mu) \rangle_\lambda \qquad (4.5)$$

Now, $< P_2(\cos\beta_\mu) >_\lambda$ indicates a weighted average over the different pigments (or excitonic states) contributing at wavelength λ. Their contributions are weighted by their (absorption) dipole strength at λ and the formal expression for $\langle P_2(\cos\beta_\mu) \rangle_\lambda$ is

$$\langle P_2(\cos\beta_\mu) \rangle_\lambda = \frac{\sum_{i=1}^{N} P_2(\cos\beta_\mu^i) A_i(\lambda)}{\sum_{i=1}^{N} A_i(\lambda)} \qquad (4.6)$$

where i enumerates the N various pigments (or exciton states) and $A_i(\lambda)$ is the absorption of pigment or exciton state i at λ. Note that upon squeezing

74

$\langle P_2(\cos\beta)\rangle$ changes, but $\langle P_2(\cos\beta_\mu)\rangle_\lambda$ remains the same. Therefore, the shape of the reduced-LD spectrum $\Delta A_{red}(\lambda)$ remains unaltered.

The fluorescence excitation anisotropy spectrum $r(\lambda)$ is related to the spectroscopic properties of the complex as follows:

$$r(\lambda) = \frac{2}{5}\langle P_2(\cos\beta_\nu)\rangle_{\lambda_{det}} \langle P_2(\cos\beta_\mu)\rangle_\lambda \qquad (4.7)$$

where λ is the wavelength of excitation and $\langle P_2(\cos\beta_\nu)\rangle_{\lambda_{det}}$ reflects a weighted average over the emitting pigments or states at detection wavelength λ_{det}. It is formally given by

$$\langle P_2(\cos\beta_\nu)\rangle_{\lambda_{det}} = \frac{\sum\limits_{i=1}^{N} P_2(\cos\beta_\nu^i)F_i(\lambda_{det})}{\sum\limits_{i=1}^{N} F_i(\lambda_{det})} \qquad (4.8)$$

where $F_i(\lambda_{det})$ is the fluorescence intensity of pigment or state i at wavelength λ_{det} for an excited-state equilibrated system. β_ν is the angle between the emitting transition dipole moment and the C_3-axis of the complex.

Equation (4.8) depends on the temperature and at sufficiently low temperatures all fluorescence stems from the lowest-energy band and $\langle P_2(\cos\beta_\nu)\rangle_{\lambda_{det}}$ becomes equal to $\langle P_2(\cos\beta_\nu^1)\rangle_{\lambda_{det}}$, where the lowest-energy band has been numbered 1.

$$r(\lambda) \approx \langle P_2(\cos\beta_\mu)\rangle_\lambda \qquad (4.9)$$

In the case of the FMO complex, the lowest energy state is well separated from the next lowest energy state at low temperature. Therefore, at sufficiently low temperature all fluorescence arises from this band, which we call state 1 or band 1. If one selectively excite this lowest-energy band, then absorption and emission

occur by/from the same state or from one of the other equivalent states in the trimer and if subunit equilibration takes place and is fast enough one obtains:

$$r(\lambda) = \frac{2}{5} P_2(\cos \beta_\nu^1) P_2(\cos \beta_\mu^1) . \qquad (4.10)$$

Since absorption and fluorescence correspond to the same electronic transition, $\beta_\nu^1 = \beta_\mu^1$ and the anisotropy provides $P_2(\cos \beta_\mu^1)$ for the lowest-energy state.

In short the shape of $P_2(\cos \beta_\mu)$ can be determined experimentally by measuring $\Delta A_{red}(\lambda)$ and furthermore, $\Delta A_{red}(\lambda)$ is proportional to $r(\lambda)$, provided that equilibration within the trimer is much faster than the excited-state lifetime in the complex. For the FMO complex the subunit equilibration occurs on a time scale of picoseconds over a wide range of temperature [25, 91, 92], whereas the excited-state lifetime is an order of nanoseconds [93]. Once the value of $r(\lambda)$ is known at (over) a suitable wavelength (range), the entire experimental reduced LD spectrum can be scaled. The isotropic absorption spectrum is also known. So, one can obtain $\Delta A^{mol}(\lambda)$ using equation (4.2). It is then straightforward to calculate $A_c(\lambda)$ and $A_a(\lambda)$ using equation (4.1) and (4.3) which lead to:

$$A_c(\lambda) = \frac{1}{3}(3A_{iso}(\lambda) + 2\Delta A^{mol}(\lambda)) \qquad (4.11)$$

$$A_a(\lambda) = \frac{1}{3}(3A_{iso} - \Delta A^{mol}(\lambda)) \qquad (4.12)$$

The resulting experimental spectra $\Delta A^{mol}(\lambda)$, $A_c(\lambda)$ and $A_a(\lambda)$ are scaled relative to the isotropic absorption spectrum. The experimental CD spectrum is also scaled relative to the corresponding measured absorption spectrum with an absorption maximum of 1.

4.2.3 Model Parameters

The formalism of exciton calculations are explained in detail in references [27, 28] and is summarized Chapter 1.

For the position of each pigment, the positions of its four nitrogen atoms are averaged. The transition dipole moment directions associated with the Q_y transitions are taken parallel to the axis passing through the N_B-N_D nitrogen atoms in the nomenclature of the PDB. The atomic coordinates [20] of the trimeric FMO complex of *Cb. tepidum* were kindly provided by Prof. J. P. Allen.

In the simulations, Monte Carlo approach [25, 28, 94] was used to account for the inhomogeneous broadening. For every Monte Carlo iteration, the site energy of each of the 21 BChls a is randomly taken from its own Gaussian inhomogeneous distribution function independently from the site energies of the other molecules.

Homogeneous broadening is accounted for by convoluting each excitonic line with a homogenous lineshape as described in Chapter 1. A homogeneous line generally consists of a zero-phonon line (ZPL) and a phonon wing (PW). Owing to the fact that the 825 nm band of the optical spectra of the FMO complex is well separated from the other bands, it can be selectively excited in the FLN measurement. Therefore, the FLN spectrum only gives information about this state. Wendling et al. [87] have used temperature-dependent absorption and FLN measurements on the FMO complex of *Pc. aestuarii* to extract the one-phonon-vibrational profile (spectral density, $\phi(\nu)$) (see Figure 4.2) and have determined the overall Huang-Rhys factor S to be 0.45. By using this information a homogeneous spectrum, shown in Figure 4.3, was constructed. Since the FLN measurement for the FMO complex from *Cb. tepidum* is not available, and the lowest-energy state of the FMO complex from both species shows very similar optical characteristics [91], we used the same spectral density and homogeneous lineshape as in reference [86] shown in Figures 4.2 and 4.3. Previously Vulto et al. [87] used the same formalism to model the excitation dynamics within the FMO

complex from both species. In that study a generic function was used for the spectral density.
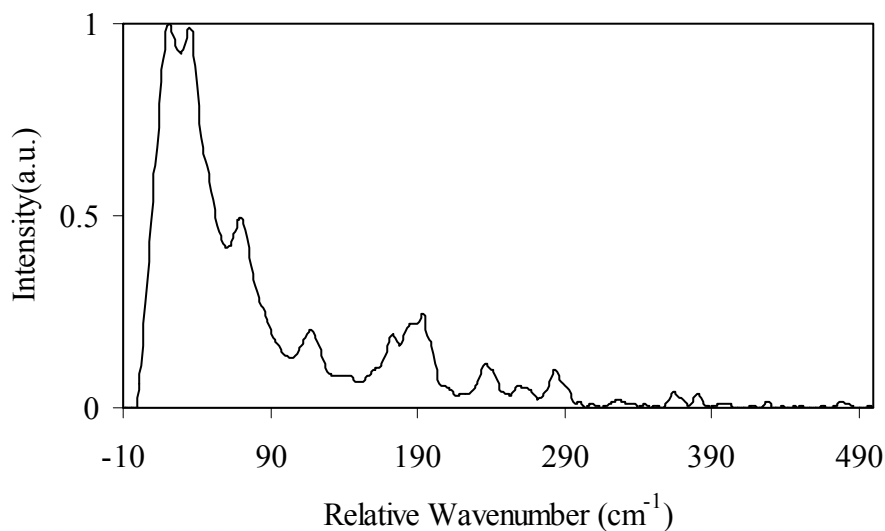

Figure 4.2. The one-photon-vibration profile of the FMO complex from *Pc. aestuarii* [86] calculated for S=0.45.
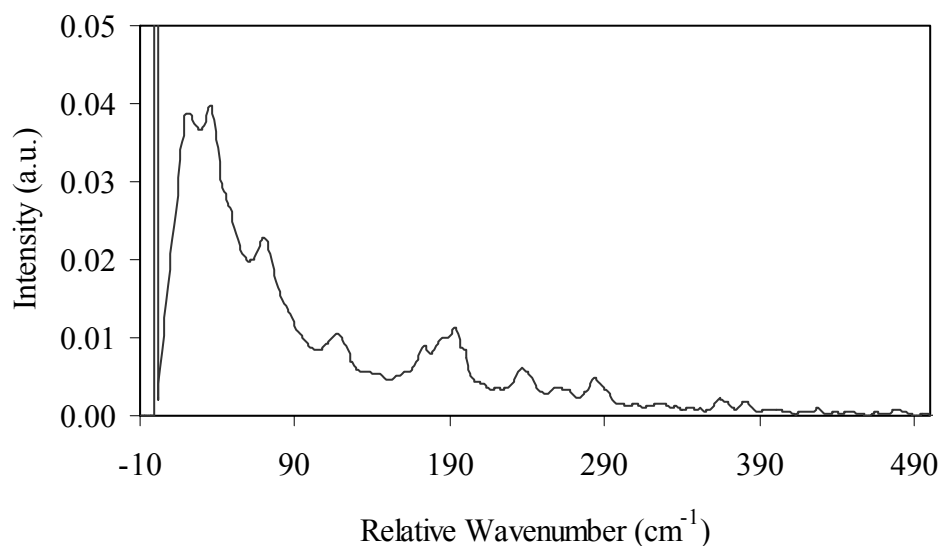

Figure 4.3. The homogeneous lineshape of the FMO complex from *Pc. aestuarii* [86].

To account for the lifetime broadening in the simulations the formalism of Leegwater et al. [29] has been used (see section 1.5.3). In equation (1.30) $\gamma(\omega)$ is the spectral density describing the frequency dependent coupling of the electronic states of the complex to their environment, and it is known up to a scaling factor γ_0 [86, 87], i.e., $\gamma(\omega) = \gamma_0 \cdot \phi(\nu)$.

The scaling factor γ_0 (ratescale) is not directly available and is an additional parameter in the simulations. In the simulations shown below, the decay rates of exciton states are calculated for each Monte Carlo iteration.

4.3 Results and Discussions

4.3.1 Experiments

Figure 4.4 shows experimental ABS, LD and CD spectra at 4 K. All spectra have common bands around 790, 805, 815 and 825 nm labeled as 1, 2, 3 and 4 in Figure 4.4.

The low-temperature absorption spectrum exhibits considerable structure characterized by four partially overlapping bands with peaks around 790, 805, 815 and 825 nm. Increase in the band intensities with a concomitant sharpening was observed upon lowering the temperature (data are also taken at 25, 50 and 75 K, not shown). The low-temperature absorption spectrum is very similar to those reported earlier [41, 95].

In the LD measurement our orientation technique produces negative LD signals for transitions oriented more or less perpendicular to the plane of the trimer whereas transitions that lie in the plane of the trimer give rise to a positive LD signal. The positive LD signals are observed at 805 and 825 nm, together with a broad positive band around 790 nm. The characteristic signature of the LD is an intense negative band at 815 nm with a shoulder around 812 nm. The LD signal around 812 nm indicates the composite character of the absorption band labeled as

3. The LD spectrum is similar to the one measured by Vulto et al. [41] except the band around 812 nm which is less pronounced in [41]. The absorption and LD band shapes at 825 nm are almost identical, which provide further evidence to the idea that this band originates from a single BChl [39].
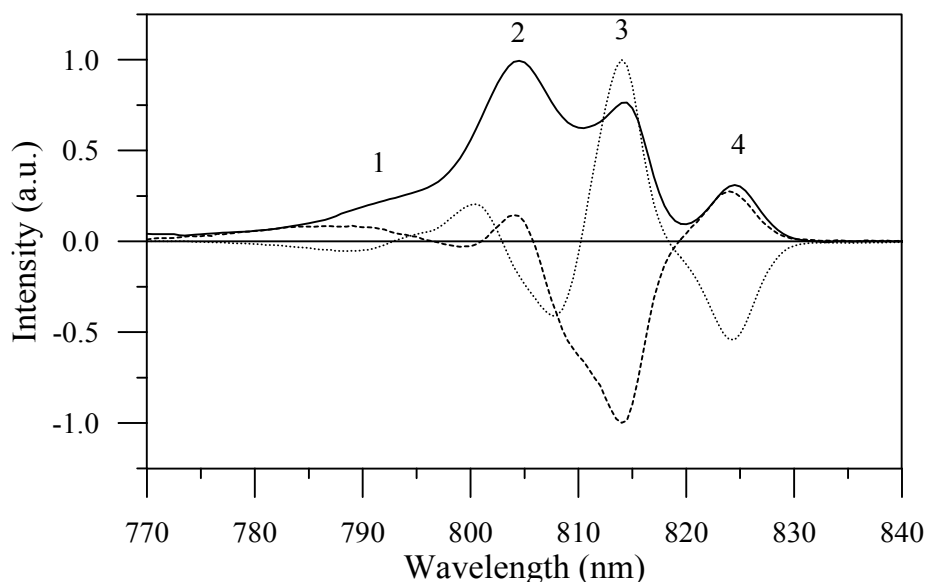

Figure 4.4. The ABS (solid lines), LD (dashed lines) and CD (dotted lines) spectra of the FMO complex from *Cb. tepidum* at 4 K. Each spectrum is normalized its own maximum.

The CD spectrum has positive bands at 802 and 815 nm and negative bands at 790, 810 and 825 nm. A composite character under absorption band labeled as 2 is evidenced by the CD subbands around 795 and 805 nm. LD also indicates a composite character between 795 and 805 nm.

As described in section 4.2.2, once the value of $P_2(\cos\beta_\mu)$ is known one can construct $\Delta A^{mol}(\lambda)$, $A_c(\lambda)$ and $A_a(\lambda)$. $P_2(\cos\beta_\mu)$ is calculated to be between -0.31 and -0.26 for the lowest excited stated of the FMO from *Pc. aestuarii* [86]. The variation of $P_2(\cos\beta_\mu)$ between -0.35 and -0.25 corresponds to a 6^0 difference in the value of (β_μ). For the reasons mentioned one does not expect major differences in the values of (β_μ) and $P_2(\cos\beta_\mu)$ between the two FMO

species. Therefore, we used the same $P_2(\cos\beta_\mu)$ value to construct, $\Delta A^{mol}(\lambda)$, $A_c(\lambda)$ and $A_a(\lambda)$ for *Cb. tepidum*. Figure 4.5 shows the difference in $P_2(\cos\beta_\mu)$ between -0.25 and -0.35 in the constructed A_a and A_c for the FMO complex from *Cb. tepidum*. The spectra show only minor differences upon changing the value of $P_2(\cos\beta_\mu)$.
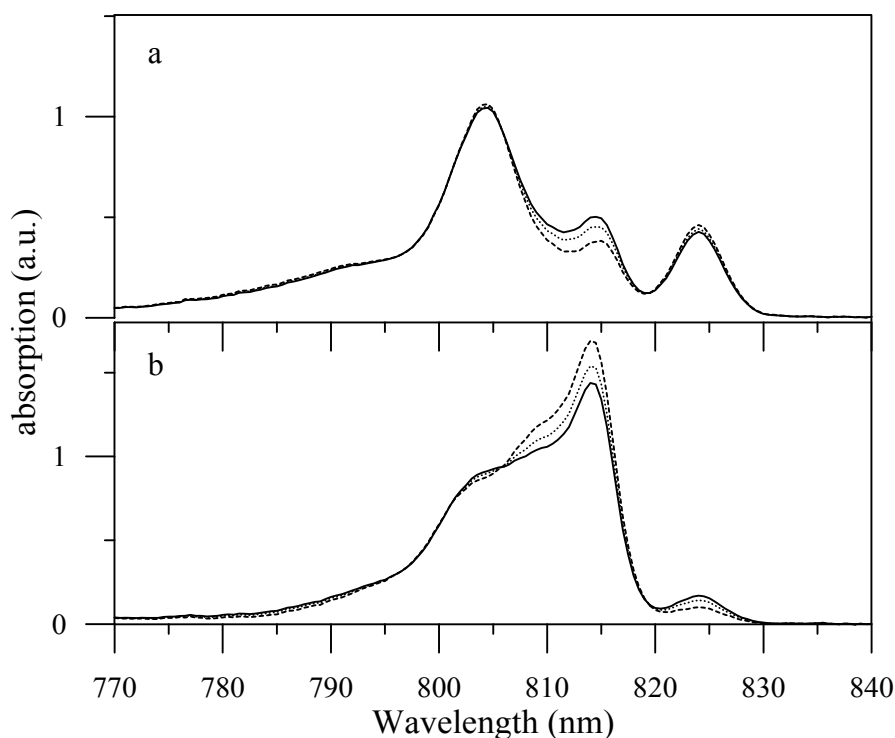

Figure 4.5. The constructed polarized absorption spectra of the the FMO complex from *Cb. tepidum* for light polarized perpendicular to the C_3-axis, $A_a(\lambda)$, (a) and parallel to it, $A_c(\lambda)$, (b). The spectra were constructed from a linear combination of the absorption and LD spectra as explained in the text, assuming that $\langle P_2(\cos\beta_\mu)\rangle$ is equal to -0.25 (solid), -0.29 (dotted) and -0.35 (dashed). Each spectrum corresponds to an isotropic absorption spectrum A_{iso} with a maximum of 1.
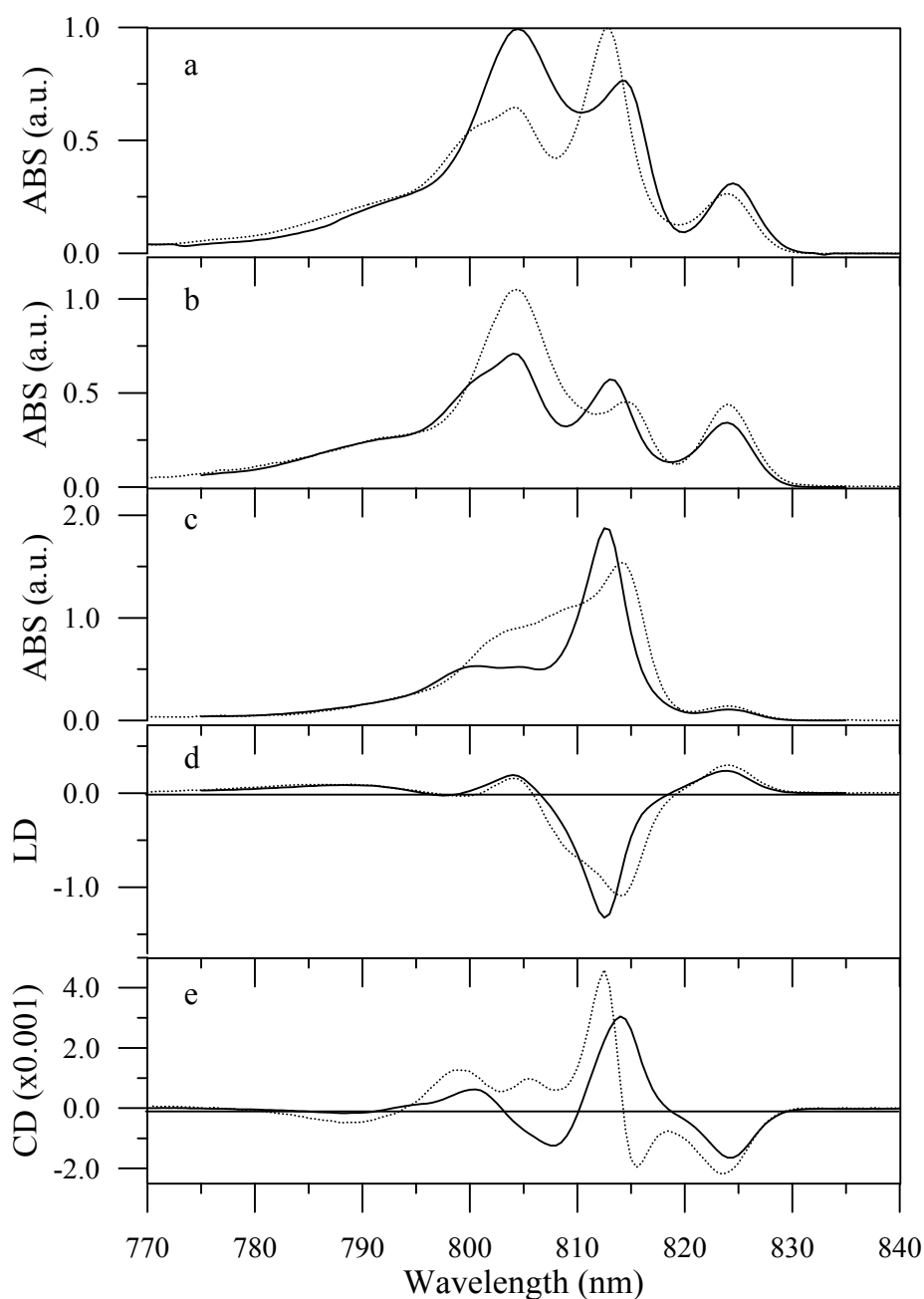
Figure 4.6. Optical spectra of the FMO complexes of *Cb tepidum* (solid) and *Pc. aestuarii* (dashed) at 4 K. (a) ABS spectrum, (b) A_a spectrum, (c) A_c spectrum, (d) LD spectrum and (e) CD spectrum. All spectra are scaled relative to the corresponding ABS spectrum with an absorption maximum of 1. *Pc aestuarii* data are taken from reference [86].

In Figure 4.6, ABS, LD, CD, A_c and A_a spectra of the FMO complexes from the two species, *Cb. tepidum* and *Pc. aestuarii*, are compared. Experimental data of *Pc. aestuarii* are taken from reference [86]. All the spectra of both

complexes were scaled relative to the corresponding ABS spectrum with an absorption maximum of 1.

The long wavelength absorption bands (near 825, 815 and 805 nm) appear at similar positions for both species, but with different relative intensities (Figure 4.6a). The 805 nm band is the most intense one in *Cb. tepidum* on the other hand the 815 nm band exhibits the largest absorption intensity in *Pc. aestuarii*. The overall shapes of the LD spectra from both complexes are similar except for the band around 813 nm where the LD signal of *Pc. aestuarii*. has no shoulder.

The overall shape of A_a spectra of both complexes is similar but the intensity of bands exhibits considerable differences. The absorption strength of the 805 nm band is more intense in *Cb. tepidum* while the 815 nm band is more intense in *Pc. aestuarii*. The major difference in A_c spectra is in the absorption strength of 805 nm band, which is more intense in *Cb. tepidum*. The CD spectra of both complexes are widely different in terms of band intensities and positions. The CD spectrum of *Pc. aestuarii* has more structure compared to *Cb. tepidum*. The 815 and 807 nm bands are the positive CD signals in *Pc. aestuarii*, whereas these bands have negative CD signals in *Cb. tepidum*.

4.3.2 Test Runs

In the following simulations the effects of different broadening mechanisms and the intersubunit interactions are tested. The diagonal and off-diagonal elements of Hamiltonian matrix are constructed by using the parameters of Vulto et al. [41] and the recently available crystal data [20]. The aim of the following simulations is to observe systematic effects of inclusion of different broadening mechanism into the simulations of optical spectra. The results are presented in Figures 4.7-4.11. Each Figure includes the spectra calculated with different broadening mechanisms in separate panels for which the further details of simulation are given in the Figure captions. For comparison, the experimental spectra, the simulation results for the monomer and, the trimer are also given in each panel.

The inclusion of inhomogeneous broadening does not change the overall shapes of the spectra. For each spectrum the bands sharpen compared to the spectrum obtained by using Gaussian synthesis (see panels a and b in Figures 4.7-4.11). The excitonic interactions lead to narrowing of the bands in the Monte Carlo simulations. This effect is known as exchange narrowing [25]. In order to arrive at the bandwidths in the calculations of dressed stick spectra, the width of distributions of the energies has to be taken as 110 cm^{-1} in the Monte Carlo simulation. This effect is more pronounced on the CD spectra. The narrowing effect is clearly visible in the CD spectrum of trimeric model of FMO complex. In addition it is important to note that the bands around 795 and 805 nm split into two contributions. The absorption band at 793 nm splits into two subbands at 790 and 795 nm, and the broad absorption band at 805 nm appear as two bands at 805 and 807 nm. The splitting is observed in A_a but it is not observed in A_c spectra. Also, the negative LD signal at 807 nm becomes more pronounced.

The effects of homogeneous broadening on the calculated spectra are shown in panel c of Figures 4.7-4.11. The inclusion of the homogeneous broadening does not lead to major differences compared to inhomogeneously broadened simulations in panel b of Figures 4.7-4.11. The major effect of homogeneous broadening is to fill out the vibrational tails on the blue side of each spectral band which cause some improvement on the blue side of the simulated spectra.

Finally, the lifetime broadening effect was considered and the simulated spectra are shown in panel d of Figures 4.7-4.11. The blue part of the simulated spectra has been affected. The band intensities decrease especially on the blue side of the spectra upon including the lifetime broadening. Moving to the higher energies the spectra are affected more by the lifetime broadened homogeneous line shape. The high-energy transitions are broadened more than the low-energy ones. This is consistent with the observations that at low temperatures the FMO complex has fast downhill excitation energy relaxation characteristics towards the lowest exciton state [40, 87, 95] and this leads to shorten the lifetime and broadens the high-energy transitions more than the low-energy transitions.
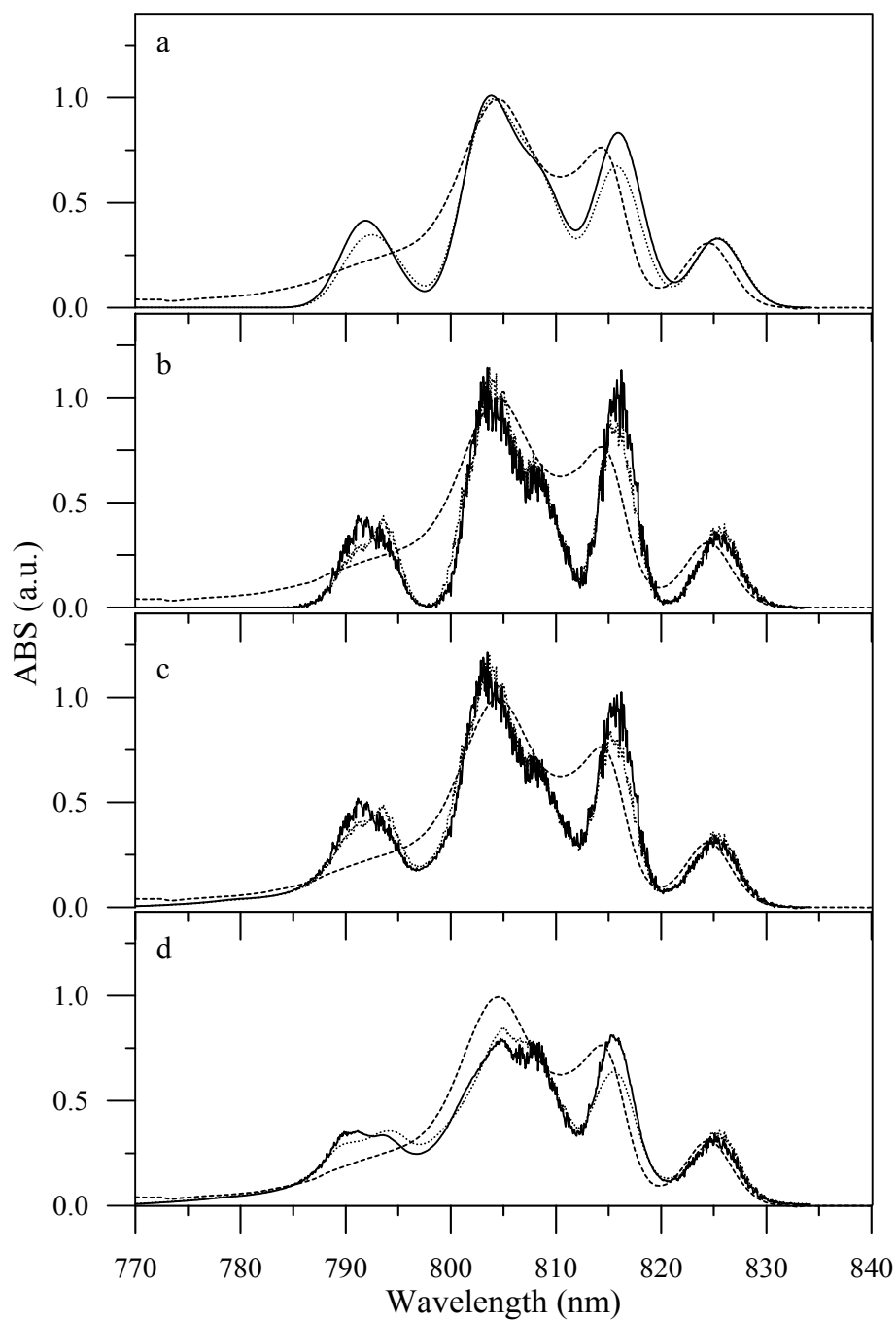
Figure 4.7. Simulated ABS spectra of monomer (solid) and trimer (dotted) models by using parameters of reference [41]. For comparison experimental ABS spectrum (dashed) at 4 K is also shown. Simulated spectra are scaled to the lowest energy experimental ABS peak. (a) The excitonic spectrum is convoluted with a Gaussian line shape with fwhm of 80 cm^{-1}. (b) Monte Carlo simulation by using IDF with a fwhm of 80 cm^{-1}. (c) Monte Carlo simulation and homogeneous line shape. (d) Monte Carlo simulation and lifetime broadened homogeneous line shape.

Figure 4.8. Simulated A_c spectra of monomer (solid) and trimer (dotted) models by using parameters of reference [41]. For comparison experimental A_c spectrum (dashed) at 4 K is also shown. Simulated spectrum is scaled with the same scaling factor corresponding to that of the ABS simulation in Figure 4.7. (a) The excitonic spectrum is convoluted with a Gaussian line shape with fwhm of 80 cm^{-1}. (b) Monte Carlo simulation by using IDF with a fwhm of 80 cm^{-1}. (c) Monte Carlo simulation and homogeneous line shape. (d) Monte Carlo simulation and lifetime broadened homogeneous line shape.
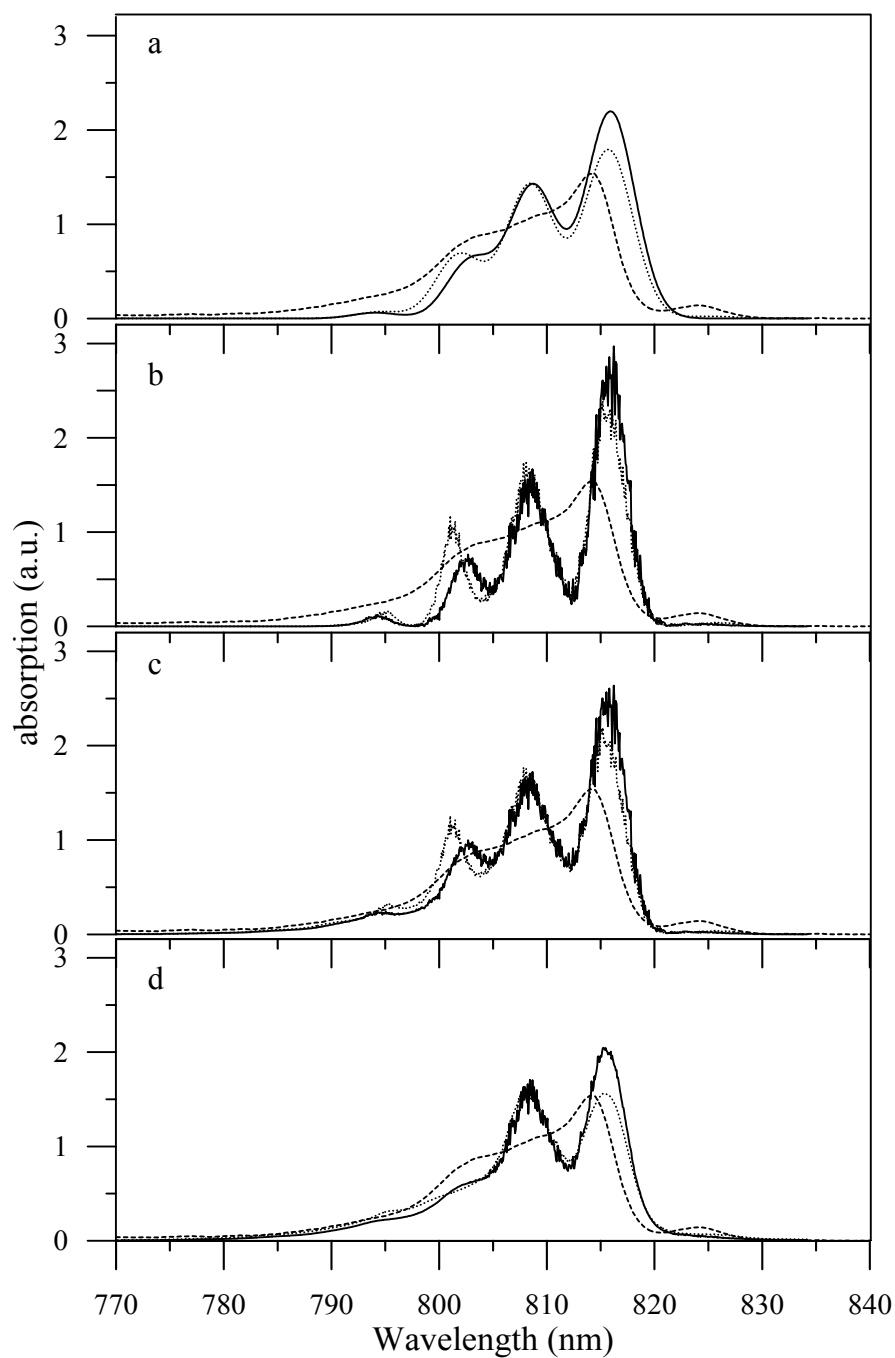
Figure 4.9. Simulated A_a spectra of monomer (solid) and trimer (dotted) models by using parameters of reference [41]. For comparison experimental A_a spectrum (dashed) at 4 K is also shown. Simulated spectrum is scaled with the same scaling factor corresponding to that of the ABS simulation in Figure 4.7. (a) The excitonic spectrum is convoluted with a Gaussian line shape with fwhm of 80 cm^{-1}. (b) Monte Carlo simulation by using IDF with a fwhm of 80 cm^{-1}. (c) Monte Carlo simulation and homogeneous line shape. (d) Monte Carlo simulation and lifetime broadened homogeneous line shape.
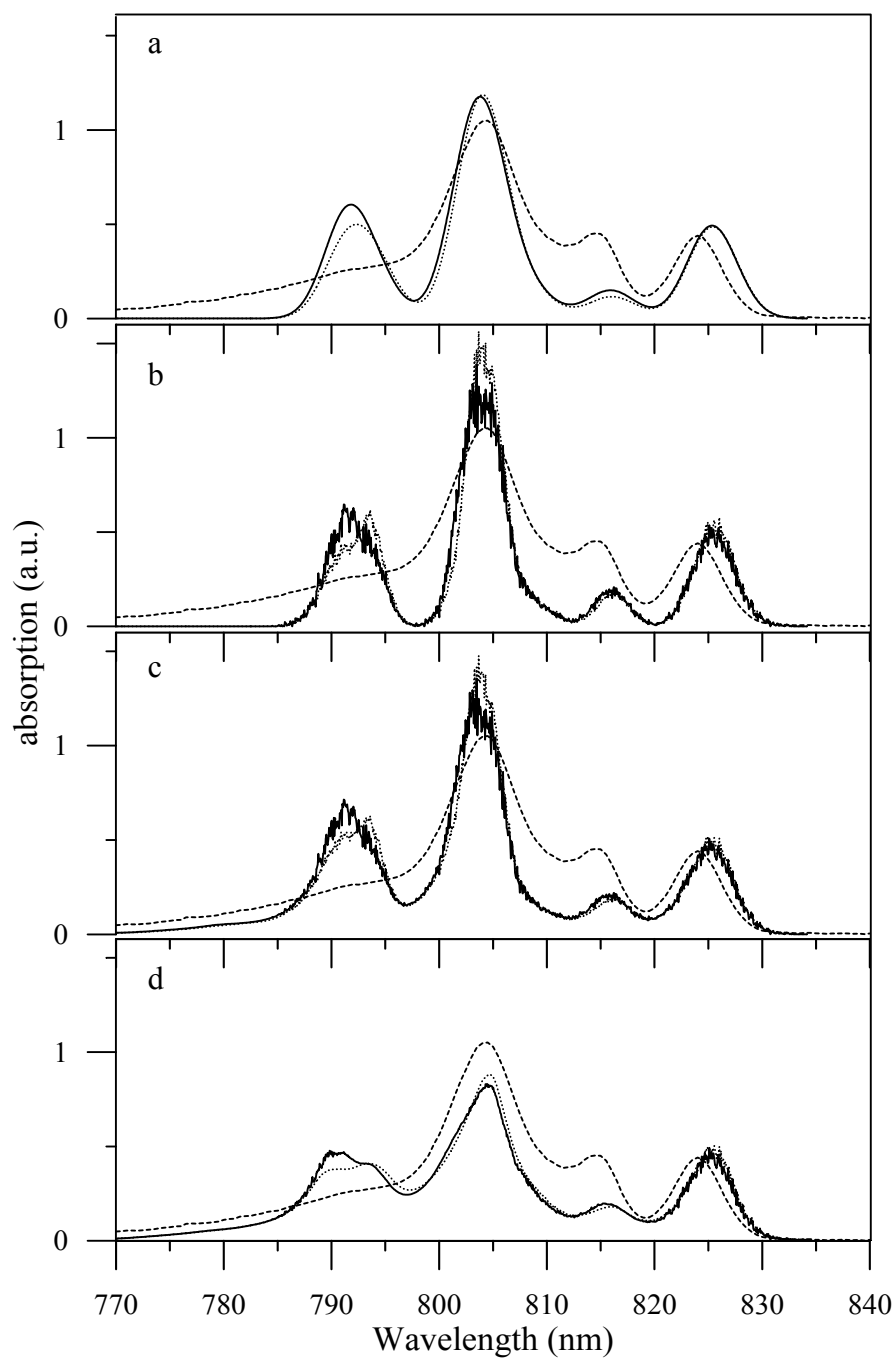
Figure 4.10. Simulated LD spectra of monomer (solid) and trimer (dotted) models by using parameters of reference [41]. For comparison experimental LD spectrum (dashed) at 4 K is also shown. Simulated spectrum is scaled with the same scaling factor corresponding to that of the ABS simulation in Figure 4.7. (a) The excitonic spectrum is convoluted with a Gaussian line shape with fwhm of 80 cm^{-1}. (b) Monte Carlo simulation by using IDF with a fwhm of 80 cm^{-1}. (c) Monte Carlo simulation and homogeneous line shape. (d) Monte Carlo simulation and lifetime broadened homogeneous line shape.
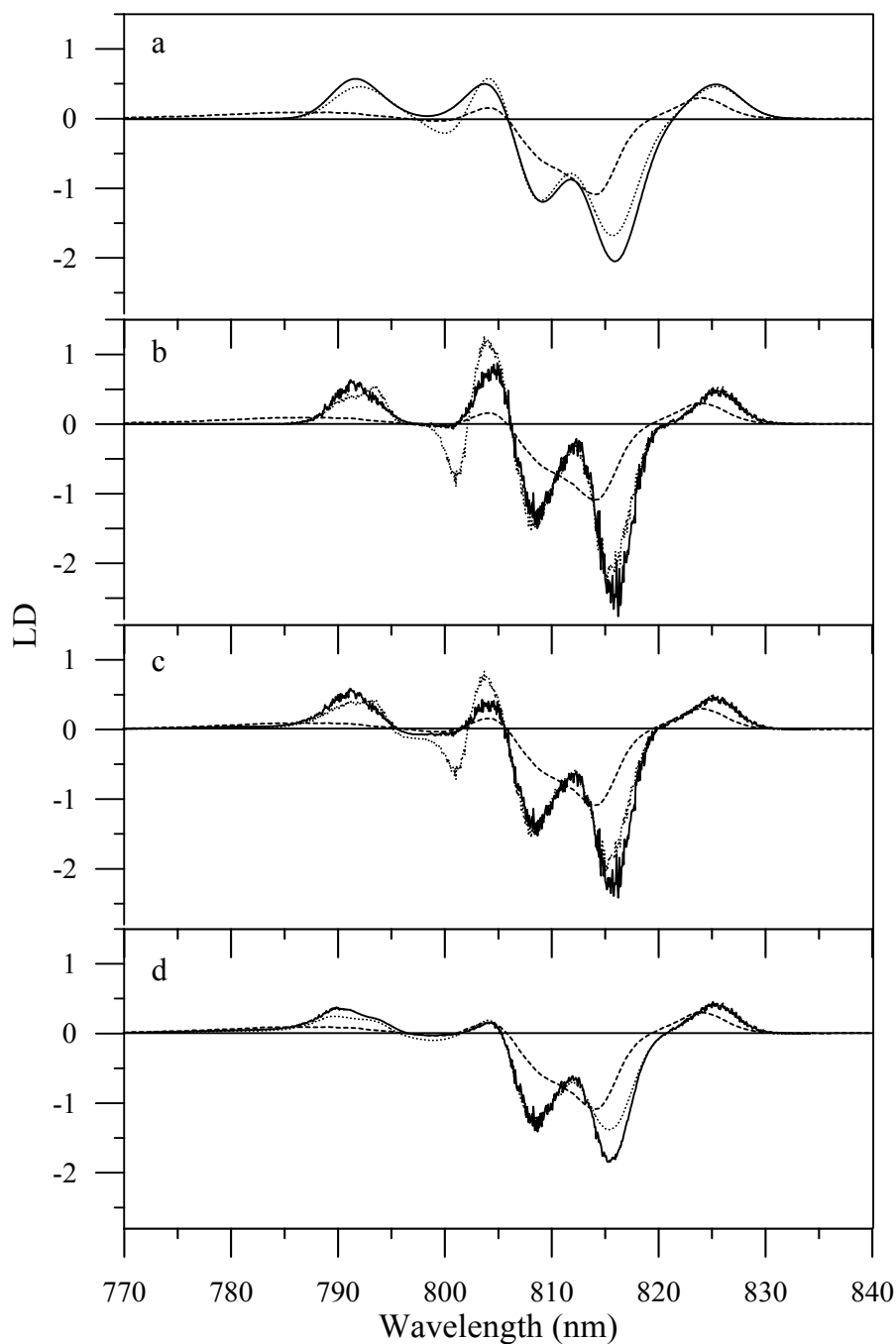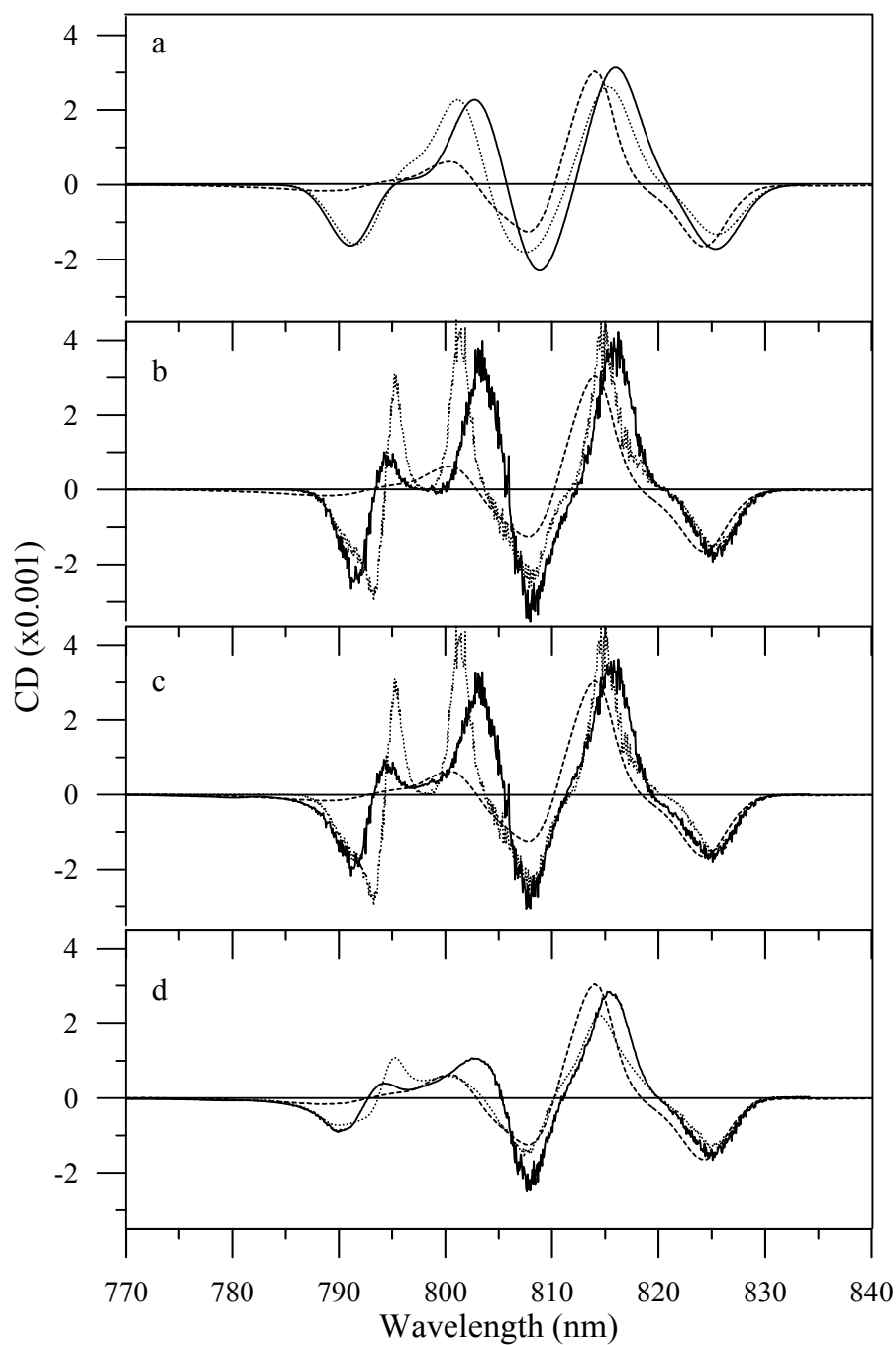
Figure 4.11. Simulated CD spectra of monomer (solid) and trimer (dotted) models by using parameters of reference [41]. For comparison experimental CD spectrum (dashed) at 4 K is also shown. Simulated spectrum is scaled with the same scaling factor corresponding to that of the ABS simulation in Figure 4.7. (a) The excitonic spectrum is convoluted with a Gaussian line shape with fwhm of 80 cm^{-1}. (b) Monte Carlo simulation by using IDF with a fwhm of 80 cm^{-1}. (c) Monte Carlo simulation and homogeneous line shape. (d) Monte Carlo simulation and lifetime broadened homogeneous line shape.
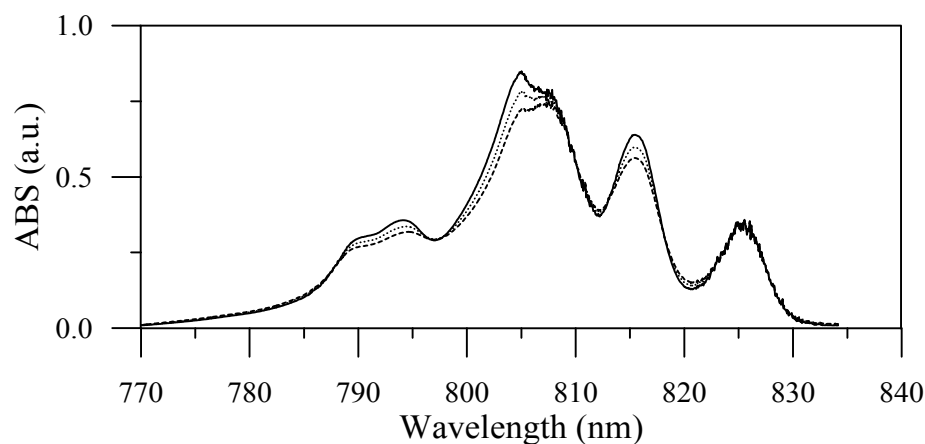
Figure 4.12. Simulated ABS spectra at three different values of γ_0; 3000 ps^{-1} (solid), 4000 ps^{-1} (dotted) and 5000 ps^{-1} (dashed) with the parameters of reference [41]. Simulations include inhomogeneous and lifetime broadened homogeneous line shape.

Figure 4.12 shows the effect of ratescale (γ_0) on the simulated ABS spectrum. The intensity of the bands (≤ 815 nm) decreases and gets broader upon increasing the ratescale from 3000 ps^{-1} to 5000 ps^{-1}. Similar effects are also observed for the other spectra (results are not shown). This is an expected result of using equation (1.30) that taking larger ratescale decrease the lifetime of the excitonic state and increases the homogeneous line width.

The difference between the spectra simulated using the monomeric and trimeric complexes of FMO is subtle (see Figures 4.7-4.11). The overall shape of the two simulations for all the spectra considered is very similar. The largest differences are observed in the absorption strengths of 792 nm and 815 nm bands. CD spectrum is seen to be more sensitive to the intersubunit interactions. The band intensities of CD spectra show larger fluctuations compared to ABS, A_a, A_c, and LD spectra and exhibit significant shift to the blue upon including intersubunit interactions. As a general trend, even though the intersubunit interactions are much smaller than the intrasubunit interactions, we observed changes in the band intensities with a shift to the blue upon including intersubunit interactions.

90

Note that the simulations presented in panel a of Figures 4.7-4.11 have differences compared to the one presented by Vulto et al. [41]. These differences are due to the use of the recently available crystal data [20] of *Cb. tepidum* which has dissimilarities compared to the model of previously determined using crystals in a different space group [23]. The largest differences between two models are reported for BChls 1, 2, and 5. The change in crystal data lead to changes in magnitude of interactions and changes in orientation of dipoles lead to differences in polarized spectra, i.e., the interaction energy between BChl 1 and 2 decreases ~17 %. In general, changes in exciton interactions produce comparable changes in both absorption intensities and peak separations [76], such as are observed here.

Now, comparing simulations with the experiments shows few problems associated with the parameters of Vulto et al. [41]. The overall shape of ABS simulation in panel d of Figure 4.7 is reasonable but still has discrepancies with the experiment. The absorption band at 790 nm absorbs more than the experiment and 805 nm less than the experiment. The 805 nm band also splits in to two subbands. In A_c simulation, in panel d of Figure 4.8, the 807 and 815 nm bands absorb much more than experiment and 815 nm band is red shifted. The 790 nm band absorbs more than experiment and 805 and 815 nm bands absorb less than experiment in A_a simulation shown in panel d of Figure 4.9. The 807 and 815 nm are much more intense and broad than experiment LD. The overall shape of CD simulation is reasonably good. The 815 and 825 nm bands are red shifted. The 800 nm and 807 nm CD signals are larger than experiment. Note that in the simulations we took the ratescale used by Wendling et al. [86] and did not attempt to improve simulations by varying ratescale only. The blue side of the ABS spectrum can be improved by using a larger ratescale, but then the intensity of 805 nm band will become too small in amplitude.

Summarizing; taking into account different broadening mechanisms explicitly lead to some fine structure that is not observed for the dressed stick spectra and inclusion of the inter-subunit interactions lead to considerable changes.

4.3.3 Control over the Simulations towards Satisfactory Fits

In view of the results we have presented above, it is necessary to reinvestigate the simulations of optical spectra of FMO complex by taking the different broadening mechanisms and intersubunit interaction into account with recently available crystal data [20].

We next try to improve simulations of FMO complex from *Cb. tepidum* following the observations summarized above. We take the site energy set of Vulto et al. [41] and the ratescale value of Wendling et al. [86] as the starting point. We then vary the site energies, the ratescale and the dipole strength to optimize the simulations. In the calculations, all 21 BChls belonging to three different subunits are considered. The simulations include all three different broadening effects.

In assigning the site energies we have the following; BChl 3 is fixed to be the red most pigment; the BChls 2, 5, and 6, whose dipole moment directions are almost perpendicular to the C_3 symmetry axis, should be contributing mostly to the bands around 800-805 nm which have positive LD signals. The largest contribution to the strong LD signal around 813 nm should be from the BChls 1, 4, and 7 whose dipole moments are more or less parallel to the C_3 symmetry axis (see Figure 1.8). One may refer to [41] and [83] for more details on this reasoning. The rate limiting step in determining the site energies of the BChls has been in relation to the choice of the relative positions of the site energies of the BChl 1 and 2 as we shall explain below.

In Figures 4.13-4.17, we present the ABS, A_c, A_a, LD and CD simulations together with the experiments for three different site energy sets (hereafter, the model A, the model B and the model C) given in Table 4.1. These models differ in the choice of the site energies for the BChls 1 and 2: model A ($E_1 < E_2$), model B ($E_1 > E_2$) and model C ($E_1 = E_2$).

The blue region characteristics of ABS spectra are reasonable in all models as shown in Figure 4.13. The 805 nm band is broader than experiment and split in two sub-bands (805 and 808 nm) in models A and B. In model C, this band is

narrower and absorbs more than experiment. In all models the 815 nm band absorbs less than experiment.

Table 4.1. Parameters used in the simulations of Figures 4.13-4.17.

	Site Energies (cm^{-1})		
BChl no	Model A	Model B	Model C
1	12458	12535	12546
2	12515	12438	12546
3	12170	12170	12170
4	12313	12313	12313
5	12558	12538	12558
6	12498	12508	12498
7	12443	12433	12443
IDF (cm^{-1})	90		
γ_0 (ps^{-1})	4350		
Dipole strength (debye^2)	32.6		

The blue region of A_a spectra is also reproduced successfully in all models as shown in Figure 4.14. The 805 nm band absorbs less than experiment in model A, is broader than experiment in model B due to splitting as in ABS simulation and fits very well in model C. None of the models could reproduce the 815 nm band properties.

The simulated A_c spectra for all models are shown in Figure 4.15. Compared to the ABS and A_a simulation the blue part of the spectra is improved

moderately in model A and C. In model B, this region is less satisfactory. The 805 nm band absorbs more than experiment in all models and also shifted to 800 nm in model C. The 815 nm band is reproduced successfully in all models.

The characteristic red-most-positive LD signal at 825 nm is reproduced in all models with the choice of BChl 3 as the red-most pigment. The main difficulty with all models is in relation to the shoulder at 812 nm. This band is either more pronounced or less pronounced than the experiment depending on the site energy choice of BChl 1 and 2. In our simulations the transition around 808 nm is mainly controlled (contributed) by the BChl 1 and BChl 2 interaction (see Table 4.2). When we change the magnitude of site energies of BChl 1 and BChl 2 relative to each other (e.g. E1>E2 or E1<E2), the respective magnitude of the contributions of BChl 1 and BChl 2 to the 808 nm state in model A and B also changed. Since BChl 1 (2) gives negative (positive) LD signal, depending on the magnitude of the contribution of each BChls to that particular state, the 812 nm LD signal is either more or less pronounced (see Figure 4.16). In addition to this, in model B, 785 - 805 nm region and in model C positive LD signal at 805 nm could not be reproduced.

The overall shape of CD spectra is well reproduced in model A presented in Figure 4.17. All CD bands are reproduced but their amplitudes are weaker than the experimental values. In model B red part of the CD spectrum is reproduced very well. While, 805 nm band splits into two sub-bands (805 and 803 nm) and 800 nm band is shifted to blue. In model C, all bands except the lowest one, are shifted to blue.

The overall idea that one get from the results of this subsection is: better fits can be achieved through a model that takes a combination of the models A, B and C.

Figure 4.13. Comparison of the simulated ABS spectra (solid) to the experimental data (dotted). Simulations are carried out for three different models (A, B, and C). Simulated spectra include all three different broadening mechanisms and the model parameters are given in Table 4.1.

Figure 4.14. Comparison of the simulated A_a spectra (solid) to the experimental data (dotted). Simulations are carried out for three different models (A, B, and C). Simulated spectra include all three broadening mechanisms and the model parameters are given in Table 4.1.
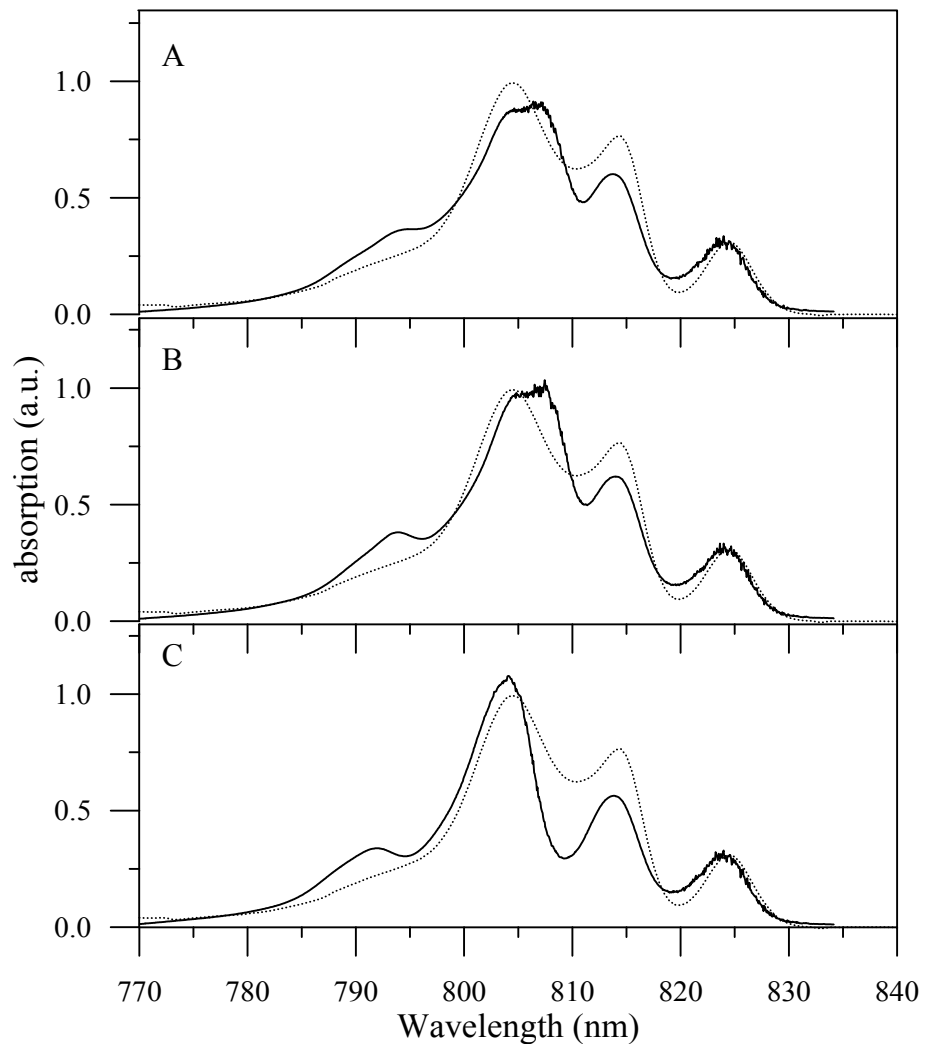
Figure 4.15. Comparison of the simulated A_c spectra (solid) to the experimental data (dotted). Simulations are carried out for three different models (A, B, and C). Simulated spectra include all three different broadening mechanisms and the model parameters are given in Table 4.1.

Figure 4.16. Comparison of the simulated LD spectra (solid) to the experimental data (dotted). Simulations are carried out for three different models (A, B, and C). Simulated spectra include all three different broadening mechanisms and the model parameters are given in Table 4.1.
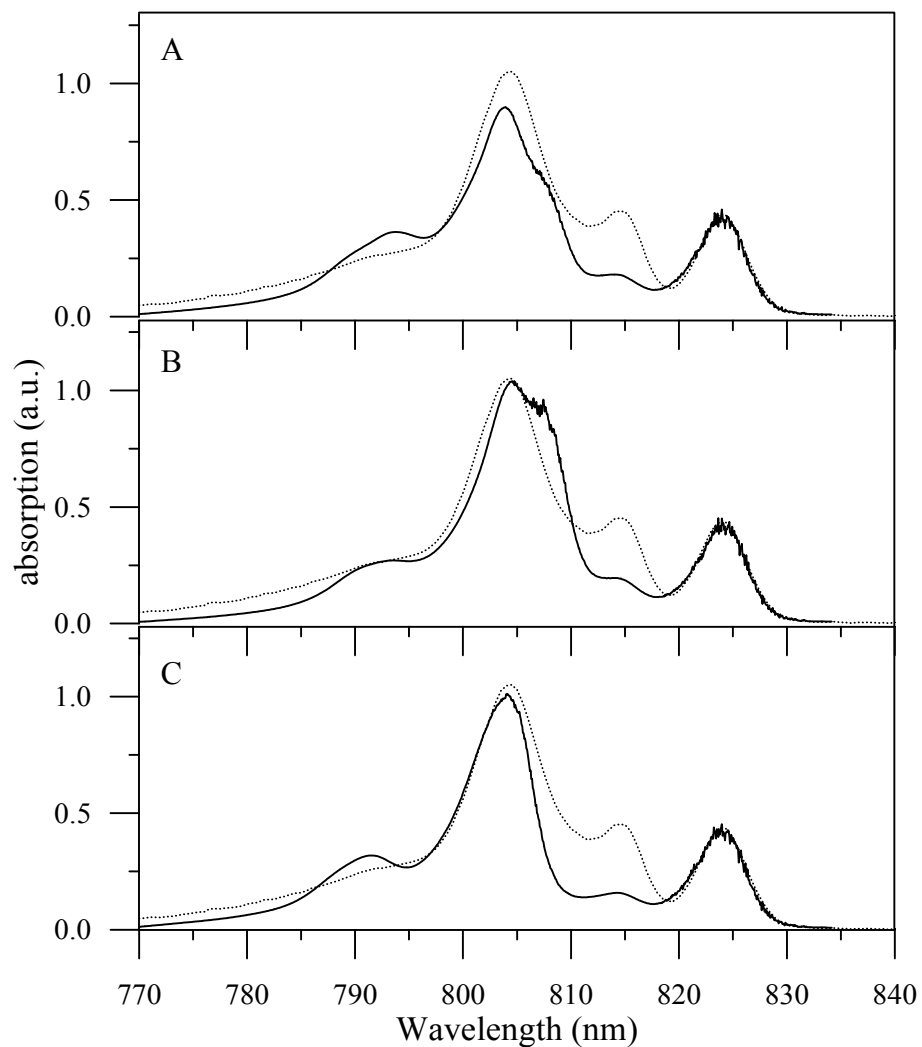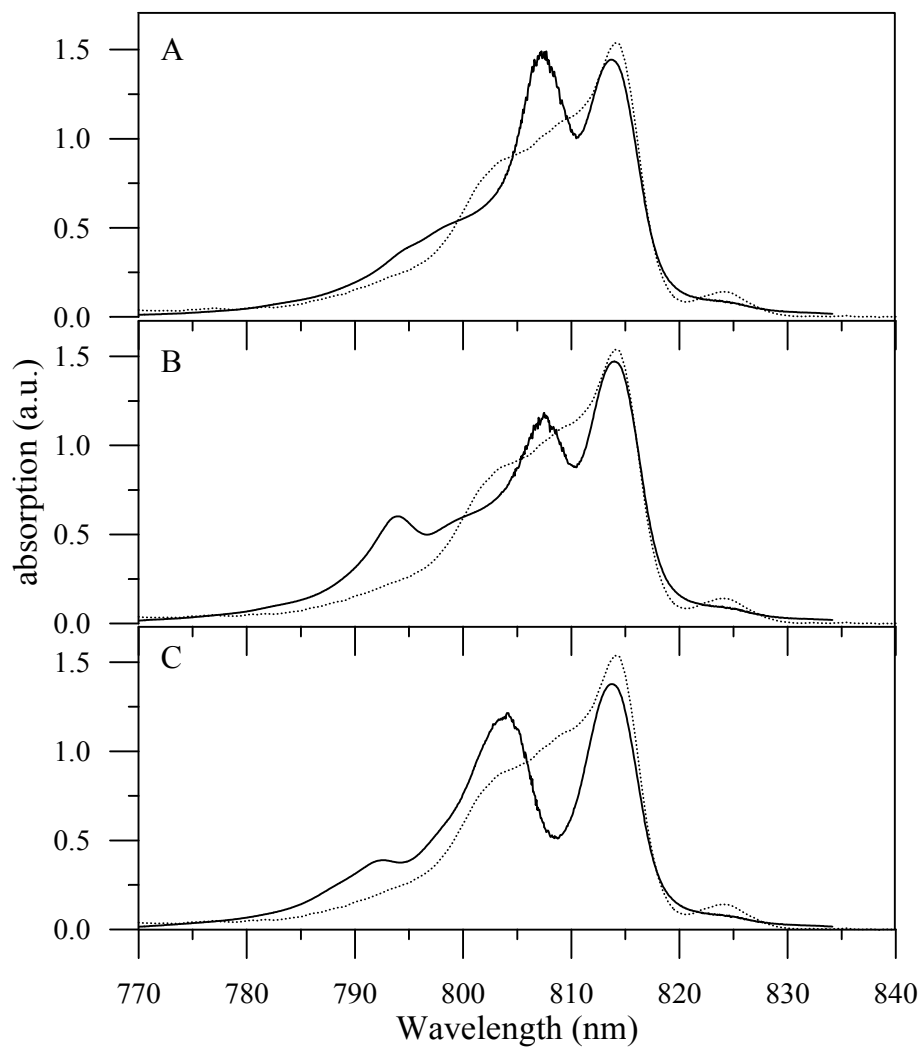
Figure 4.17. Comparison of the simulated CD spectra (solid) to the experimental data (dotted). Simulations are carried out for three different models (A, B, and C). Simulated spectra include all three different broadening mechanisms and the model parameters are given in Table 4.1.
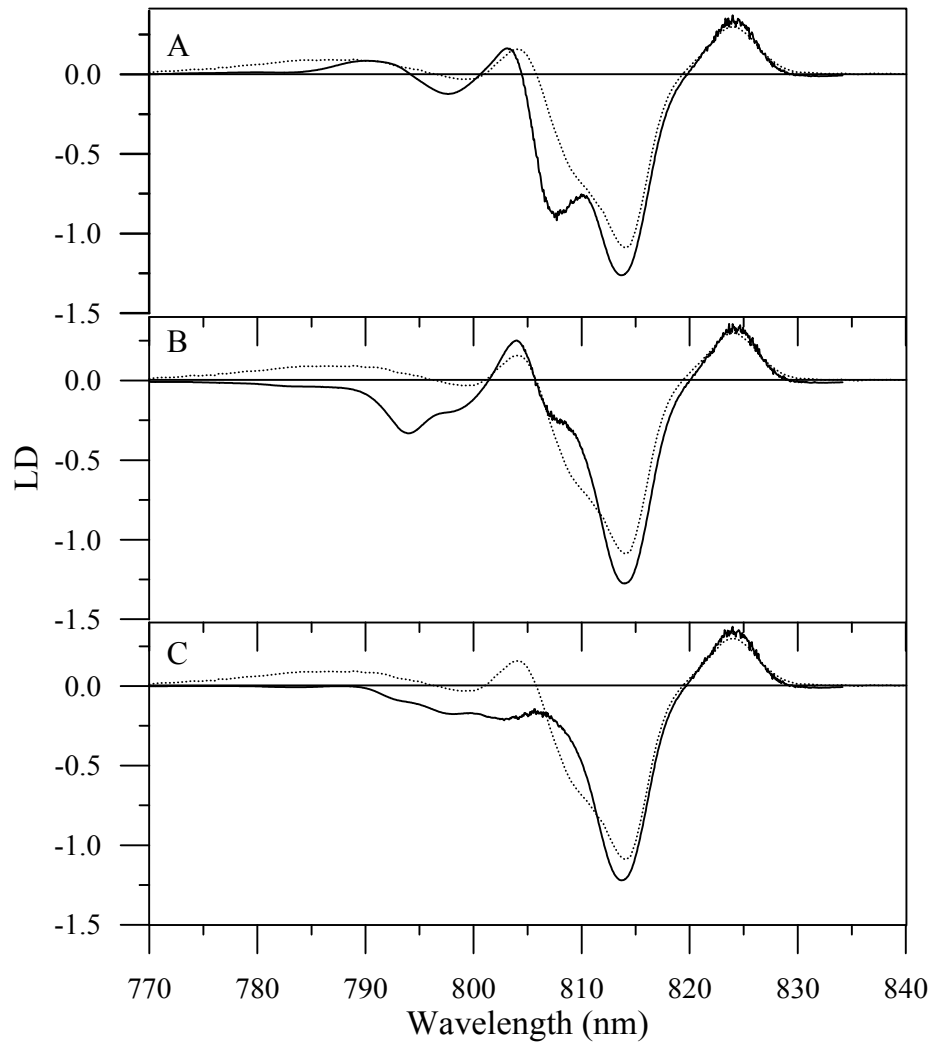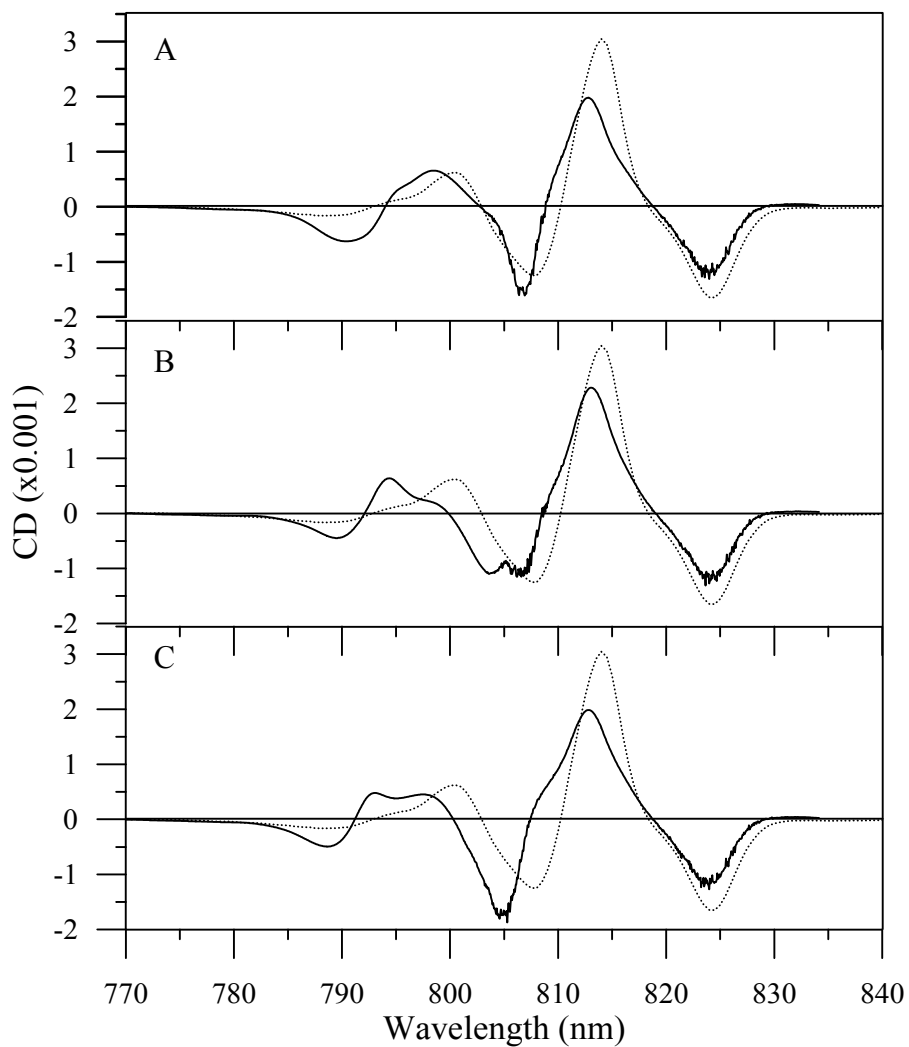
Table 4.2. Contributions of each BChl to the occupation characteristics of the monomeric excited states in Models A, B and C. The numbers in parentheses indicate the percentage contribution of the respective BChl to the occupation probability.

Model A		Model B		Model C	
Excited state energy (nm)	BChl #	Excited state energy (nm)	BChl #	Excited state energy (nm)	BChl #
823.8	3 (83)	823.9	3 (82)	823.8	3 (83)
814.2	4 (60), 7 (17)	814.4	4 (59), 7 (17)	814.2	4 (60), 7 (17)
807.6	1 (62), 2 (35)	807.9	1 (28), 2 (69)	804.2	6 (53), 7 (17)
804.1	6 (55), 7 (20)	804.1	6 (49), 7 (24)	803.1	1 (45), 2 (44)
801.5	5 (25), 7 (59)	802	5 (30), 7 (53)	801.4	5 (25), 7 (57)
794.2	1 (36), 2 (58)	793.8	1 (67), 2 (26)	791.2	5 (47), 6 (17)
790.8	5 (56), 6 (30)	791.2	5 (50), 6 (35)	790.1	1 (35), 2 (36)

4.3.4 Best Fits

Upto now we have assumed that (also a common assumption in all the previous models for the trimeric FMO complex), the symmetry-related BChl a molecules of different subunits have the same site energy and experience the same IDF. Being symmetry-related does not necessarily justify this assumption and it can be considered as an assumption made for convenience. In fact one could argue against this assumption. For example, some of the BChls may exhibit different conformational properties in different subunits, which may lead to differences in the electronic properties of that BChls or the motion of proteins may be different from one subunit to other which can change the pigment-protein interactions in different subunits.

In the FMO complex the BChls1 and 2 are exposed on the surface of each of the protein subunits forming the trimer and the other BChls are buried in the core of the protein. Therefore, it is conceivable that these two BChls are more susceptible to the changes in their site energies, IDFs and intermolecular interactions (in fact the strongest pairwise interaction of the BChls 1 and 2 are with each other), although these possibilities could not be excluded for the other BChls. We next introduced these possibilities into the modeling and we apply them to the BChls 1 and 2.

Figure 4.18 shows the best fit (hereafter, the BChl1_2 model) obtained by assigning different site energies of BChl 1 and 2 belonging to different subunit in the trimer. When the site energies are chosen in this way, the simulations of the corresponding experimental data are in better agreement than the previous approach. Parameters of the BChl1_2 model are given in Table 4.3.

Table 4.3. Parameters used in simulations of Figure 4.18.

BChl no	Site Energies (cm^{-1})		
	Subunit 1	Subunit 2	Subunit 3
1	12420	12536	12525
2	12525	12536	12420
3	12163	12163	12163
4	12313	12313	12313
5	12553	12553	12553
6	12493	12493	12493
7	12443	12443	12443
IDF (cm^{-1})	90		
γ_0 (ps^{-1})	3750		
Dipole strength ($debye^2$)	32.6		

The overall shape and size of ABS simulation fits almost perfectly. The splitting of 805 nm is corrected and additionally the amplitude of this band fits perfectly. The amplitude of 815 nm band improved but it still absorbs less than experiment. The red-most band and the blue region of the simulated spectra are reproduced rather satisfactorily.

In simulations of A_a, A_c and LD, the corrected A_a, A_c, and LD of the experimental spectra which are scale with respect to the ABS spectra are shown for $P_2(\cos \theta)$ = -0.29 and -0.33. As it is seen from the Figures, the simulations and the experiments show better agreement when we choose $P_2(\cos \theta)$ to be equal to -0.33.
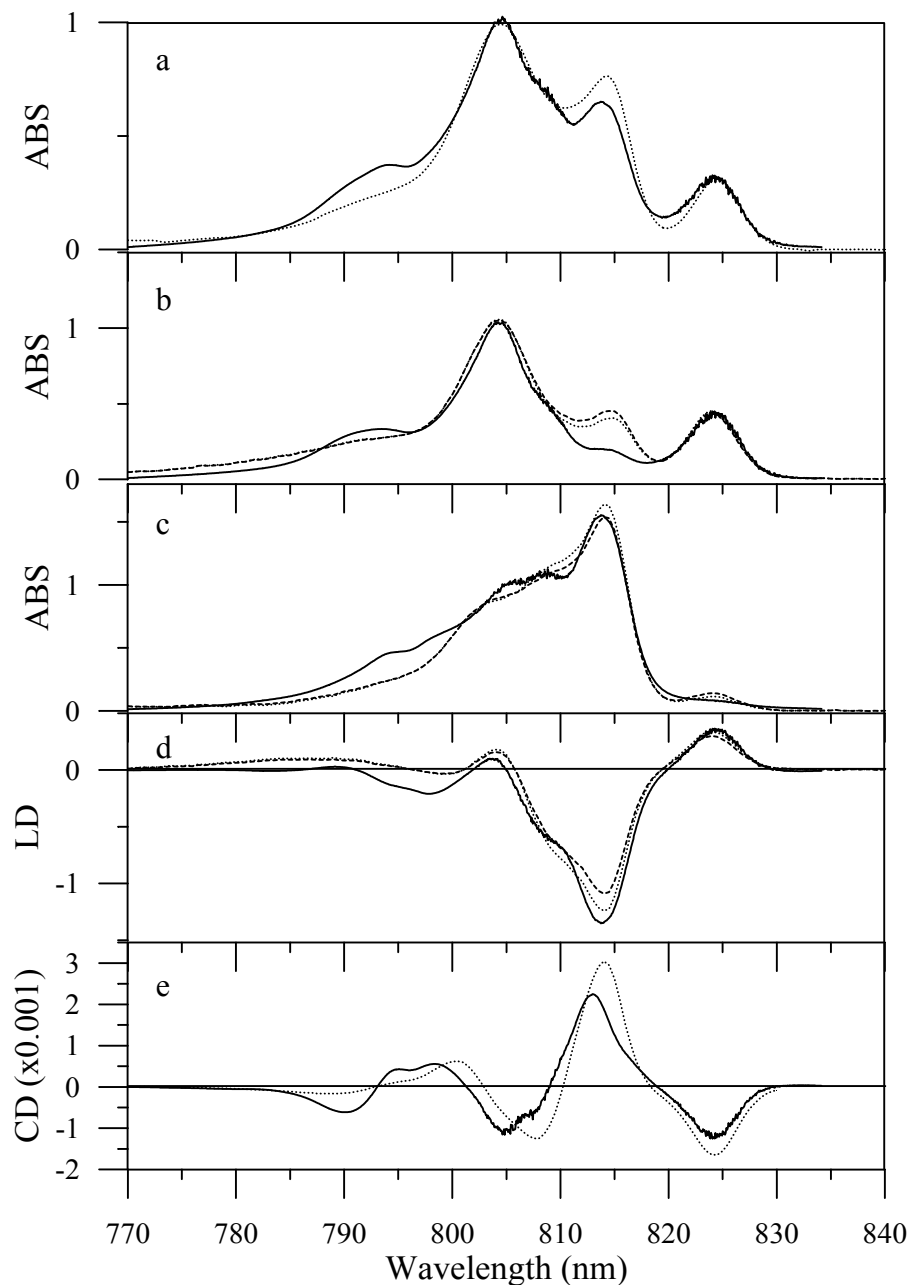
Figure 4.18. Comparison of the simulated ABS (a), A_a (b), A_c (c), LD (d), and CD (e) spectra (solid) to the experimental data (dotted). Simulated spectra include all three different broadening mechanisms and the model parameters are given in Table 4.3. The corrected experimental A_a, A_c and LD are calculated for two values of $P_2(\cos \theta)$; -0.29 (dotted) and -0.33 (dashed).

The shape of simulated CD spectra is in good agreement with the experiment. The positive 825 and 815 nm CD signals are reproduced but the intensities of these bands are less than experiment. On the blue region the simulated CD bands are blue shifted.

The simulations could also be improved if we assign broader site energy fluctuation (IDF) to BChl 1 or 2 with their site energies identical in different subunits. The best fits obtained by assigning different IDF to site energies of BChl 1 and BChl 2 (hereafter, the BChl1 and the BChl2 models respectively) are presented in Figures 4.19 and 4.20 respectively. In Table 4.4, the parameters are given for both models.

Table 4.4. Parameters used in simulations of Figures 4.19 and 4.20.

|	Site Energies (cm^{-1}), IDF (cm^{-1})	
BChl no	BChl1 model	BChl2 model
1	12458, 150	12460, 90
2	12515, 90	12468, 150
3	12163, 90	12170, 90
4	12313, 90	12313, 90
5	12548, 90	12518, 90
6	12488, 90	12513, 90
7	12433, 90	12436, 90
γ_0 (ps^{-1})	4350	
Dipole strength (debye^2)	32.6	

Figure 4.19. Comparison of the simulated ABS (a), Aa (b), Ac (c), LD (d), and CD (e) spectra (solid) to the experimental data (dotted). Simulated spectra include all three different broadening mechanisms and the model parameters are given in Table 4.4.
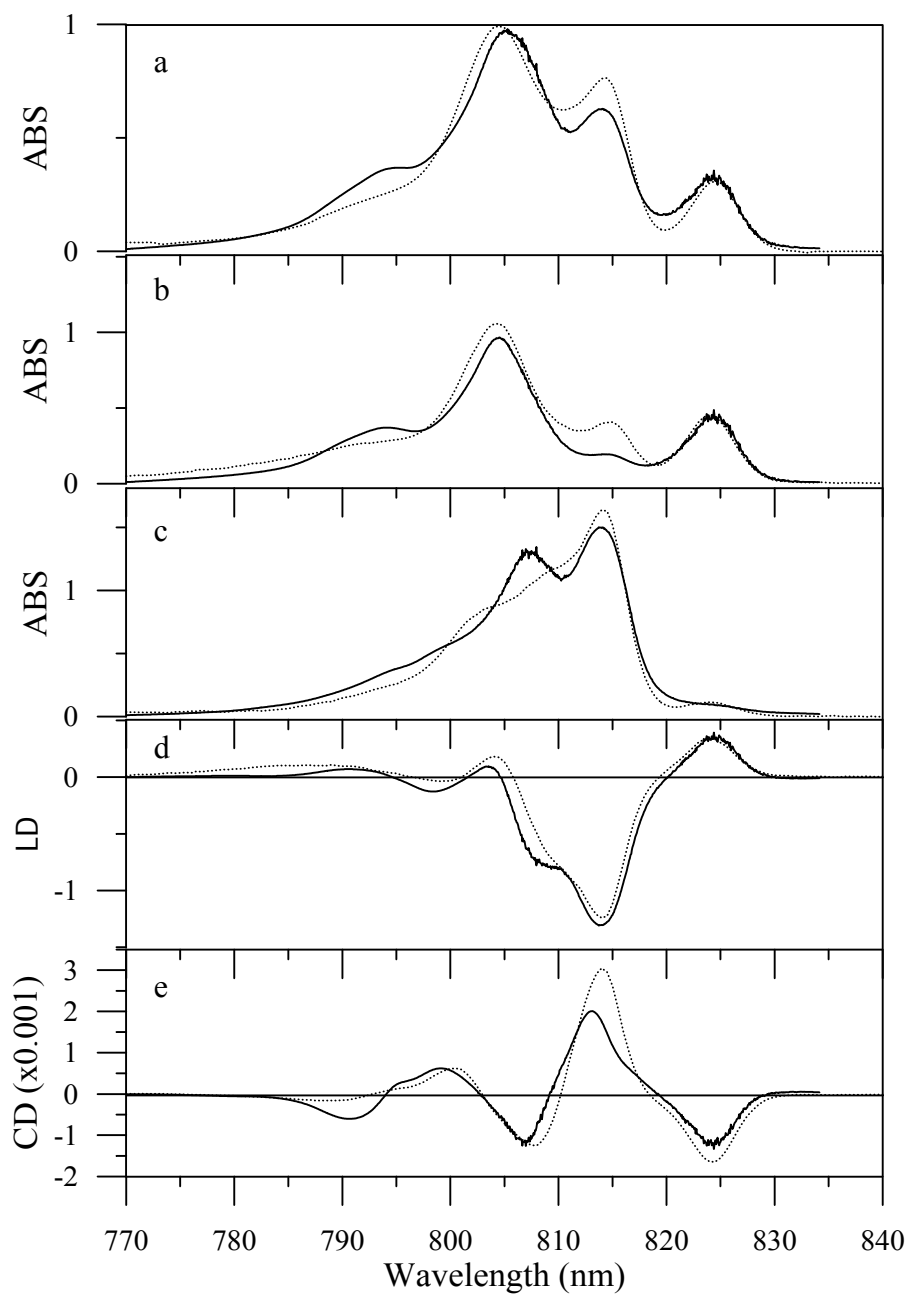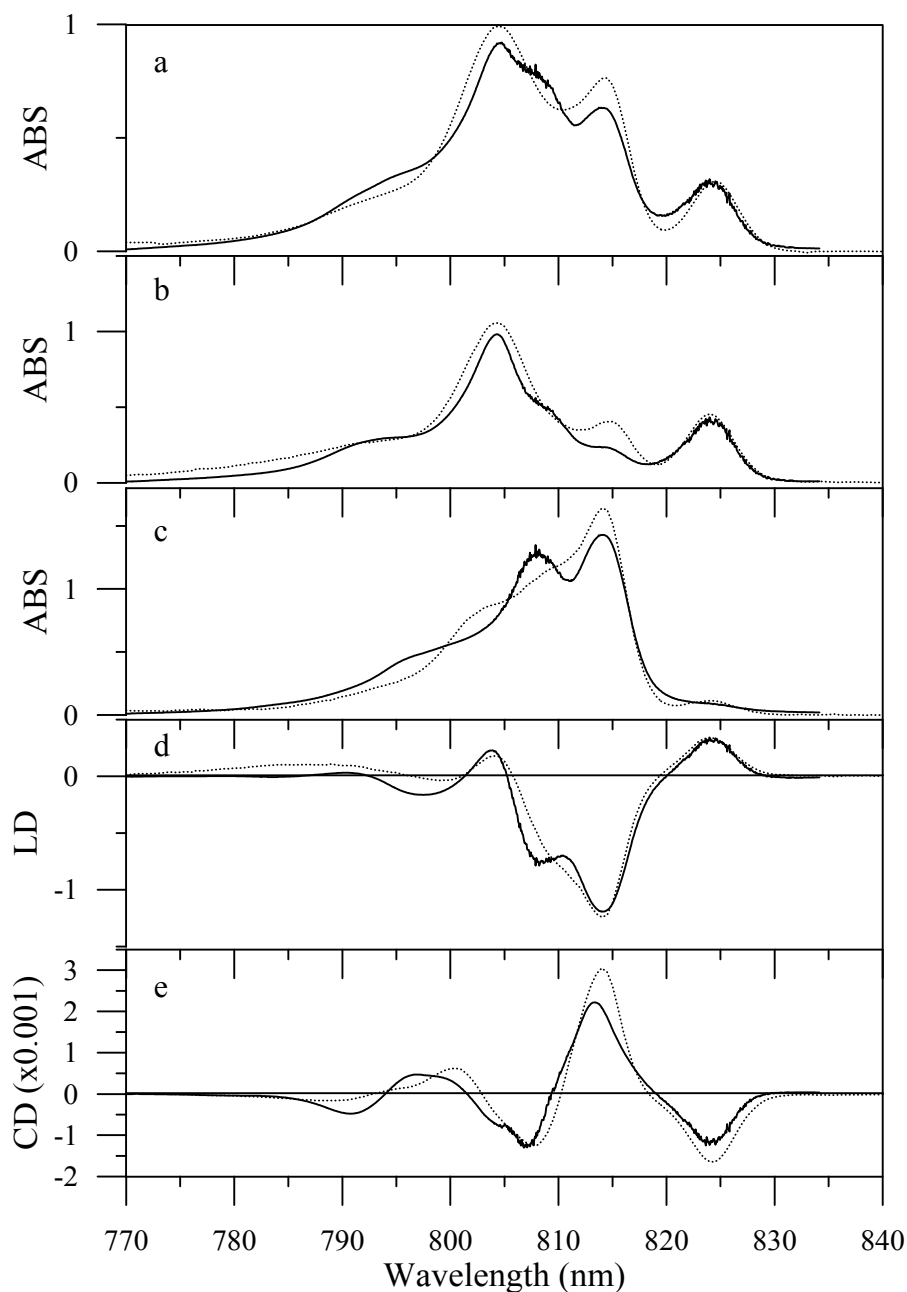
Figure 4.20. Comparison of the simulated ABS (a), Aa (b), Ac (c), LD (d), and CD (e) spectra (solid) to the experimental data (dotted). Simulated spectra include all three different broadening mechanisms and the parameters are given in Table 4.4.

In the BChl1 model the 805 nm band is reproduced reasonably, but this band is broader than experiment. In the both models the overall simulation of A_a spectra did not get affected. The simulation of the 805 nm band of A_c spectra could be improved moderately and still absorb more than experiment. The problematic

band at 808 nm of LD spectra is somewhat improved in both models. In the simulation of CD spectra the prominent features are reproduced in both models. Even though the simulations improved, overall comparison of the simulations with respect to the BChl1_2 model is rather poor.

We would also like to note that the calculated spectra for off-diagonally disordered ensembles show similar features as those for diagonal disordered ensembles (the results are not shown).

Summarizing, through the simultaneous simulations of ABS, A_a, A_c, LD and CD, we have concluded that the experimental spectra can be satisfactorily simulated by choosing different (broader) IDF to either BChl 1 or BChl 2 or by assigning different site energies to the BChl 1 and 2 belonging to different subunit in the trimeric FMO.

4.3.5 Comparison of the Excited State Structure of *Cb. tepidum* and *Pc. aestuarii*

Finally we compare our results (the BChl12 model) with the results of the Wendling et al. [86] obtained for the FMO complex from *Pc. aestuarii*. Table 4.5 shows the delocalization characteristics of both models. It is clear that in *Cb. tepidum* the excited states are more delocalized than in the *Pc. aestuarii*.

In both models the red-most transition has contribution from the BChl 3 of all three subunit. BChl 4 is predominantly contributes to the spectra at the 814 nm in both models. The 814 nm transition in *Cb. tepidum* model is also contributed from BChl 7. The transition around 809 nm is contributed from BChl 1 and 2 in *Cb. tepidum*. The corresponding transition in *Pc. aestuarii* is the transition around 811 nm and also mainly contributed, almost equally, from BChl 1 and 2.

Table 4.5. Contributions of each BChl to the occupation probabilities of the excited state of *Cb. tepidum* and *Pc. aestuarii* .

Cb. tepidum		*Pc. aestuarii*	
Excited state energy (nm)	Contribution (BChl no)	Excited state energy (nm)	Contribution (BChl no)
824.3, 824.2, 824.1	3	823.41*, 823.1	3
814.5, 814.5, 814	4, 7	813.51*, 812.9	4
809.1, 808.8	1, 2	811.62*, 811.58	1, 2
804.7, 804.5, 804.4, 803.9	4, 6, 7 (1), 1, 2, 6 (2), 6 (3)	804.2, 804.12*	6, 7
802.1*, 800.5	5, 7	801.66*, 800.66	6, 7
794.5, 794.3	1, 2	797.88*, 797.58	1, 2
791.7, 791.1*, 790.5	1, 2 (2), 5, 6 (1, 2, 3)	788.19*, 787.96	5, 6

The (*) next to the energy values indicate that the transition is degenerate. The numbers in parenthesis indicate the subunit number.

The excitation around at 804 nm is delocalized over many molecules in *Cb. tepidum*. These molecules are the BChl 4, 6 and 7 of first subunit, the BChl 1, 2 and 6 of second subunit and BChl 6 of third subunit. This is the result of assigning different site energy fluctuation to BChl 1 and 2 of different subunits. In *Pc. aestuarii* BChl 6 and 7 contributed to the 804 nm transition. The transition around 801 nm is mainly contributed from the BChl 5 and 7 in *Cb. tepidum* and BChl 6 and 7 in *Pc. aestuarii*.

The transition around 794 nm is contributed from BChl 1, 2 in both models. The blue most transition, 791 nm, is also show large delocalization characteristics in *Cb. tepidum*. This transition is contributed from BChl 1, 2 of second subunit and BChl 5, 6 of all subunits. The corresponding transition in *Pc. aestuarii* is the transitions around 797 nm and is contributed from BChl 5 and 6.

Although the positioning and orientation of the corresponding BChls are very similar, comparison of the structure of *Cb. tepidum* and *Pc. aestuarii* reveals many structural differences such as the protein environment, the ligand binding, the H-bonding and the conformations of the tetrapyrroles and phytyl chains of the BChls [20, 23]. The most significant differences are observed in the planarity of several BChls and it has been noted that the BChls 2 and 6 are most different. Differences in the planarity of tetrapyyrole, including the position of Mg atom relative to the macrocycle, can influence the electronic states of the BChls [96, 97]. This is consistent with the site energies determined from the simulations of the spectra. Although the out-of-plane distances for the central magnesium atoms of Bchls 3 and 7 are much larger in the *Pc. aestuarii* structure compared to the *Cb. tepidum* structure [20], these two molecules exhibit the similar site energies in both models. When the hydrogen bond lengths of the two FMO complexes are compared, it seems that for all the BChls in the FMO complex of *Cb. tepidum* the hydrogen bonds are weaker than in *Pc. aestuarii* [20, 23]. It is reported for LHI and LH2 of several species of purple bacteria that the Q_y absorption maximum shifts toward lower energy when the degree of hydrogen bonding is enhanced [98, 99].

4.4 Conclusions

In this Chapter the new experimental absorption, LD and CD spectra for the FMO complex of *Cb. tepidum* are presented and the simulations of these spectra within an exciton model, which is more realistic than the ones used previously [41] have been presented.

The major result of this chapter has been that satisfactory simultaneous fits to all three spectra can only be obtained by assigning different site energies to the particular BChls (BChl 1 and BChl 2) in the three different subunits of the complex or different IDF to a particular BChl (BChl 1 or BChl). Some discussion on how to reconcile this result with the reality of such systems is given.

The major contributions by the author have been his participation in the experimental data-taking process and his implementation of the codes provided kindly by Dr. Markus Wendling to carry out the simulations reported above.

This study has been initiated with the purpose of providing a more controlled research towards providing some explanation for an experimental fact. The experimental fact of interest had been the observation of rather distinctive spectral features for the FMO complexes from *Pc. aestuarii* and *Cb. tepidum* despite their very similar structures. The author has provided a comparison of his results with a previous work on *Pc. aestuarii*, but failed to extend his simulations achieve this purpose.

CHAPTER 5

SUMMARY

The simulations described in this thesis were aimed at understanding the structure-function relationship of light-harvesting complexes. Three different antenna systems were investigated based on exciton theory and Förster mechanism namely, CP29 and LHCII from green plants and the FMO complex from the green sulfur photosynthetic bacterium *Cb. tepidum*. The spectral properties of the LHC are strongly affected by interactions between the pigment and the protein environment and by the so called excitonic interactions which occur between the pigments themselves (embedded in the protein). The rate of energy transfer between weakly interacting pigments depends on the distance between them, their mutual orientation and spectral properties according to Förster mechanism.

CP29 is a monomeric peripheral light harvesting complex and is part of the photosystem II from green plants. CP29 share significant amino acid sequence homology and spectral similarity with the major light harvesting complex LHCII. However, CP29 is simpler system than LHCII, as it binds fewer pigments: 6 Chls a, 2 Chls b and 2 Cars. At the current structural resolutions, the dipole moment orientation of each Chl molecules was not determined. Since each Chl can have a transition dipole in two possible directions (Y or X) for a given conformation there are 2^{12} possible configuration for the orientational arrangement of the transition dipole moment for the LHCII structural model. Although, through the series of studies, the number of configuration has been limited, this is still an open question. Owing to a fewer number of Chl molecule, CP29 is less complicated than LHCII and understanding of CP29 should help to a better interpretation of LHCII. In Chapter 2, we have presented the simulations of the various optical spectra and the

kinetic information concerning the transport of excitation within the CP29. As a result, the orientation of the chlorophyll Q_y transition dipole moments, which have not been unraveled in the crystal structure, has been determined for all of the Chls. Rotating the transition dipole moments of some Chls in the plane of their porhyrins had been necessary to obtain a much better description of spectral properties of CP29. In addition, our results showed the compartmental properties of energy transfer in CP29, i.e., energy equilibration occurs first locally in the compartments (with only a few Chls involved) less than a picoseconds, and then globally between the compartments over many picoseconds. These results were used further in the LHCII modeling (see below).

Another light harvesting complex of green plants, LHCII is the major light-harvesting pigment-protein complex of higher plants and responsible for binding of about 50% of all Chls on Earth. It facilitates energy transfer to the core of Photosystem II and also to the minor light-harvesting complexes CP29, CP26 and CP24. In Chapter 3 we have used the same approach as in the case of CP29 to investigate the structure-function relation of the LHCII by incorporating the results obtained on the CP29. Again the orientation of the chlorophyll Q_y transition dipole moments has been determined for all of the Chls and the energy pathways have been calculated in the frame of Förster mechanism.

Since the structure of the FMO complex from *Pc. aestuarii* was resolved by means of X-ray diffraction early in the 1970s, significant scientific effort has been focused on the understanding of the structure-function relationship. With the availability of the structural information of the FMO complex from another green sulfur bacterium, *Cb. tepidum*, provides some kind of opportunity to cross-check the exciton theory by correlating structural differences with the observed spectral differences between two complexes. In Chapter 4, we examined the FMO complex from *Cb. tepidum*. We present the ABS, LD and CD measurements at 4 K on the FMO complex from *Cb. tepidum*. Furthermore, by using the results of recent fluorescence anisotropy measurements on the FMO complex from *Pc. aesuarii* we calculated the absolute LD spectrum which enabled us to simulate the size of the LD spectrum relative to its absorption spectrum besides its shape. For this purpose

we have used the $P_2(\cos\beta_\mu)$ determined in reference [85] by using the fluorescence excitation anisotropy measurements on the FMO complex from *Pc. aestuarii* since these measurements are not available for *Cb. tepidum*. The consistency in the size of LD between the simulated and the experiment has been achieved by using slightly different value of $P_2(\cos\beta_\mu)$ than the one used in reference [85]. By using an extended exciton model which includes different broadening mechanisms explicitly we have discussed the effect of broadening by including the information on homogeneous and lifetime broadenings obtained in two recent studies [86, 87]. Note that the homogeneous line shape and the spectral density that we have used in the simulations were calculated for the FMO complex of *Pc. aestuarii*, which do not necessarily have to be same for the FMO complex of *Cb. tepidum*. Although we have discussed that there shouldn't be major differences, using the data created for *Cb. tepidum* may lead to further improvements in the simulations.

REFERENCES

[1] Knox, R. S., "Excitation energy transfer and migration: theoretical considerations", In: Bioenergetics of Photosynthesis (Govindjee, ed.), Academic Press, 183-221 (1975).

[2] Barber, J., "Biophysics of photosynthesis", Rep. Prog. Phys,. 41, 1157-1199 (1977).

[3] Youvan, D. C. and Marrs, B. L., "Molecular mechanisms of photosynthesis", Scientific American, 42-48 (June, 1987).

[4] Hunter, N., "Molecules of the green machine", New Scientist, 60-63 (April 28, 1988).

[5] Fleming, G. R. and van Grondelle, R., "The primary steps of photosynthesis", Physics Today, 47, 48-55 (1994).

[6] Bacon, K., "Photosynthesis: Photobiochemistry and Photophysics", In: Advances in Photosynthesis, Boston Kluver Academic Publishers, 10, (2001).

[7] Blankenship, R. M., "Molecular Mechanisms of Photosynthesis", Blackwell Science, Oxford, UK (2002).

[8] Gouterman, M., "Spectra of Porphyrins", J. of Mol. Spectrosc., 6, 138-145 (1961).

[9] Frigaard, N. U., Larsen, K. L. and Cox, R. P., "Spectrochromatography of photosynthetic pigments as a fingerprinting technique for microbial phototrophs", FEMS, Microbiol. Ecol., 20, 69-77 (1996).

[10] Kliger, D. S., Lewis, J. W. and Randall, C. E., "Polarized Light in Optics and Spectroscopy", Academic Press Inc. (1990).

[11] Deisenhofer, J., Epp, O., Miki, K., Huber, R., and Michel, H., "X-ray structure analysis of a membrane protein complex. Electron density map at 3 Å resolution and a model of the chromophores of the photosynthetic reaction center from Rhodopseudomonas viridis.", J. Mol. Biol., 180, 385-398 (1984).

[12] Boekema, E. J., van Roon, H., Calkoen, F., Bassi R., and Dekker, J. P., "Multiple types of association of photosystem II and its largest light-harvesting antenna in partially solubilized photosystem II membranes", Biochemistry, 38, 2233-2239 (1999).

[13] Boekema, E, J., van Roon, H., van Breemen J. F. L. and Dekker, J. P., "Supramolecular organization of photosystem II and its light-harvesting antenna in partially solubilized photosystem II membranes", Eur. J. Biochem., 266, 444-452 (1999).

[14] Kühlbrandt, W., Wang, D. N., and Fujiyoshi, Y., "Atomic model of plant light-harvesting complex by electron crystallography", Nature, 367, 614-621 (1994).

[15] Remelli R., Varotto C., Sandona D., Croce R. and Bassi R., "Chlorophyll binding to monomeric light-harvesting complex", J. Biol. Chem., 274, 33510-33521 (1999).

[16] Bassi, R., Croce, R., Cugini, D., and Sandona, D., "Mutational analysis of a higher plant antenna protein provides identification of chromophores bound into multiple sites", Proc. Natl. Acad. Sci., USA, 96, 10056-10061 (1999).

[17] Gradinaru, C. C., Pascal, A., van Mourik, F., Robert, B., Horton, P., van Grondelle, R., and van Amerongen, H., "Ultrafast evolution of the excited states in the minor chlorophyll a/b complex CP29 from green plants studied by energy-selective pump-probe spectroscopy", Biochemistry, 37, 1143-1149 (1999).

[18] Ruban, A. V., Walthers, R. G., and Horton, P., "The molecular mechanism of the control excitation energy dissipation in chloroplast membranes. Inhibition of pH-dependent quenching of chlorophyll fluorescence by dicylohexylcarbodiimide", FEBS. Lett., 309, 175-179 (1992).

[19] Olson, J. M., "Chlorophyll organization and function in green photosynthetic bacteria", Photochem. and Photobiol., 67, 61-75 (1998).

[20] Camara-Artigas, A., Blankenship, R. E. and Allen, J. P., "The structure of the FMO potein from Chlorobium tepidum at 2.2 $\overset{\circ}{A}$ resolution", Photosynthesis Research, 75, 49-55 (2003).

[21] Fenna, R. E. and Matthews B. W., "Chlorophyll arrangement in a bacteriochlorophyll protein from *Chlorobium limicola*", Nature, 258, 573-577 (1975).

[22] Tronrud, D. E., Schmid, M. F. and Matthews, B. W., "Structure and X-ray amino acid sequence of a bacteriochlorophyll a protein from *Prosthecochloris aestuarii* refined at 1.9 $\overset{\circ}{A}$ resolution", J. Mol. Biol., 188, 443-454 (1986).

[23] Li, Y. F., Zhou, W., Blankenship, R. E. and Allen, J. P., "Crystal structure of the bacteriochlorophyll a protein from *Chlorobium tepidum*", J. Mol. Biol., 271, 456-471 (1997).

[24] Krueger, B. P., Scholes, G. D. and Fleming, G. R., "Calculations of Couplings and Energy-Transfer Pathways between the pigments of LH2 by the ab Initio Transition Density Cube Method", J. Phys. Chem. B, 5378-5386 (1998).

[25] van Amerongen, H., Valkunas, L. and van Grondelle, R., "Photosynthetic Excitons", World Scientific, Singapore (2000).

[26] May, V. and Kühn, O., "Charge and energy transfer dynamics in molecular systems", WILEY-VCH (2000).

[27] Pearlstein, R. M., "Theoretical interpretation of antenna spectra", In: Scheer H. (ed), Chlorophylls. CRC Press, Boca Raton, 1047-1078 (1991).

[28] Fidder, H., Knoester, J. and Wiersma, D. A., "Optical properties of disordered molecular aggregates: a numerical study", J. Chem. Phys. 95, 7880-7890 (1991).

[29] Leegwater, J. A., Durrant, J. R. and Klug, D. R., "Exciton equilibration induced by phonons: Theory and Application to PSII Reaction Centers", J. Phys. Chem. B, 101, 7205-7210 (1997).

[30] Förster, Th., "Zwischenmolekulare Energiewanderung und Fluoreszenz", Ann. Phys.[6] 2, 55-75 (1948).

[31] Förster, Th., "Delocalization excitation and excitation transfer", In: Sinanoğlu, O., (ed) Part II.B.1 of Modern Quantum Chemistry: İstanbul Lectures. Part III, Action of Light and Organic Crystals, 93-137 (1965).

[32] Shipman, L. L. and Hausman, D. L., "Förster transfer rates for chlorophyll a", Photochem. Photobiol., 29, 1163-1167 (1979).

[33] Jean, J. M., Chan, C. K. and Fleming, G. R., "Electronic energy transfer in photosynthetic bacterial reaction centers", Israel J. of Chem., 28, 169-175 (1988).

[34] van Grondelle, R., Dekker, J. P., Gillbro, T., and Sundström, V., "Energy transfer in photosynthesis", Biochim. Biophys. Acta, 1187, 1-65 (1994).

[35] Zucchelli, G., Dainese, P., Jennings, R. C., Breton, J., Garlaschi, F. M., and Bassi, R., "Gaussian decomposition of absorption and linear dichroism spectra of outer antenna complexes of photosystem II", Biochemistry, 33, 8982-8990 (1994).

[36] Giuffra, E., Zucchelli, G., Sandona, D., Croce, R., Cugini, D., Garlaschi, F. M., Bassi, R., and Jennings, R. C., "Analysis of some optical properties of native and reconstituted photosystem II antenna complex, CP29: pigment

binding sites can be occupied by chlorophyll a or chlorophyll b and determine spectral forms", Biochemistry, 36, 12984-12993 (1997).

[37] Pascal, A., Gradinaru, C. C., Wacker, U., Peterman, E., Calkoen, F., Irrgang, K-D., Horton, P., Renger, G., van Grondelle, R., Robert, B., and van Amerongen, H., "Spectroscopic characterization of the spinach Lhcb4 protein (CP29), a minor light-harvesting complex of photosystem II", Eur. J. Biochem., 262, 817-823 (1999).

[38] Simonetto, R., Crimi, M., Sandona, D., Croce, R., Cinque, G., Breton, J., and Bassi, R.: "Orientation of chlorophyll transition dipole moments in the higher-plant light-harvesting complex CP29", Biochemistry, 38, 12974-12983 (1999).

[39] Louwe, R.J.W., Vrieze, J., Hoff, A.J., and Aartsma, T.J., "Towards an integral interpretation of the optical steady-state spectra of the FMO-complex of Prosthecochloris aestuarii. II. Exciton simulations", J. Phys. Chem. B, 101, 11280-11287 (1997).

[40] İşeri, E. İ. and Gülen, D., "Electronic excited states excitation transfer kinetics in the FMO protein complex of the photosynthetic bacterium *Prosthecochloris aestuarii* at low temperatures", Eur. Biophys. J., 28, 243-253 (1999).

[41] Vulto, S. I. E., de Baat, M. A., Louwe, R. J. W., Permentier, H. P., Neef T., Miller, M., van Amerongen, H., and Aartsma, T. J., "Exciton simulations of optical spectra of the FMO complex from the green sulphur bacterium *Chlorobium tepidum* at 6 K", J. Phys. Chem. B., 102, 9577-9582 (1998).

[42] İşeri, E. İ., "Electronic excited states and excitation transfer kinetics in the FMO protein complex of the photosynthetic bacterium *Prosthecochloris aestuarii* at low temperatures", M.S. Thesis, METU, Ankara, Turkey (1998).

[43] Kleima, F. J., Hofmann, E., Gobets, B., van Stokkum, I. H., van Grondelle, R., Diederichs, K., and van Amerongen, H., "Förster excitation energy transfer in peridinin-chlorophyll-a-protein", Biophys. J., 78, 344-353 (2000).

[44] Sauer, K., Schmidt, J. R. L., and Schultz, A. J., "Dimerization of chlorophyll a, chlorophyll b and bacteriochlorophyll in solution", J. Am. Chem. Soc., 88, 2681-2688 (1966).

[45] Gülen, D., van Grondelle, R., and van Amerongen, H.: "Structural information on light-harvesting complex II as obtained from exciton calculations and polarized spectroscopy", In: Photosynthesis: From Light to Biosphere, (Mathis, P., ed.)Volume I, Kluwer, Dordrecht, pp. 335-338 (1995).

[46] Gülen, D., van Grondelle, R., and van Amerongen, H., "Structural information on the light-harvesting complex II of green plants that can be deciphered from polarized absorption characteristics", J. Phys. Chem. B, 101, 7256-7261 (1997).

[47] Gradinaru, C. C., Özdemir, S., Gülen, D., van Stokkum, I. H. M, van Grondelle, R., and van Amerongen, H., "The flow of excitation energy in LHCII monomers: Implications for the structural model of the major plant antenna", Biophys. J., 75, 3064-3077 (1998).

[48] Kiraly, A. P., and Knox, R. S., "Excitation energy flow through light-harvesting chlorophyll proteins", University of Rochester, Biological Physics Group Technical Report, 147 (1995).

[49] van Zandvoort, M. A. M. J., Wrobel, D., Lettinga, P., van Ginkel, G., and Levine Y. K., "The orientation of the transition dipole moments of chlorophyll a and pheophytin in their molecular frame", Photochem. Photobiol., 62, 299-308 (1995).

[50] Hofmann, E., Wrench, P., Sharples, F. D., Hiller, R. G., Welte, W., and Diederichs, K., "Structural basis of light-harvesting by carotenoids-Peridinin-Chlorophyll a-Protein from *Amphidinium carterae*", Science, 272, 1788-1791 (1996).

[51] Moog, R. S., Kuki, A., Fayer, M. D., and Boxer, S. G., "Excitation transport and trapping in a synthetic chlorophyllide substituted hemoglobin: Orientation of the chlorophyll S1 transition dipole", Biochemistry, 23, 1564-1571 (1984).

[52] Fragata, M., Norden, B., and Kurucsev, T., "Linear dichroism (250-700 nm) of chlorophyll a and pheophytin a oriented in a lamellar phase of glycerylmonooctaonate/ H_2O-characterization of electronic transitions", Photochem. Photobiol., 47, 133-143 (1988).

[53] Kleima, F. J., Hobe, S., Calkoen, F., Urbanus, M. L., Peterman E. J. G., van Grondelle, R., Paulsen, H., and van Amerongen, H., "Decreasing the chlorophyll a/b ratio in reconstituted LHCII: structural and functional consequences", Biochemistry, 38, 6587-6596 (1999).

[54] Visser, H. M., Kleima, F. J., van Stokkum, I. H. M., van Grondelle, R., and van Amerongen, H., "Probing many energy-transfer processes in the photosynthetic light-harvesting complex II at 77 K using energy selective sub-picosecond transient absorption spectroscopy", Chem. Phys., 210, 297-312 (1996). Erratum: Chem. Phys., 215, 299 (1997).

[55] Connelly, J. P., Müller, M. G., Gatzen, G., Mullineaux, C. W., Ruban, A. V., Horton, P., and Holzwarth A. R., "Ultrafast spectroscopy of trimeric light-harvesting complex II from higher plants", J. Phys. Chem. B, 101, 1902-1909 (1997).

[56] Özdemir, S., "Identification of several energy transfer pathways in the light-harvesting complex II of green plants using current structural and spectroscopic information", M.S. Thesis, METU, Ankara, Turkey (1997).

[57] İşeri, E. İ., Albayrak, D. and Gülen, D., "Electronic excited states of the CP29 antenna complex of green plants. A model based on exciton calculations", J. Biol. Phys., 26, 321-339 (2000).

[58] Eads, D. D., Castner, E. W., Alberte, R. S. and Mets L., "Direct observation of energy transfer in a photosynthetic membrane: chlorophyll b to chlorophyll a transfer in LHC", J. Phys. Chem., 93, 8271-8276 (1989).

[59] Hemelrijk, P. W., Kwa, S. L. S., van Grondelle, R. and Dekker, J. P., "Spectroscopic properties of LHCII, the main light-harvesting chlorophyll *a*/*b* protein from chloroplast membranes", Biochim. Biophys. Acta, 1098, 159-166 (1992).

[60] Krawzcky, S., Krupa, Z. and Maksymiec, W., "Stark spectroscopy of chlorophylls and carotenoids in antenna pigment proteins LHC-II and CP-II", Biochim. Biophys. Acta. 1143, 273-281 (1992).

[61] Kwa, S. L. S., van Amerongen, H., Lin, S., Dekker, J. P., van Grondelle R. and Struve W. S., "Ultrafast energy transfer in LHC-II trimers from the Chl a/b light –harvesting antenna of photosystem II", Biochim. Biophys. Acta., 1101, 202-212 (1992).

[62] van Amerongen, H., van Bolhuis, B. M., Betts, S., Mei, D., van Grondelle, R., Yocum, C. F. and Dekker, J. P., "Polarized fluorescence and absorption of macroscopically aligned light harvesting complex II", Biophys. J., 67, 837-847 (1994).

[63] Bittner, T., Wiederrecht, K. D., Irrgang, K-D., Renger, G. and Wasielewski, M., "Femtosecond transient absorption spectroscopy on the light-harvesting Chl a/b protein complex of photosystem II at room temperature and 12 K", Chem. Phys., 194, 312-322 (1994).

[64] Du, M., Xie, X., Mets, L. and Fleming, G. R., "Direct observation of ultrafast energy-transfer processes in light-harvesting complex II", J. Phys. Chem., 98, 4736-4741 (1994).

[65] Nussberger, S., Dekker, J. P., Kühlbrandt, W., Bolhuis, B. M., van Grondelle, R. and van Amerongen, H., "Spectroscopic characterization of three different

monomeric forms of the main chlorophyll a/b binding protein from chloroplast membranes", Biochemistry, 33, 14775-14783 (1994).

[66] Palsson, L. O., Spangfort, M. D., Gulbinas, V. and Gillbro, T., "Ultrafast chlorophyll b-chlorophyll a excitation transfer in the isolated light-harvesting complex, LHC, of green plants", FEBS Lett., 339, 134-138 (1994).

[67] Reddy, N. R. S., van Amerongen, H., Kwa, S. L. S., van Grondelle, R. and Small, G. J., "Low-energy exciton level structure and dynamics in light-harvesting complex II of green plants", J. Phys. Chem., 98, 4729-4735 (1994).

[68] Savikhin, S., van Amerongen, H., Kwa, S. L. S., van Grondelle, R. and Struve, W. S., "Low-temperature energy transfer in LHC-II trimers from the Chl a/b light-harvesting antenna of photosystem II", Biophys. J., 1597-1603 (1994).

[69] Lokstein, H., Leupold, D., Voight, B., Nowak, F., Ehlert, J., Hoffman, P. and Garab, G., "Nonlinear polarization spectroscopy in the frequency domain of light-harvesting complex II: absorption band structure and exciton dynamics", Biophys. J., 69, 1536-1543 (1996).

[70] Kleima, F. J., Gradinaru, C. C., Calkoen, F., van Stokkum, I. H. M., van Grondelle, R. and van Amerongen, H., "Energy transfer in LHC-II monomers at 77 K studied by subpicosecond transient absorption spectroscopy", Biochemistry, 36, 5262-5268 (1997).

[71] Agarwal, R., Krueger, B. P., Scholes, G. D., Yang, M., Yom, J., Mets L. and Fleming G. R., "Ultrafast energy transfer in LHC-II revealed by three-pulse photon echo peak shift measurements", J. Phys. Chem. B, 104, 2908-2918 (2000).

[72] Trinkunas, G., Connelly, J. P., Müller, M. G., Valkunas, L. and Holzwarth, A., "Model for excitation dynamics in the light-harvesting complex II from green plants", J. Phys. Chem. B, 101, 7313-7320 (1997).

[73] Renger, T. and May, V., "Simulations of frequency-domain spectra: structure-function relationships in photosynthetic pigment-protein complexes", Phys. Rev. Lett., 84, 5228-5231 (2000).

[74] Renger, T. and May, V., "Exciton motion in photosynthetic antenna systems: the FMO system", J. Phys. Chem. A, 102, 4381-4391 (1998).

[75] Sumi, H., "Theory on rates of excitation-energy transfer between molecular aggregates through distributed transition dipoles with application to antenna system in bacterial photosynthesis", J. Phys. Chem. B, 103, 252-260 (1999).

[76] Pearlstein, R. M. and Hemenger, R. P., "Bacteriochlorophyll electronic transition moment directions in bacteriochlorophyll a protein", Proc. Natl. Aca. Sci., USA, 75, 4920-4924 (1978).

[77] Blankenship, R. E., Olson, J. M. and Miller, M., "Antenna complexes from green photosynthetic bacteria",In: Blankenship, R. E., Madigan, M. T., Bauer, C. E., (ed), Anoxygenic photosynthetic bacteria., Kluwer, Dordrecht, 399-435 (1995).

[78] Savikhin, S., Buck, D. R. and Struve, W. S., "Towards level-to-level energy transfers in photosynthesis: The Fenna-Matthews-Olson protein", J. Phys. Chem. B, 102, 5556-5565 (1998).

[79] Savikhin, S., Buck, D. R. and Struve, W. S., "The Fenna-Matthews-Olson protein: a strongly coupled photosynthetic antenna" In: Andrews, D. L. and Demidov, A. A., (ed), John Wiley and Sons, 399-434 (1999).

[80] Pearlstein, R. M., "Theory of the optical spectra of the bacterichlorophyll a antenna protein trimer from *Prosthecochloris aestuarii*", Photosynth. Res., 31, 213-226 (1992).

[81] Lu, X. and Pearlstein, R. M., "Simulations of *Prosthecochloris* bacteriochlorophyll a protein optical spectra improved by parametric computer search", Photochem. and Photobiol., 57, 86-91 (1993).

[82] Gülen, D., "Interpretation of the excited state structure of the Fenna-Matthews-Olson pigment complex of *Prosthecochloris aestuarii* based on the simultaneous simulation of the 4 K absorption, linear dichroism and singlet-triplet absorption difference spectra: A possible excitonic explanation?", J. Phys. Chem. B, 100, 17683-17689 (1996).

[83] İşeri, E. İ. and Gülen, D., "Absorption and linear dichroism of the Fenna-Matthews-Olson pigment-protein complex of *Prosthecochloris aestuarii*: An exciton model", Doğa-Tr. J. of Physics, 21, 1129-1143 (1997).

[84] Louwe, R. J. W., Aartsma, T. J. and Hoff, A. J., "Towards an integral interpretation of the optical steady-state spectra of the FMO-complex of *Prosthecochloris aestuarii*. I An investigation with linear-dichroic absorbance-detected magnetic resonance", J. Phys. Chem. B, 101, 11280-11287 (1997).

[85] Owen, G. M. and Hoff, A. J., "Absorbance detected magnetic resonance spectra of the FMO complex of *Prosthecochloris aestuarii* reconsidered: Exciton simulations", J. Phys. Chem. B, 105, 1458-1463 (2001).

[86] Wendling, M., Przyjalgowski, M. A., Gülen, D., Vulto, S. I. E., Aartsma, T. J., van Grondelle, R. and van Amerongen, H., "The quantitative relationship between structure and polarized spectroscopy in the FMO complex of *Prosthecochloris aestuarii*: refining experiments and simulations", Photosynthesis Research, 71, 99-123 (2002).

[87] Vulto, S. I. E., de Baat, M. A., Neerken, S., Nowak, F. R., van Amerongen, H., Amesz, J. and Aartsma, T. J., "Excited state dynamics in FMO antenna complex from photosynthetic green sulfur bacteria: A kinetic model", J. Phys. Chem. B, 103, 8153-8161 (1999).

[88] Wendling, M., Pullerits, T., Przyjalgowski, M. A., Vulto, S. I. E., Aartsma, T. J., van Grondelle, R. and van Amerongen, H., "Electron-Vibrational Coupling in the Fenna-Matthews-Olson Complex of *Prosthecochloris aestuarii*

Determined by Temperature-Dependent Absorption and Fluorescence Line Narrowing Measurement", J. Phys. Chem., B, 104, 5825-5831 (2000).

[89] Francke, C. and Amesz, L., "Isolation and pigment composition of the antenna system of four species of green sulfur bacteria", Photosynth. Res., 52, 137-146 (1997).

[90] Van Amerongen, H. and Struve, W. S., "Polarized optical spectroscopy of chromoproteins", Meth. Enzymol., 246, 259-283 (1995).

[91] Louwe, R. J. W. and Aartsma, T. J., "On the nature of energy transfer at low temperatures in the BChl a pigment-protein complex of green sulfur bacteria", J. Phys. Chem. B, 101, 7221-7226 (1997).

[92] Matsuzaki, S., Zazubovich, V., Räpset, M., Hayes, J. M. and Small, G. J., "Energy transfer kinetics and low energy vibrational structure of the three lowest energy Q_y-states of the Fenna-Matthews-Olson antenna complex", J. Phys. Chem. B, 104, 9564-9572 (2000).

[93] Räpset, M., Blankenship, R. E. and Small, G. J., "Energy transfer and spectral dynamics of the three lowest energy Qy-state of the Fenna-Matthews-Olson antenna complex", J. Phys. Chem. B, 103, 5736-5741 (1999).

[94] Monshouwer, R., Abrahamsson, M., van Mourik, F. and van Grondelle, R., "Supperradiance and exciton delocalization in bacterial photosynthetic light-harvesting systems", J. Phys. Chem. B, 101, 7241-7248 (1997).

[95] Buck, D. R., Savikhin, S. and Struve, W. S., "Ultrafast absorption difference spectra of the Fenna-Matthews-Olson protein at 19 K: Experiment and simulations", Biophys J., 72, 24-36 (1996).

[96] Gudowska-Nowak, E., Newton, M. D. and Fajer, J., "Conformational and environmental effects on bacteriochlorophyll optical spectra: Correlation of calculated spectra with structural results", J. Phys. Chem., 94, 5795-5801 (1990).

[97] Gentemann, S., Nelson, Y. N., Jaquinod, L. Nurco, D. J., Leung, S. H., Medfort, C. J., Smith, K. M., Fajer, J. and Holten, D., "Varitions and Temperature Dependence of the Excited State Properties of Conformationally and Electronically Perturbed Zinc and Free Base Porphyrins", J. Phys. Chem. B, 101, 1247-1254 (1997).

[98] Sturgis, J. N. and Robert, B., "The role of chromophore coupling in tuning the spectral properties of peripheral light-harvesting protein of purple bacteria", Photosynth. Res., 50, 5-10 (1996).

[99] Sturgis, J. N. and Robert, B., "Pigment binding-site and electronic properties in light-harvesting proteins of purple bacteria", J. Phys. Chem. B, 101, 7277-7231 (1997).

[100] http://www.gnu.org.

[101] Press W. H, Flannery B. P., Teukolsky S. A. and Vetterling W. T., "Numerical recipes in C: The art of scientific computing", Cambride University Press (1988).

[102] Mathews J. H., "Numerical methods for mathematics, science and engineering", Prentice Hall, 2nd ed. (1992).

[103] Knuth D. E., "The Art of Computer Programming: Seminumerical Algorithms", Addison-Wesley, Vol 2, 3rd ed. (1997).

APPENDIX A

NUMERICAL METHODS

The numerical procedures are written in the C and the FORTRAN language by using GCC. GCC is the GNU compiler collection [100], which currently contains front ends for C, C++, objective-C, FORTRAN, Java and Ada; as well as libraries for these languages. Figure A.1 shows the flowchart of numerical procedure(s) used in the calculations. The Hamiltonian matrix has been numerically diagonalized by using TQL2 [101] function which finds the eingenvalues and eigenvectors of a symmetric tridiagonal matrix by the QL method [102]. The TRED2 [101] function has been also used to reduce the Hamiltonian matrix to a symmetric tridiagonal matrix using an accumulating orthogonal similarity transformation.

For the simulations of Chapter 4, a program written by Markus Wendling has been used with some modifications. The same procedure described above has been applied for the Monte Carlo simulation with typically 10,000 iterations. For the Monte Carlo simulations, standard UNIX srand48 random number generator function has been used with Box-Muller algorithm [103] to obtain Gaussian distributed random numbers. In each Monte Carlo iteration the site energy for each pigment is allowed to vary around the mean value according to a Gaussian distribution function (IDF).
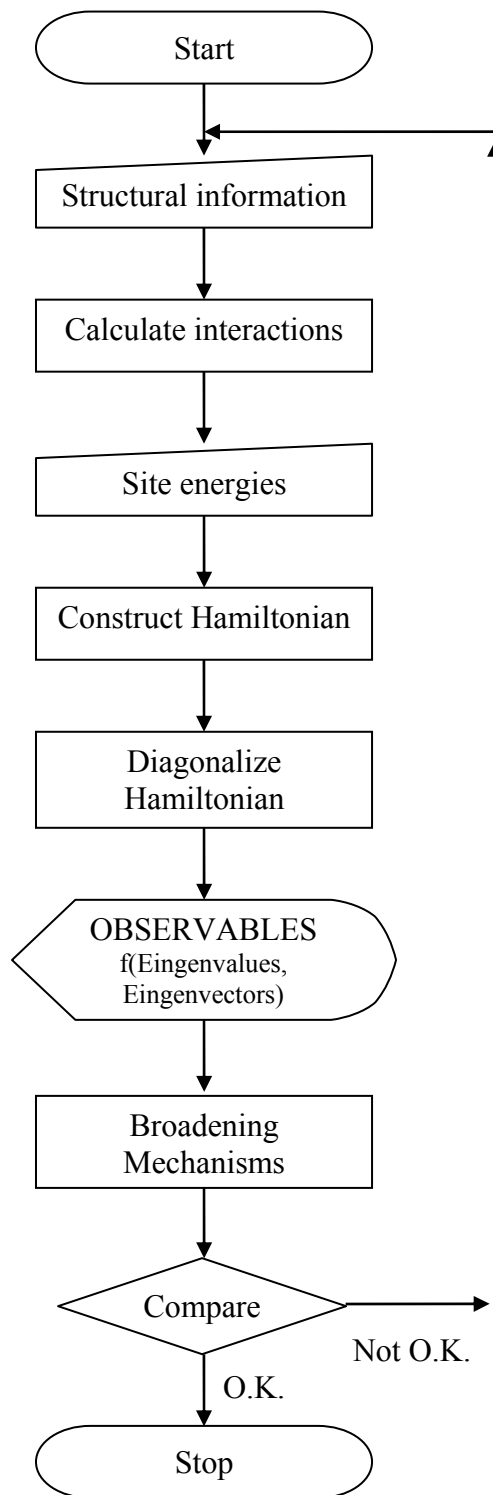
Figure A.1. Flowchart of the the numerical procedure(s) used in this thesis.

Figures A.2-4 depict the results of the simulation steps for the Gaussian dressed stick ABS spectrum, which is calculated by using the formalism described in Chapter1 and the parameters of reference [40], of the monomeric FMO complex of *Prosthecochloris aestuarii* [22]. Figure A.5 shows the ABS spectrum of the same complex resulted from Monte Carlo simulation with and without of (lifetime broadened) homogeneous lineshape (See Figure captions for further details).
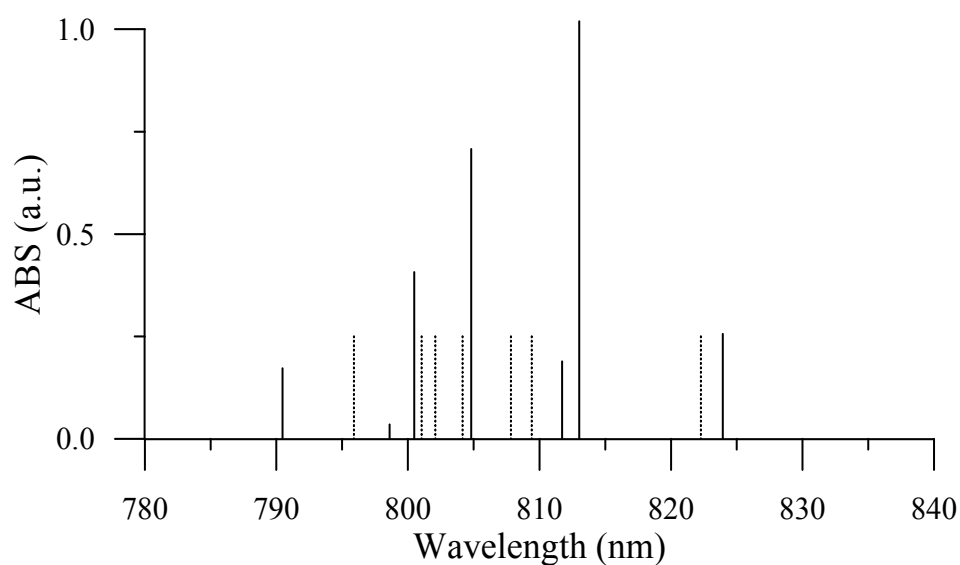

Figure A.2. Stick spectrum (solid lines) for ABS of the FMO complex of *Prosthecochloris aestuarii* with the absorption strength of 32.5 Debye^2. Dotted lines indicates the position of site energies of BChl molecules.
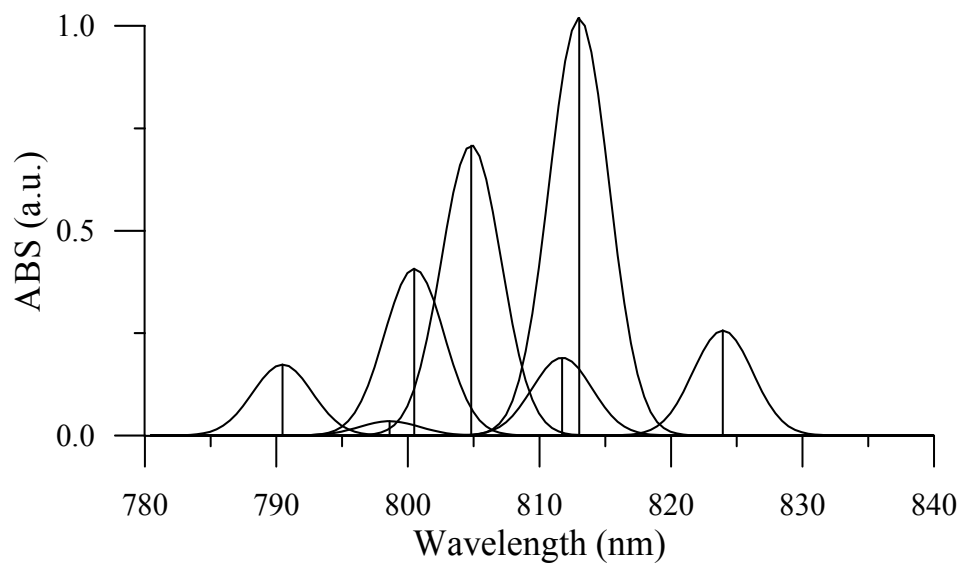
Figure A.3. Gaussian dressed absorption spectrum. Each one-exciton transition is dressed with a symmetric Gaussian of 80 cm^{-1} linewidth.
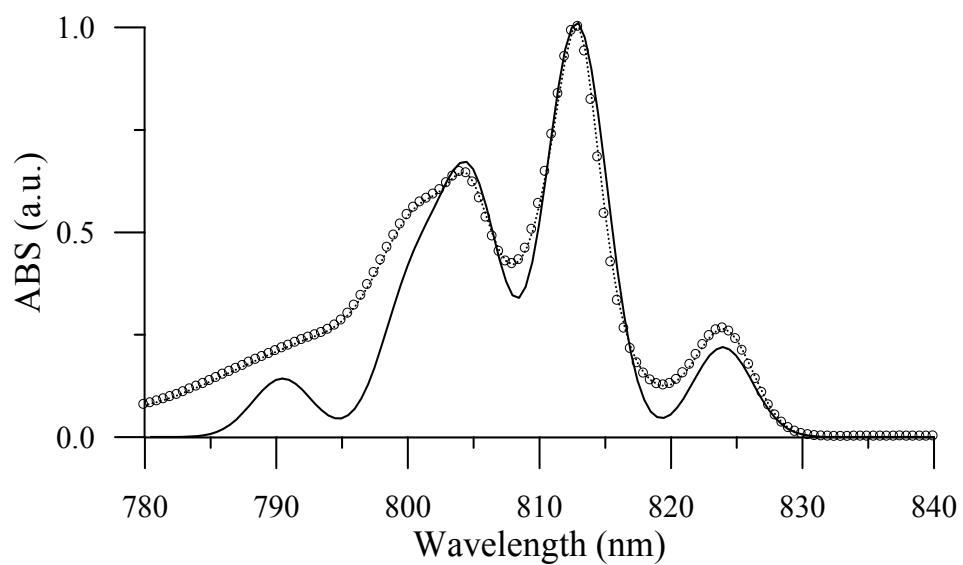

Figure A.4. Comparison of the simulated (solid lines) and the experimental (open dots) ABS spectra. Experimental data are taken from reference [86].
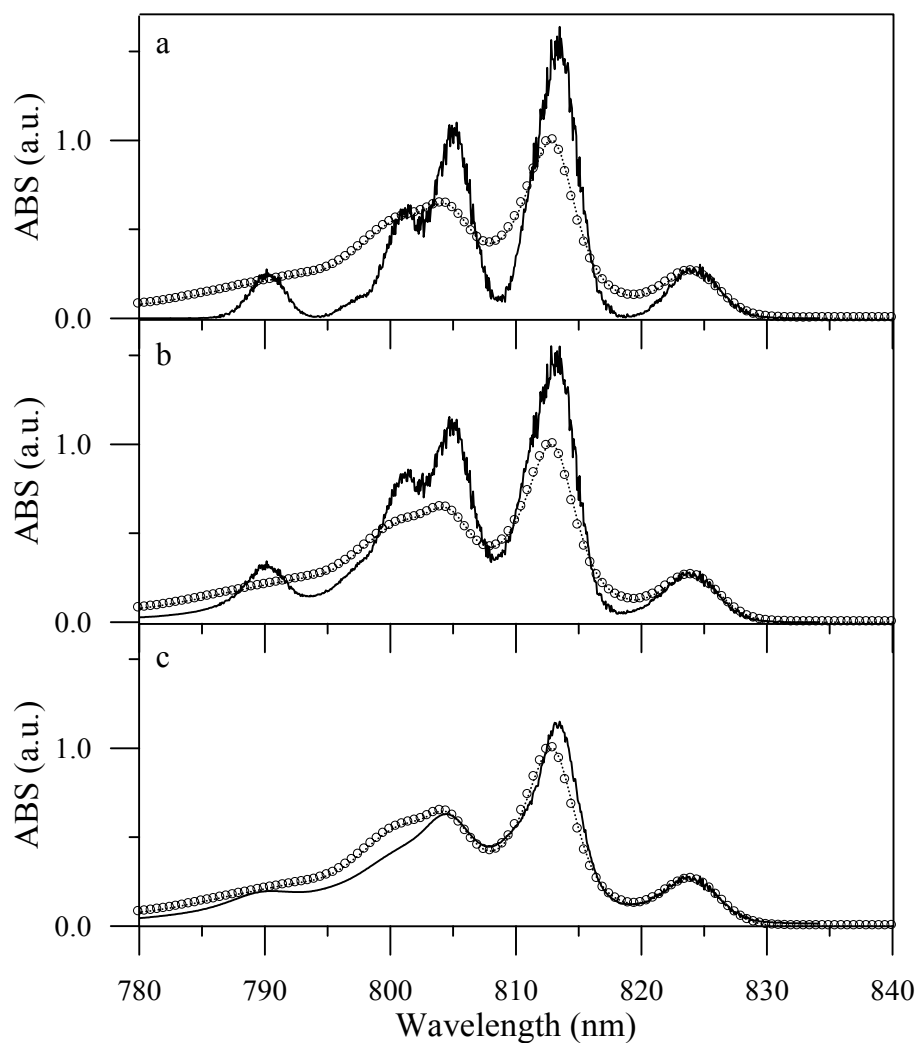
Figure A.5. Simulated ABS spectra of monomeric FMO complex (solid) by using parameters of reference [40]. For comparison experimental ABS spectrum (dashed lines) at 4 K is also shown [86]. Simulated spectra were scaled to the lowest experimental ABS peak. (a) Monte Carlo simulation by using IDF with a fwhm of 80 cm^{-1}. (b) Monte Carlo simulation and homogeneous line shape. (c) Monte Carlo simulation and lifetime broadened homogeneous line shape.

APPENDIX B

ACKNOWLEDGMENTS

I would like to express my deep gratitude to my supervisor Prof. Dr. Demet Gülen for her unceasing interest, guidance, encouragement and support during the course of this thesis.

I would like to thank to Prof. Dr. Werner Kühlbrandt for providing the data file containing the atomic coordinates of the LHCII model. I also would like to thank to Prof. Dr. Roberto Bassi for sharing some of the results on CP29 and LHCII from his laboratory with us prior to publication.

I thank to Prof. Dr. Jim Allen for providing the file containing the trimeric FMO structure data and to Dr. Thijs J. Aartsma for providing FMO samples.

Part of the Chaper 4 was done at the Vrije Universiteit, Amsterdam, when I was visiting Prof. Dr. Rienk van Grondelle's laboratory under the under the support of European Science Foundation 'Femtochemistry and Femtobiology' ULTRA Programme for three-months in May-August 2001. I am thankful to ESF for the financial support. I thank to Prof. Dr. Rienk van Grondelle and to Prof. Dr. Herbert van Amerongen for giving me a chance to work in the Biophysics group in Vrije Universiteit.

I would like to thank to Dr. Markus Wendling for providing the program codes used in Chapter 4.

Finally I would also like to thank to Miguel A. Palacios for helping me in taking the experimental data presented in Chapter 4.

CURRICULUM VITAE

Erkut İnan İşeri was born in Nicosia, Turkish Republic of Northern Cyprus on June 28, 1973. He received his B.S degree in Physics from the Middle East Technical University in June 1996. He received his M.S degree in Physics from the Middle East Technical University in June 1998. He has been working as a research assistant in the Department of Physics of Middle East Technical University since 1999. He has visited Prof. Dr. Rienk van Grondelle's Laboratory, Vrije University, Amsterdam, under the European Science Foundation 'Femtochemistry and Femtobiology' ULTRA Programme, for three months in 2001.

List of Publications

Papers in Refereed Journals

1. E. İ. İşeri and D. Gülen, "Absorption and linear dichroism of the Fenna-Matthews-Olson pigment-protein complex of *Prosthecochloris aestuarii*: An exciton model", Doğa-Tr. J. of Physics, **21**, 1129-1140, 1997.

2. E. İ. İşeri and D. Gülen, "Electronic excited states and excitation transfer kinetics in the Fenna-Matthews-Olson protein of the photosynthetic bacterium *Prosthecochloris aestuarii* at low temperatures", Eur. Biophys. J., **28/3**, 243-253, 1999.

3. E. İ. İşeri, Duygu Albayrak and D. Gülen, "Electronic excited states of the CP29 antenna complex of green plants: a model based on exciton calculations", J. of Biol. Phys., **26**, 321-339, 2000.

4. E. İ. İşeri and D. Gülen, "Chlorophyll transition dipole moment orientations and pathways for flow of excitation energy among the chlrophylls in the major plant antenna LHCII", Eur. Biophys. J., **30**, 344-353, 2001.

5. H. Yıldırım, E. İ. İşeri and D. Gülen, "A quantitative analysis of exciton superhyperchromism in porphyrin J-/H-aggregates", Chem. Phys. Lett. 391, 302-307 (2004).

Proceeding Papers

1. E. İ. İşeri and D. Gülen, in: *Photosynthesis: Mechanisms and Effects*, vol. I, pp. 181-184, G. Garab and J. Pusztai (eds.), "Low-temperature excitation transfer in the FMO complex. Simulations", Kluwer 1998.

Abstracts

1. E. İ. İşeri, H. van Amerongen and D. Gülen, "Excited state structure and subpicosecond excitation dynamics in FMO complex from the green photosynthetic bacterium *Prosthecochloris aestuarii*: simulations of the absorption difference spectra at low temperatures", European Science Foundation Workshop on Green and Heliobacteria, August 31-September 4 1997, Urbino, Italy.

2. E. İ. İşeri and D. Gülen "Low-temperature electronic excitation transfer in the FMO complex. Simulations", ESF International Workshop on Light-Harvesting Systems, August 14-16 1998, Tata, Hungary.

3. E. İ. İşeri and D. Gülen, "Low-temperature excitation transfer in the FMO complex. Simulations", XIth International Congress on Photosynthesis, August 17-22 1998, Budapest, Hungary.

4. E. İ. İşeri and D. Gülen, "Electronic excited states and excitation transfer kinetics in the Fenna-Matthews-Olson complexes of photosynthetic green

sulphur bacteria at low temperatures", Colloquium Spectroscopicum Internationale XXXI, September 5-10 1999, Ankara, Turkey.

5. E. İ. İşeri, D. Albayrak and D. Gülen, "Electronic excited states of the CP29 and LHCII antenna complexes of green plants", Photophysics and Photochemistry 2000, October 18-21 2000, Costa do Estoril, Portugal.

6. E. İ. İşeri, D. Albayrak and D. Gülen, "Chlorophyll transition dipole moment orientations and pathways for flow of excitation energy among the chlrophylls in CP29 and LHCII", 1st General Meeting of the ESF/ULTRA Programme, October 23-25 2000, Coimbra, Portugal.

7. E. İ. İşeri and D. Gülen, "Structure-spectroscopy relationship in the LHCII: a model study on the chlorophyll transition dipole moment orientations and flow of excitation energy among the chlorophylls", LHC2001, Satellite Workshop to the XIIth International Congress of Photosynthesis, August 15-18 2001, Surfers Paradise, Australia.

8. E. İ. İşeri and D. Gülen, "Structure-spectroscopy relationship in the LHCII: a model study on the chlorophyll transition dipole moment orientations and flow of excitation energy among the chlorophylls", XIIth International Congress of Photosynthesis, August 18-23 2001, Brisbane, Australia.

9. A. S. Taisova, D. Gülen and E. İ. İşeri, V. A. Drachev, T. A. Cherenkova, Z. G.Fetisova, "Antenna-size dependent hyperchromism of the Q_y absorption band of the chlorosomal oligomeric bacteriochlorophyll (BChl) c antenna of the green bacteria, XIIth International Congress of Photosynthesis, August 18-23 2001, Brisbane, Australia.

10. Z. G. Fetisova, A.S. Taisova, D. Gülen, E. İ. İşeri, "Antenna-size dependent hyperchromism of the Q_y absorption band of the chlorosomal oligomeric bacteriochlorophyll c antenna of the green bacterium *Chloroflexus aurantiacus*, July 2001, Voronez, Russia.

11. A. S. Taisova, D. Gülen and E. İ. İşeri, V.A. Drachev, T.A. Cherenkova, Z.G.Fetisova, "Antenna-size dependent hyperchromism of the Q_y absorption band of the chlorosomal oligomeric bacteriochlorophyll (BChl) c antenna of the green bacteria, Satellite Meeting on the Evolution of Photosynthesis, XIIth International Congress of Photosynthesis, August 25-28 2001, Heron Island, Australia.

12. H. van Amerongen, M. Wendling, M. A. Przyjalgowski, M. A. Palacios, R. van Grondelle, T. J. Aartsma, S. I. E. Vulto, E. I. Iseri, D. Gülen., "The relation between structure and polarized spectroscopy of the FMO complex of *Prosthecochloris aestuarii* and *Chlorobium tepidum* ", EMBO Workshop on Green and Heliobacteria, April 19-23, 2002, Passau, Germany.

13. E. İ. İşeri, M. Wendling, M. A. Palacios, R. van Grondelle, T. J. Aartsma, S. I. E. Vulto, D. Gülen and H. van Amerongen, "Spectroscopic measurements and spectral simulations of the FMO protein from Chlorobium tepidum", ESF "Femtochemistry and Femtobiology" Ultra Programme Workshop on Femtosecond Dynamics in Photosynthetic Light-harvesting Complexes, October 9-13 2002, Belek, Antalya, Turkey.

14. E. İ. İşeri, H. Yıldırım, and D. Gülen, "Antenna size dependent hyperchromism of the Q_y absorption band of linear and tubular BChl c aggregates", ESF "Femtochemistry and Femtobiology" Ultra Programme Workshop on Femtosecond Dynamics in Photosynthetic Light-harvesting Complexes, October 9-13 2002, Belek, Antalya, Turkey.

Conferences and Workshops Attended

1. "ESF-Biophysics of Photosynthesis Programme Workshop" on Interactions Between Chlorophylls and Carotenoids in Photosynthesis, 7-11 October, 1999, Kemer–Antalya, Turkey.

2. Colloquium Spectroscopicum Internationale XXXI, September 5-10 1999, Ankara, Turkey.

3. "ESF Femtochemistry and Femtobiology-ULTRA Programme Workshop" on Femtosecond Dynamics in Photosynthetic Light Harvesting Complexes, 9-13 October, 2002, Belek–Antalya, Turkey.